Revista Brasileira de Ciências Mecânicas

Journal of the Brazilian Society of Mechanical Sciences

1

PUBLICAÇÃO DA ABCM - ASSOCIAÇÃO BRASILEIRA DE CIÊNCIAS MECÂNICAS

VOL. XVII - Nº 1 - 1995 ISSN 0100-7386

REVISTA BRASILEIRA DE CIÊNCIAS MECÂNICAS
JOURNAL OF THE BRAZILIAN SOCIETY OF MECHANICAL SCIENCES

REVISTA BRASILEIRA DE CIÊNCIAS MECÂNICAS
JOURNAL OF THE BRAZILIAN SOCIETY OF MECHANICAL SCIENCES
Vol. 1, Nº 1 (1979) -
Rio de Janeiro: Associação Brasileira de Ciências Mecânicas
Trimestral
Inclui referências bibliográficas.
1. Mecânica
ISSN-0100-7386

A REVISTA BRASILEIRA DE CIÊNCIAS MECÂNICAS publica trabalhos que cobrem os vários aspectos da ciência e da tecnologia em Engenharia Mecânica, incluindo interfaces com as Engenharias Civil, Elétrica, Química, Naval, Nuclear, Aeroespacial, Alimentos, Agrícola, Petróleo, Materiais, etc., bem como aplicações da Física e da Matemática à Mecânica.

Publicação da /Published by
ASSOCIAÇÃO BRASILEIRA DE CIÊNCIAS MECÂNICAS
THE BRAZILIAN SOCIETY OF MECHANICAL SCIENCES

Secretária da ABCM: Ana Lucia Fróes de Souza
Av. Rio Branco, 124 - 18º andar - Tel./Fax (021) 222-7128
20040-001 - Rio de Janeiro RJ - Brasil

Presidente: **Arthur Palmeira Ripper**
Vice-Presidente: **Sidney Stuckenbruk**
Secret. Geral: **Agamenon R. E. Oliveira**
Secretário: **Carlos Alberto de Almeida**
Diretora de Patrimônio: **Aura Conci**

REVISTA FINANCIADA COM RECURSOS DO
Programa de Apoio a Publicações Científicas
MCT CNPq FINEP
FAPESP - Fundação de Amparo a Pesquisa do Estado de São Paulo

RBCM - J. of the Braz. Soc. Mechanical Sciences
Vol. XVII - nº1 - 1995 - pp. 1-13

ISSN 0100-7386
Printed in Brazil

Advances and Applications of Laser Velocimetry

E.P. Tomasini
Dip. Meccanica Univ. di Ancona
via Brecce Bianche
60131 ANCONA
Tel. +71 2204487 Fax +71 2204813

Abstract

This paper is a critical review of the most recent advances in laser measurement techniques and their different applications. It is worth underling that these techniques are used both for measuring fluids motion characteristics and conditions, and for measuring motion, vibrations in particular, in solids.
Those applications which, until today, had been carried out in laboratories, are now being extended to the industrial field, especially in the control of processes and products. It is therefore desirable that associations, meetings and conferences will contribute to a more extensive use and knowledge of these techniques.
Keywords: Laser Doppler, Dual Focus, PIV, Doppler Global Velocimetry, Scalar Quantities, Laser Vibrometry, Vibrations, Flames.

Introduction

Non-intrusive measurement techniques have expanded in scope and have achieved fruitful results in laser metrology.

In particular, optical techniques (interferometry, speckle, holography and so on, combined with advanced techniques of analysis, treatment and interpretation of the signal) are fundamental to solve many measurement problems in bigger, various application fields. Laser velocimetry has played a decisive role as regards the development of experimental techniques on fluids and solids; in particular, combined with other optical methods, it has been the starting point in the growth of a laser applied measurement culture.

Therefore, it is clear that nowadays talking about advances of laser velocimetry means also talking about all the changes that the metrological approach has had. Particularly, it is very important to underline that the use of cheaper, more compact laser construction techniques, the use of fibre optics components, the miniaturization also in integrated optics of the well known, expensive and very delicate optical benches, the realization of electro-optical components and the development of techniques of analysis and the quick processing of signals and images have made velocimetry, and all the techniques connected with it, more and more interesting, useful and well known.

As far as Italy is concerned, in order to expand and consolidate different application fields and with the aim of creating a common ground for both market and research, the Italian Association of Laser Velocimetry (AIVELA) was founded in 1991. The AIVELA aims to promote every kind of activities concerning laser velocimetry and any similar techniques: from research to industrial application and even to realization. Therefore, the AIVELA wishes to collect researches, users and producers of laser metrology systems.

In order to point the most interesting themes out, I would like to synthesize some of the most meaningful techniques, some of their aspects that let us foresee an enormous development, as regards measurements on fluids and solids, and newest results achieved by our research group.

Velocity measurement has got many applications in the most various fields:

control of industrial processes and machines;

- quality process control of mechanical and electronic products;
- fluid dynamics, both in laminar flow and in turbulent flow;
- study of structure vibrations;
- transfer phenomena;

Invited Paper: December 1994. Technical Editor: Leonardo Goldstein Jr.

- noise generation, and
- fatigue.

It is therefore important to use velocity measuring instruments, which have metrological characteristics and operative capabilities suitable for an experimental research of different phenomena.

Laser Doppler Velocimetry

Nowadays, Laser Doppler Velocimetry (LDV) (Durst et al., 1976, Darin, 1980) is quite know in all the Universities and all the research centres. Although its applications could be on a much larger scale, it is not yet widespread in the industrial field perhaps because of the difficulty of use, due to a not specifically trained staff or, perhaps, because of the high cost of amortization.

Until today, there has been a progressive development of performances. Thus, the head-on products of the market have become high quality instruments, suitable for the measurement of the three components of the velocity vector in a wide range of different applications. Likewise, to meet many users' needs, more simple systems have been developed, with average performances, realized thanks to the availability of primary components, a kind of opto-mechanical-electronic "tool box", by using processors which are aimed at the not very strong specifications of many applications.

In the next future, one can foresee that the development of LDV systems will head not only towards general purpose, very simple and cheap instruments, but they should also be suitable for specific applications and have simple configurations so to make use of less powerful lasers. Thanks to a favourable cos-performances ratio such systems could be employed in the most diverse fields of applied research and, especially, of industry.

Among the most advanced applications, it is worth mentioning those in flames, in biological flows (Fig. 1) (Pinotti et al., 1994), "in vivo" as well, as for example (Einav, 1993), in the study of boundary layers with little measurement volumes, in two-phase flows.

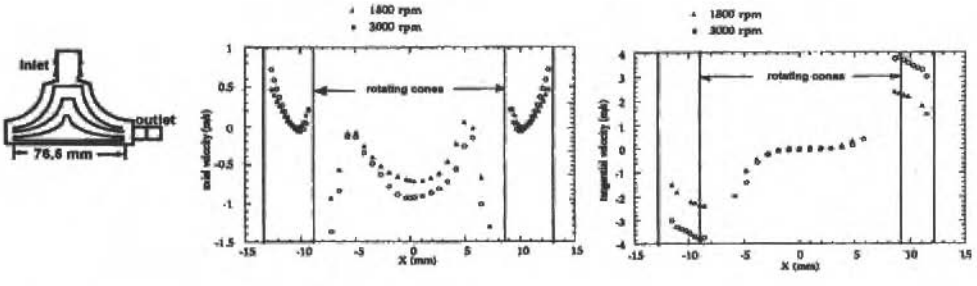

Fig. 1 Axial and tangential velocity along X axis at 5 mm from the inlet of a vaneless centrifugal blood pump (Pinotti et al., 1994)

Dual Focus Velocimetry

Dual Focus Laser Velocimetry is a non-intrusive measurement technique for liquid or gas velocity, based on the analysis of luminous pulses, produced by seeding particles passing through two adjacent focal points. The velocity is calculated by measuring the time-of-flight of the particles between the two focal points, whose location in the space is known. Compared to LDV systems, this technique has advantages, in terms of the signal-noise ratio, but it is less suitable for measuring high turbulent flows. Here as well, recent developments have led to realize two-colour systems, so that they can allow the measurement of two or three components of the velocity vector (Sriram, 1992).

Among the most interesting applications of Dual Focus systems, are those in turbomachines. In them, in fact, the high signal-noise ratio allows measuring even in difficult optical access areas and the presence of strong guided flows reduces problems related to turbulence, thus allowing an accurate, easy velocity measurement on a wide, dynamic range.

In the first months of 1995, a new experimental phase will start at the Dept. of Mechanics of Ancona University. The aim will be of assessing the potential of the most recent systems which are now commercially available. In addition to this, comparison will be made with the more classical Laser Doppler System.

Particle Image Velocimetry PIV

PIV can be considered as the development of classical flow visualization techniques into quantitative measurements of fluid velocity. Of these techniques, PIV has kept the possibility of a quantitative, global observation of a flow field in just a moment, "the flowing ... moment". This capability allows a quick acquisition of the velocity field, related to stationary phenomena and, in particular, the study of non-stationary phenomena and spatial structures. This last characteristic mostly distinguishes PIV from punctual measurement systems, such as LDV, which become valid complements to the PIV measurement. The most recent PIV technique developments regard, on the one hand the set-up of the measurement chain. On the other hand, they are also concerned with the study of the applications, for which the system has to be developed and optimized each time.

In spite of PIV conceptual simplicity, this measurement technique is complex and articulated at the same time. That is why trends of the PIV development move towards electronic measurement chains, from the acquisition of the image to its digitization and processing. Until now, problems linked to a limited resolution of CCD sensors have reduced applications of digital PIV to small-size flows (Cenedese et al., 1980). For these reasons, all the studies on the use of such technique on areas of big flow, such as the one described next, are of great importance. Resort to high resolution systems and the development of parallel computation of systems with transputer or neural networks will allow the development of PIV digital systems which are competitive with the photographic ones. Another developing trend concerns the use of completely optical processors, capable of operating Fourier transforms and correlations on photographic negatives in real time.

The use of holographic supports (Royer, 1988) or stereoscopic acquisition techniques (Prasad and Adrian, 1992) gives the opportunity of measuring in 3-D and also of a complete knowledge of the whole velocity field and not only of one of its "sections".

The main aspect for the development of the PIV technique is the study of its applications to particular flows. In fact, the main difficulty of PIV measurements is that of realizing multiexposed images of such quality as to allow the following processing, in other words provided with a high contrast and a high contrast and a high signal-noise ratio.

This first step of the measuring process corresponds to the phase in which the primary information is extracted from the physical system. In fact, no algorithm of processing can increase the information recorded by the image. If the image is not a good quality one, it will not be possible to extract any information that has been by now lost.

Among the most recent applications, let us focus our attention on PIV measurements in high velocity flows, in flames and in large wind tunnels.

Works on PIV measurements in transonic and supersonic flows in wind tunnels have recently been published (Humphreys et al., 1993, Rafael and Kompenhans, 1993). In order to operate high velocity measurements, it is necessary to use micro metrical particles and pulsed lasers, if one wants to obtain good images: in particular, pulsed lasers are necessary to freeze the images of the particles and to increase the signal-noise ratio.

Problems linked to the possibility of photographing seeding particles are also present in measuring combusting flows, where the main problem is the radiation emitted by the flame which represents an intense source of noise in the images. One can try to solve the problem by using an interferential, narrow band optical filter in order to eliminate the radiation of the wavelength different from that of the utilized laser light. In (Paone, 1994), measurements made in methane premixed flames (combustion chamber at 14000 kcal/h) are described. The measurements (see Fig. 2 and 3) show the spatial structures of the motion field, which are interesting for studying transfer phenomena in flames.

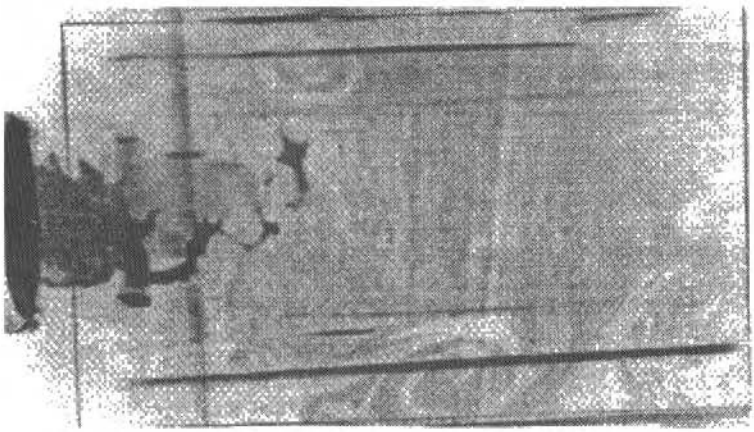

Fig. 2 Seeding particles of the 14,000 kcal/h burner (Paone, 1994)

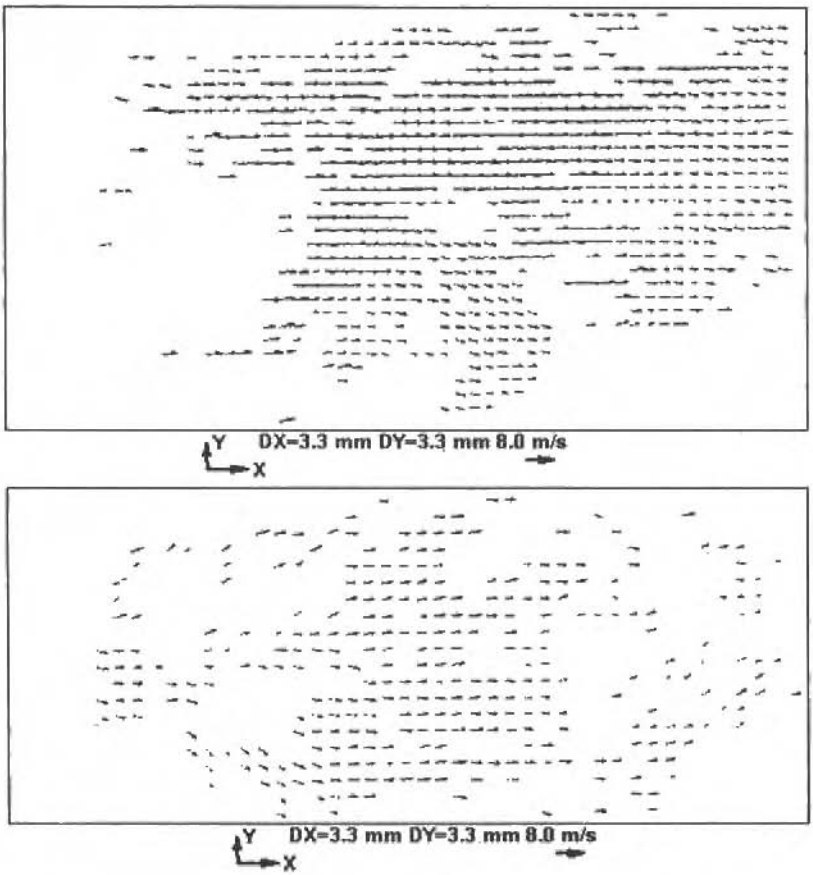

Fig. 3 Velocity fields obtained through PIV in a 14,000 kcal/h burner (Paone, 1994)

An important aspect of the PIV technique is the capability of measuring the whole motion field, limiting the duration of data acquisition to few moments. This peculiarity makes it very advantageous, even when the hourly cost of the experiment is extremely high, as in large wind tunnels. The PIV flowing application in large scale presents many difficulties in the acquisition of images in an area of more than 1 m^2. In (Castelini et al., 1994a), the application of the PIV technique to the measurement of a flow in a wind tunnel in full size scale 1:1, is illustrated on an area as large as up to 1.40 x 1.74 m2 and wind tunnel operating at 60 Km/h, using successfully both the photographic acquisition and the digital one. The results thus obtained, as illustrated in Fig. 4, show PIV potential for this kind of applications.

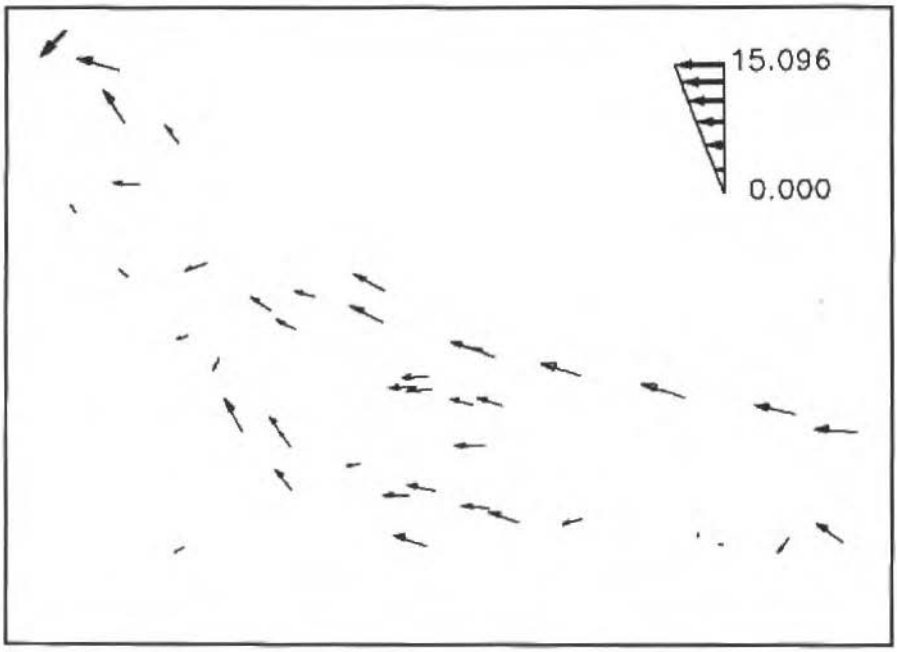

Fig. 4 Velocity field obtained in a full size scale automotive wind tunnel (Castellini et al., 1994a)

Doppler Global Velocimetry DGV

The Doppler Global Velocimetry technique represents an interesting development in laser velocimetry techniques; like PIV, it allows to measure velocity by analyzing images. It is therefore a measurement technique in which many vectors are measured on a field at the same time. The measurement principle (Meyers et al., 1991) is based on the direct observation of the wave length shifting of the radiation scattered by the moving particles within a fluid, due to the Doppler effect. The inseminated flow is illuminated by a laser light plane propagating in the i-direction and the scattered light is collected in the o direction by a CCD video camera. The particle scattered light is shifted by the Doppler effect:

$$\Delta\nu = \frac{\nu_0 (o - i) \bullet V}{c}$$

where ν is the frequency of the incident radiation, c is the speed of light, V is the velocity vector. The scalar product indicates that the Doppler shift is linked to the velocity vector component in the (o-i) direction, perpendicular to the bisecting line between o and i, as shown in Fig. 5; therefore, it contains

In these technique, it is necessary to resort to a laser source, since this guarantees highest levels of spectral purity of the incident radiation and an accurate placement of such radiation in the spectrum of the analysed gas. The fact that lasers can emit a varying frequency allows to optimize scattering phenomena in relation to the atomic characteristics of the chemical species in the fluid. The main advantage of these techniques is that they allow to measure many quantities characterizing flows which, otherwise, would be difficult to approach. These techniques have been particularly employed in the study of flames and in the process control both of products of combustion and of the reasons that have caused such products.

Laser Vibrometry

One of the major problems in Mechanics regards the measurement of motion and vibration of solids. In particular, the motion of an object can be thought of as obtained from the overlap of three components of macroscopic motion, either of the translatory or rotational kind, each with a superimposed component of vibratory motion.

The laser vibrometers of the interferometric type allow the measuring of a single component of velocity and of the surface shifting along the axis of the measure laser beam or, when tangential vibrometers are used, in the perpendicular direction. Their resolution and dynamics response guarantee the measurement of both the global and vibratory motion: as a result, it is sufficient, in the case of wide rigid motions, to follow the moving object with the measurement probe volume.

The development of laser vibrometers has been encouraged by two different sets of needs: on the one hand the need for higher accuracy, resolution and measurement range, which have been achieved by operating both on the optical configuration and the electronic section of the system. On the other hand new instruments have been developed to offer, although with an acceptable and foreseen reduction in performance, higher practicability, cost-effectiveness and therefore wider diffusion.

A further development in the compactedness of the instruments has been obtained with the introduction of laser diodes and fibre components. It has therefore become possible to separate the probe from the body of the vibrometer, thus allowing the acquisition of information on locations not easy to gain access to, or the differential measurements between objects which are not necessarily close. Finally, with the advent of integrated optics, it is now possible to obtain miniaturized instruments whose components are contained in a single chip. Together with this evolution in terms of components, new technique have been developed for the analysis of the signal.

Important applications have been made in diverse fields throughout the years, and in many cases the laser vibrometer has proved to be of vital importance, as for example in the vibration measurement in the automotive industry, the study of the dynamics in electro-mechanical components, the vibration measurement in the membrane of the ear-drum, the calibration and certification of transducers, the study of the interactions between fluids and their structure, to name only a few. Figure 6 shows the results of the measurement of motion of a value in an internal combustion engine. The solution of anomalous phenomena such as the bounce within the valve seat is also shown (Paone et al., 1994).

A recent development in laser vibrometry is represented by the scanning vibrometer; its probe is fitted with mobile mirrors which, when properly controlled, allow the measure beam to be place at several locations on the surface to analyse. In this way, measurements can be made either on grids or by following points in motion (Sriran et al., 1992).

This technique can be applied in laboratory tests and also in field tests, for example on hand-guided vibrating tools, vehicles, machines. Tests with sinusoidal vibrations up to 250 Hz have been performed on different subjects with their hand on three test devices, designed in accordance with ISO standards. An electrodynamic exciter was used as vibration source. Comparisons of simultaneous measurements, performed by the vibrometer and by the accelerometer installed on the vibrating devices, in accordance with ISO standards, have been used to verify the measurement technique.

information on a component of the velocity. To observe such a frequency shift, this technique uses a filter, whose transmissivity varies with the frequency of the radiation passing through it. Thus, an observer viewing a field with moving particles sees the luminosity of the particles increase or decrease, in relation to the motion direction and to the modules of the velocity vector, linked to the Doppler shift. Therefore, the light intensity becomes a measure of a component of velocity. The underlying principle is simple and it can be implemented by using an Argon ion laser ($\lambda = 514$ mm), a CCD video camera, a iodine cell used as a filter and a digital image acquisition system. By illuminating the field from three different directions, or by using three video cameras and only one light plane, it is possible to build systems for a tridimensional measurement of the velocity vector (Meyers et al., 1992). In fact, because of the variation of the quantity of light scattered by every single particle, it is necessary to use a second camera observing the field without any filter, so that the measuring video camera is normalized with that of the reference video camera.

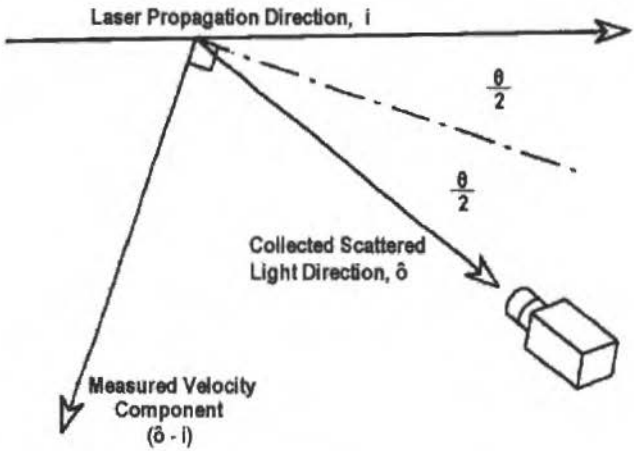

Fig. 5 Doppler Global Velocimetry: operating principle (Meyers and Komine, 1991)

This system developed by NASA has been successfully used in wind tunnels on complex, high velocity flows (100-250 m/s). Higher velocity applications are presently under study.

Unlike the PIV technique, Global Doppler Velocimetry has some important advantages, such as the possibility of working in real time, of having a completely digital measurement chain which allows automatization and, finally, of acquiring, simultaneously, the three velocity components.

Scalar Quantities Measurement

Measurement techniques based on the analysis of light scattered by the molecules of an analyzed gas illuminated by the laser radiation have been recently developed (Durão e Heitor, 1990; Eckbreth, 1988; Taylor, 1993).

Among the most used techniques are those based on elastic scattering of molecules (Rayleigh Scattering) for density, temperature and velocity measurement and those based on anelastic scattering (CARS, CSRS and IRS) for temperature, density, chemical species and velocity measurement.

In these techniques, the values of measured quantities have been deduced by the absorption and emission profile of the molecules of the analysed fluid. For example, concentration and partial pressure of a chemical species are deduced by the quantity of emission, whereas concentration of the species is deduced by the emission and absorption spectrum.

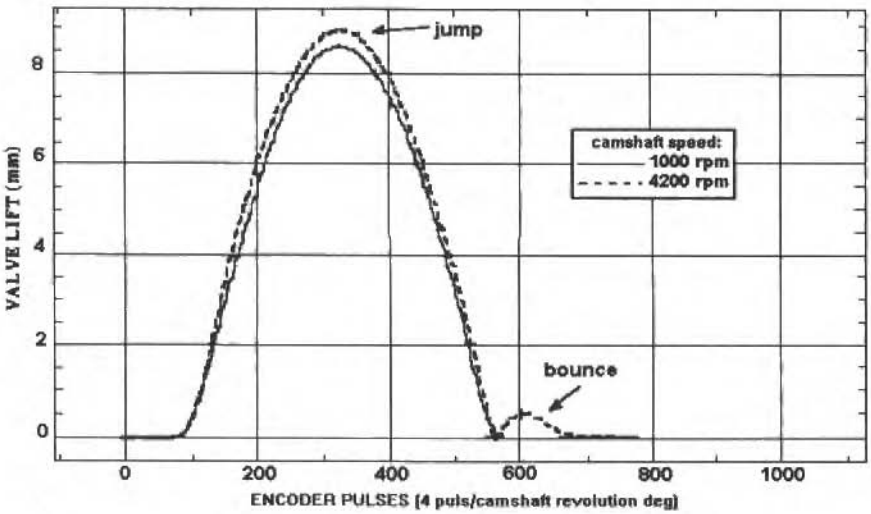

Fig. 6 Diagram representing the shifting of a valve obtained through laser vibrometer (Paone et al., 1994)

Further work has started in order to develop a measurement system for mapping the mechanical impedance function by using the scanning vibrometer and a force film sensor array. This technique has proved very powerful for analysing hand-arm dynamic characteristics on humans, and it also represents a step forward in the range of possible applications (Fig. 7) (Rossi and Tomasini, 1994).

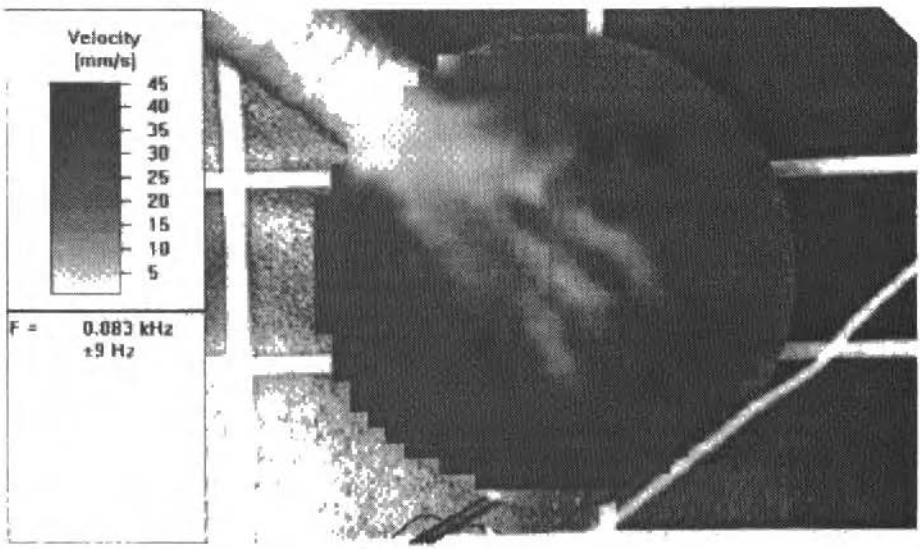

Fig. 7 Application of scanning laser vibrometry to the study of the human hand vibrations (Rossi and Tomasini, 1994)

As shown in Fig. 8, this technique can be used to detect damages of frescoes paintings.

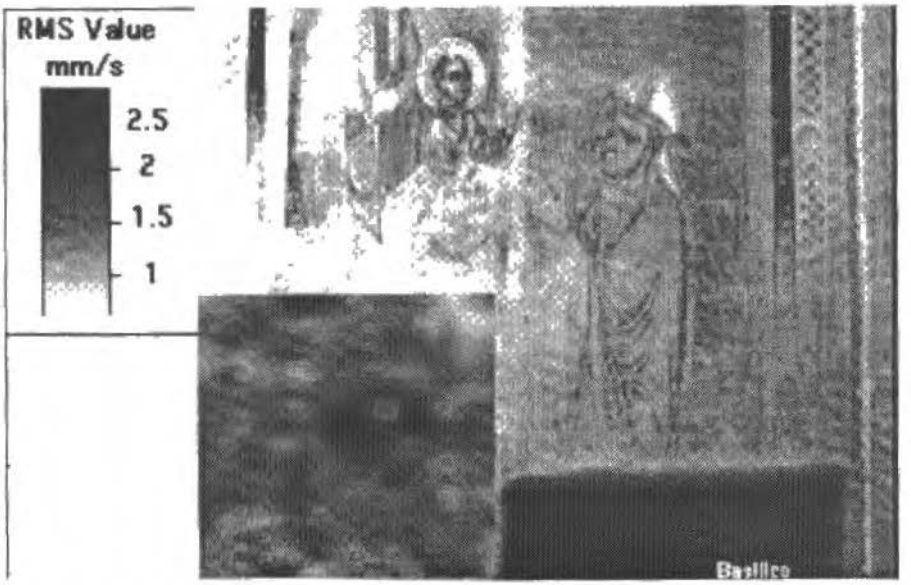

Fig. 8 Application of scanning laser vibrometry to the study of the detachments of the fresco surface Castellini et al., 1994b)

As part of a research by Dept. of Mechanics of Ancona University, experimental verification was carried out on a wall where detachments of the external layer from the inner substrate were artificially introduced. Impulse excitation showed that frequency response functions identify the presence of any damage. Laser beam scanning can therefore provide a way to remotely investigate large areas of paintings.

With a simple laser vibrometer, it is also possible to measure the angular velocity of shafts and, therefore, their torsional vibrations (lewin et al., 1994); when applied to a shaft, in fact, this instrument measures the tangential velocity component in the direction of its optical axis, which is a function of the angular velocity. Two parallel laser beams are generally used and they are located symmetrically to the rotation axis. In this way the measurement becomes insensitive to the radial motion of the shaft.

In order to measure the tangential motion of a surface, this being a major problem in the control of rolling mills, rotary presses, turbomachines etc., systems are now commercially available whose underlying principle is the same as the Doppler velocimeters in which the Doppler shifting is caused by the motion of the surface whose roughness represents a light scattering factor. These systems are highly valued in terms of measurement but their cost is still extremely high.

A valid alternative to the systems based on the Doppler effect is represented by correlation-based systems. In a fibre-optics system which has been developed at the Department of Mechanics of the University of Ancona (Massi, 1994), see Fig. 9, it is possible to measure tangential velocity and normal shift of surfaces at the same time. The operating principle is based on the modulation of the intensity of light scattered by three collimated laser beams, which is operated by the roughness of the surface itself. The velocity of the tangential translation is determined by operating the cross correlation between signals coming from perpendicular beams. The perpendicular shift to the surface is determined by the cross correlation between the signal coming from one of the two perpendicular beams, and the signal coming from the inclined beam. Nor being based on interferometric techniques, this system is advantageous both in terms of cost-effectiveness and in terms of ease of construction.

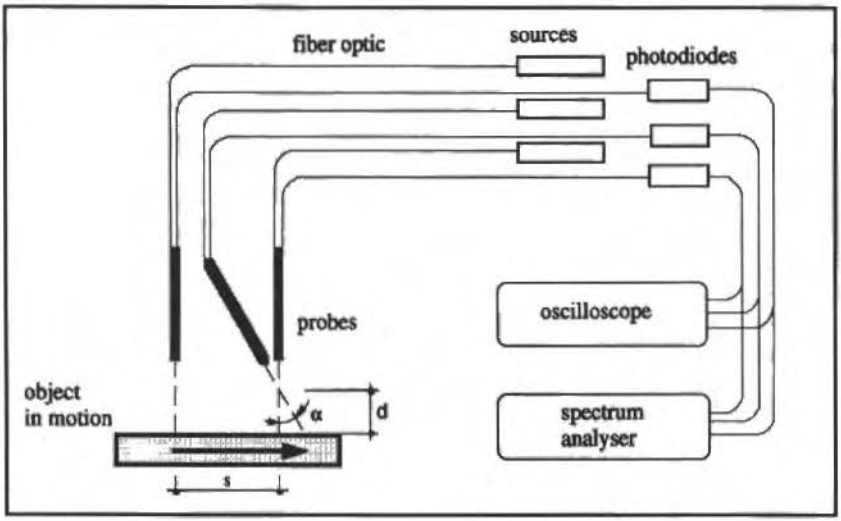

Fig. 9 Correlation technique for the measurement of tangential velocity and distance from a solid surface (Massi, 1994)

By resorting to laser systems it is also possible to develop measurement systems in diagnostic, especially for turbomachines; at the Department of Mechanics of the University of Ancona a technique has been developed for the measurement of rotating blade vibration in operating turbomachines (Nava et al., 1994).

In this kind of application, the object under study is moved by rigid motion at a considerable velocity and it is also animated by a vibratory motion in the same direction.

The system is based on the measurement of the time which elapses between two rotations of a rotating blade before two observators consisting of proximity pickups without contact with the surface. If the rotating blade was infinitely rigid, the measured time would only depend on the angular velocity of the rotor. But a real blade, having a limited rigidity, will vibrate as a result of inertial and fluid-dynamic stresses. The blade, therefore, after having passed before the first observator, will reach the second one either earlier or later than what is expected by a rigid blade. The time elapsed between the two rotations before the two observators will thus differ from the time of rigid motion of a value which is proportional to the vibration deflection of the blade. Once the instantaneous velocity of the rotor is known, the deflection of the blade becomes known, too.

To realise such system, laser proximity pickups had to be used and, in particular, fibre-optics systems.

In fact, in the case of peripherical velocity values of 300 m/s and with vibration amplitudes of 0.05 mm, in order to have a resolution of around 5%, it is necessary to use observators with a bandwidth in the region of 100 - 120 MHz, which would be otherwise impossible with traditional sensors.

A description of this measurement system is given in Fig. 10. The laser source emits a beam which, through a fibre-optics system and a coupler, is taken to the two sensitive heads and focused on the top of the blades. As the rotating blade passes through, the light reflected by the surface is taken to the photo diode, where is converted into electric pulse. After processing, this signal provides the measure of the vibration. Such system is an example of how electro-optical technology can have successful applications in the diagnostics of industrial machines.

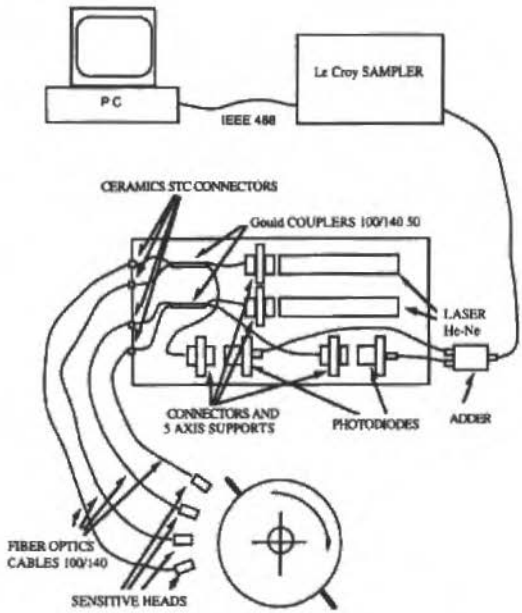

Fig. 10 Diagram showing the measurement system of vibrations of rotating blades in turbomachines (Nava et al., 1994)

Conclusions

Within the global field of mechanic measurements, laser measurement techniques offer the widest range of applications. However, their potential will not fully develop unless problems are tackled with a more open-minded approach, therefore not limited to a sectorial analysis. The need, thus, arises for a meeting ground where optics on one side and fluid or experimental mechanics on the other, can work together.

For its own nature, A.I.V.E.L.A. must be an autonomous body whose scope of interest and research is half way between optics and mechanics.

Considering the possibility of further development in the near future and the extreme vitality of the research and the market for this field, the need is felt for other initiatives which could promote the development and the diffusion of such techniques as those of laser measurement.

It was with this attitude that the First International Conference on "Vibration Measurements by Laser Techniques" was held in Ancona in October 1994. On this occasion, more than 120 researchers in the field of vibrometry, coming from 17 different countries, gathered to present and discuss their work. Either for economic or technical reasons, even more researchers who would have liked to participle were unable to attend the conference. Considering the success of this initiative and the possibility of extending the attendance, it was decided to hold the conference every two years.

The next Conference will take place in Ancona in September 1996. Until then, all possible efforts will be made to increase both the diffusion and the attendance to this event, also making use of specific financial support. The ALFA program, sponsored by the EEC, will especially help promoting co-operation and exchanges between Latin American countries and the EEC. Therefore, it is to be hoped that further possibilities of collaborative scientific research between Italy and Latin American countries, and in particular Brazil, will also develop.

Within the COBEM Congress, a special session will be held in December 1995, particularly devoted to the applications of those techniques described in this paper and supported by an exhibition of the most interesting equipment in this field.

Acknowledgement

The author wish to thank P. Castellini and N. Paone, from Ancona University, for the contribution in the preparation of this paper.

References

Castellini, P., Paone, N., and Tomasini and E.P.,1994a, "Applicazione della PIV a Grandi Flussi in Galleria del Vento Automobilistica Scala 1:1 (Application PIV to Large Flows in Full Size Scale Automotive Wind Tunnel)", 3o Conv. Naz.le Strum. e Metodi di Misura Elettrottici, 25-27 magio, Pavia.

Castellini, P., Paone, N., Tomasini, E.P., 1994b, "Application of a Laser Doppler Vibrometer to Non-Intrusive Diagnostic of Frescoes Damage", 1st Int. Conf. on Vibration Measurements by Laser Techniques: Advances and Applications", 3-5 October, Ancona, Italy.

Cenedese, A., Palmieri, G. and Romano, G.P., 1990, "Turbulent Intensity Evaluation with PIV", 5th Int. Symp. on spplic. of Laser Techniques to Fluid Mech., 5-7 July, Lisbon, Portugal.

Darin, L.E., 1980, "The Laser Doppler Technique", J. Whiley & Sons, New York.

Durão, D.F.G., and Heitor, M.V., 1990, "Modern Diagnostic Techniques for Combusting Flows: An Overview", from Combustion Flow Diagnostic, NATO ASI Series, Kluwer Academic Publishers.

Durst, F., Melling, A., and Whitelaw, J,H., 1976, "Principles and Practice of Laser Doppler Anemometry" Academic Press, London.

Eckbreth, A.C., 1988, "Laser Diagnostic for Combustion Temperature and Species", Abacus Press, Worcester.

Einav, S., 1993, "In Vivo Laser Anemometry Blood Flow System", in Laser Anemometry: Advances and Applications, Fifth International Conference, Koningshof, Veldhoven, 23-27 August, The Nederlands.

Humphreys, W.M., Rallo, R.A., Hunter, W.W., and Bartram, S.M., 1993, "Application of Particle Image Velocimetry to Mach 6 Flow" in Laser Anemometry:Advances and Applications, Fifth International Conference, Koningshof, Veldhoven, 23-27 August, The Nederlands.

Lewin, A.C., Roth, V., and Siegmund, G., 1994, "New concept for Interferometric Measurement of Rotational Vibrations", 1st Int. Conf. on Vibration Measurements by Laser Techniques: Advances and Applications", 3-5 October, Ancona, Italy.

Massi, O., 1994, "Simultaneous Measurement of Surface Tangential Velocity and Normal Displacement; Advantages of a New Fiber Optic Probe", 1st Int. Conf. on Vibration Measurements by Laser Techniques: Advances and Applications", 3-5 October, Ancona, Italy.

Meinhart, C.D., Barnhart, D.H., and Adrian, R.J., 1994, "A High-Speed Processing System for Holographic Particle Image Velocimetry", 7th Int. Symp. on Applic. of Laser Techniques to Fluid Mech., 11-14 July, Lisbon Portugal.

Meyers, J.F., and Komine, H., 1991, "Doppler Global Velocimetry: a New Way to Look at Velocity", ASME 4th Int. Conference on Laser Anemometry Advances and Applications, 5-9 August, Cleveland OH.

Meyers, J.F., Lee, J.W., and Cavone, A.A., 1992, "Three Component Doppler Global Velocimenter Measurements on the Flow above a Delta Wing", 6th Int. Symp. on Applic. of Laser Techniques to Fluids Mech., 20-23 July, Lisbon, Portugal.

Nava, P., Paone, N., Rossi, G.L., and Tomasini, E.P., July 1994, "Design and Experimental Characterisation of a Non-Instrusive Measurement System of a Rotating Blade Vibration", Journal of Engineering for Gas Turbines and Power, Vol. 116.

Paone, N., Santolini, C., and Tomasini, E.P., 1994, "Application of a Laser Doppler Vibrometer to Evaluate Engine Poppet Valve Kinematics", 12th Int. Modal Analysis Conf., 31 January-3 Febrary, Honolulu Hawaii.

Paone, N., 1994, "Velocity Measurements in Turbulent Premixed Flames by LDV and PIV", 7th Int. Symp. on Applic. of Laser Techniques to Fluid Mech., 11-14 July, Lisboa, Portugal.

Pinotti, M., Paone, N., and Tomasini, E.P., 1994, "Laser Doppler Velocimetry in a Centrifugal Ventricular Assist Device", 7th Int. Symp. on Applic. of Laser Techniques to Fluid Mech., 11-14 July, Lisboa, Portugal.

Pedrazzo, G., Rossi, G.L., Santolini, C., and Tomasini, E.P., 1994, "Vibration Measurements of the Human Body by the Laser Scanner Vibrometer", 12th Int. Modal Analysis Conf., 31 January-3 Febrary, Honolulu Hawaii.

Prasad, A.K., and Adrian, R.J., 1992, "Stereoscopic Particle Image Velocimetry Applied to Liquid Flows", 6th Int. Symp. on Applic. of Laser Techniques to Fluid Mech., 20-23 July, Lisboa, Portugal.

Raffel, M., and Kompenhans, J., 1993, "PIV Measurements of Unsteady Transonic Flow Field above a NACA 0012 Airfoil", in Laser Anemometry: Advances and Applications, Fifth International Conference, Koningshof, Veldhoven, 23-27 August, The Nederlands.

Rossi, G.L., and Tomasini, E.P., 1994, "Proposal of a New Measurement Techniques for Hand-Arm Vibration Analysis", 1st Int. Conf. on Vibration Measurements by Laser Techniques: Advances and Applications", Ancona, 3-5 October, Italy.

Royer, H., 1988, "Full 3-D Measurements: the Holographic Approach", in Lectures Series 1988-06, von Karman Institute for Fluid Dynamics, Brussels Belgium.

Schodl, R., 1986, "Laser Two-Focus Velocimetry", Advanced Instrumentation for Aero Engine Components, AGARD Conf. Preprint, No. 399.

Sriram, P., Hanagud, S.V., and Craig, J.I., 1992, "Scaning Laser Doppler Technique for Modal Testing of Distributed-Parameter System", AIAA Journal, Vol. 30, No. 3, pp. 765-766.

Taylor, A.M.K.P., 1993, "Instrumentation for Flows with Combustion", Academic Press, London.

Tomasini, E.P., and Savant Aira, G., 1993, "La Sensoristica Elettroottica nel Controllo dei Processi Industriali (Electro-Optical Sensor Systems in the Control of Industrial Processes)" in Convegno del PFTEO.

RBCM - J. of the Braz. Soc. Mechanical Sciences
Vol. XVII - nº 1- 1995 - pp. 14-25

ISSN 0100-7386
Printed in Brazil

Simulação Numérica da Redistribuição de Escoamentos Bifásicos entre Passes de um Trocador de Calor

Numerical Simulation of the Two-Phase Flow Redistribution Between Two Passes of a Heat Exchanger

Luiz Felipe M. Moura
Antonio José C. Rego
José Rubens Avancini
Departamento de Engenharia Térmica e de Fluidos
Faculdade de Engenharia Mecânica
Universidade Estadual de Campinas
Tel. (0192) 39-8415 Fax. (0192) 39-3722
Caixa Postal 122 - Campinas - 13081 - SP - Brazil

Abstract

This work deals with the numerical simulation of the two-phase flow distribution inside a common header placed between two passes of a shell-and-tube heat exchanger. The Numerical results have been obtained from a computer code based on the two-dimensional two-fluid model. The interfacial momentum transfer was modeled as a function of the flow patterns observed in the heat exchanger common header. The influence of the total mass flow rate and the mixture quality (the inlet flow conditions) on the phase distributions at the common header outlet were investigated. The numerical simulations of the two-phase flow distribution inside the common header were compared qualitatively with other numerical and experimental results, showing the capability of the proposed model.
Keywords: Two-Phase Flow, Numerical Simulation, Two-Fluid Model, Heat Exchanger.

Resumo

A redistribuição das fases de um escoamento bifásico dentro de uma caixa de retorno, localizada entre dois passes de um trocador de calor, foi estudada numericamente. As simulações numéricas foram realizadas utilizando-se um programa computacional baseado no modelo de dois fluidos. Um modelo de transferência interfacial de quantidade de movimento foi desenvolvido a partir dos padrões de escoamento existentes na caixa de retorno do trocador de calor. Foram investigados os efeitos da vazão mássica total e do título da mistura, ou seja, das condições de entrada do escoamento, na distribuição das fases na saída da caixa de retorno. Os resultados das simulações numéricas foram comparados qualitativamente com outros resultados numéricos e com alguns resultados experimentais, mostrando a validade do modelo proposto.
Palavras-chave: Escoamento Bifásico, Simulação Numérica, Modelo de Dois Fluidos, Trocador de Calor.

Introdução

Em várias instalações industriais, tais como refinarias de petróleo, indústrias químicas e termoelétricas, é comum a utilização de trocadores de calor. Muitas vezes, nestes trocadores de calor ocorrem escoamentos bifásicos gás-líquido. A previsão adequada do comportamento destes escoamentos, em algumas regiões do trocador de calor, pode facilitar o projeto ou a operação e a manutenção destes equipamentos.

No presente trabalho será apresentado um estudo numérico de escoamentos bifásicos gás-líquido em uma caixa de retorno localizada entre dois passes de um trocador de calor. A distribuição das fases na saída da caixa de retorno é de fundamental importância para a avaliação das trocas térmicas no segundo passe do trocador de calor. Um estudo realizado por Mueller e Chiou (1988) descreve os efeitos da distribuição irregular do escoamento no coeficiente global de transferência de calor em equipamentos térmicos.

Poucos trabalhos foram publicados sobre a análise da distribuição de escoamentos bifásicos em trocadores de calor. A maioria deles aborda o problema da distribuição do escoamento em redes de tubos conectados em paralelo, como por exemplo o trabalho de Kubo e Ueda (1973). Por outro lado,

Manuscript received: October 1993. Technical Editor: Carlos Alberto Carrasco Altermani

existem vários trabalhos disponíveis sobre a distribuição de escoamentos bifásicos em tês. O trabalho de Hwang, Soliman e Lahey (1988) apresenta uma excelente revisão bibliográfica sobre o estudo da separação de escoamentos bifásicos em tês.

As simulações numéricas do escoamento bifásico na caixa de retorno de um trocador de calor foram realizadas a partir de um programa computacional baseado no modelo de dois fluidos. Foram estudadas diferentes condições de entrada do escoamento na caixa de retorno de modo a caracterizar a distribuição das fases nestas geometrias.

Modelo Teórico

O modelamento teórico do escoamento bifásico em caixas de retorno de trocadores de calor é uma tarefa bastante complexa, devido à interação dinâmica entre as fases. Para este tipo de escoamento é utilizado o modelo de dois fluidos, que é descrito por um conjunto de equações de conservação para cada fase, além das equações de transporte através das interfaces.

O modelo de dois fluidos consiste em um tratamento rigoroso do escoamento bifásico através de uma formulação local e instantânea. Esta formulação pode ser simplificada através de um processo de média no tempo, conforme o procedimento apresentado em Ishii (1975).

Neste trabalho foram adotadas algumas hipóteses simplificadoras de modo a possibilitar uma solução numérica das equações que formam o modelo de dois fluidos:

- Escoamento bidimensional no plano de simetria;
- Escoamento isotérmico e sem transferência de massa;
- Equilíbrio local de pressão entre as fases, e
- Difusão turbulenta desprezível.

O conjunto de equações de balanço do modelo de dois fluidos (Ishii, 1975), quando simplificado através das hipóteses descritas acima, pode ser escrito da seguinte forma:

Balanço de massa do líquido:

$$\frac{\partial}{\partial t}(\alpha_l \rho_l) + \frac{\partial}{\partial x}(\alpha_l \rho_l u_l) + \frac{\partial}{\partial y}(\alpha_l \rho_l v_l) = 0 \qquad (1)$$

Balanço de massa do gás:

$$\frac{\partial}{\partial t}(\alpha_g \rho_g) + \frac{\partial}{\partial x}(\alpha_g \rho_g u_g) + \frac{\partial}{\partial y}(\alpha_g \rho_g v_g) = 0 \qquad (2)$$

Balanço de quantidade de movimento de líquido na direção x:

$$\frac{\partial}{\partial t}(\alpha_l \rho_l u_l) + \frac{\partial}{\partial x}(\alpha_l \rho_l u_l^2) + \frac{\partial}{\partial y}(\alpha_l \rho_l u_l v_l) = -\alpha_l \frac{\partial P}{\partial x} + \alpha_l \rho_l g_x + K_{lg}(u_g - u_l) + \mu_l \left[\frac{\partial}{\partial x}\left(\alpha_l \frac{\partial u_l}{\partial x} \right) + \frac{\partial}{\partial y}\left(\alpha_l \frac{\partial u_l}{\partial y} \right) \right] \qquad (3)$$

Balanço de quantidade de movimento de gás na direção x:

$$\frac{\partial}{\partial t}(\alpha_g \rho_g u_g) + \frac{\partial}{\partial x}(\alpha_g \rho_g v_g^2) + \frac{\partial}{\partial y}(\alpha_g \rho_g u_g v_g) = -\alpha_g \frac{\partial P}{\partial x} + \alpha_g \rho_g g_x + K_{lg}(u_l - u_g) + \mu_g \left[\frac{\partial}{\partial x}\left(\alpha_g \frac{\partial u_g}{\partial x} \right) + \frac{\partial}{\partial y}\left(\alpha_g \frac{\partial u_g}{\partial y} \right) \right] \qquad (4)$$

Balanço de quantidade de movimento de líquido na direção y:

$$\frac{\partial}{\partial t}(\alpha_l \rho_l v_l) + \frac{\partial}{\partial x}(\alpha_l \rho_l u_l v_l) + \frac{\partial}{\partial y}(\alpha_l \rho_l v_l^2) = -\alpha_l \frac{\partial P}{\partial y} + \alpha_l \rho_l g_y$$
$$+ K_{lg}(v_g - v_l) + \mu_l \left[\frac{\partial}{\partial x}\left(\alpha_l \frac{\partial v_l}{\partial x}\right) + \frac{\partial}{\partial y}\left(\alpha_l \frac{\partial v_l}{\partial y}\right)\right] \quad (5)$$

Balanço de quantidade de movimento de gás na direção y:

$$\frac{\partial}{\partial t}(\alpha_g \rho_g v_g) + \frac{\partial}{\partial x}(\alpha_g \rho_g u_g v_g) + \frac{\partial}{\partial y}(\alpha_g \rho_g v_g^2) = -\alpha_g \frac{\partial P}{\partial y} + \alpha_g \rho_g g_y$$
$$+ K_{lg}(v_l - v_g) + \mu_g \left[\frac{\partial}{\partial x}\left(\alpha_g \frac{\partial v_g}{\partial x}\right) + \frac{\partial}{\partial y}\left(\alpha_g \frac{\partial v_g}{\partial y}\right)\right] \quad (6)$$

onde:

- l = líquido
- g = gás
- P = pressão
- u = velocidade na direção x
- v = velocidade na direção y
- α = fração de vazio
- ρ = densidade
- g = gravidade
- K_{gl} = coeficiente de atrito interfacial

Este sistema de seis equações contém nove variáveis dependentes. São necessárias, portanto, três relações adicionais:

$$\alpha_l + \alpha_g = 1 \quad (7)$$

$$\rho_l = f(P) \quad (8)$$

$$\rho_g = f(P) \quad (9)$$

Apesar da formulação adotada no modelo matemático ser restrita à escoamentos incompressíveis, é possível calcular as densidades das fases (principalmente a densidade do gás) em função das variações de pressão no interior do domínio.

A solução deste conjunto de equações depende de uma equação constitutiva para o coeficiente de atrito interfacial. Avaliar corretamente este termo é de extrema importância para obter uma solução consistente para o modelo de dois fluidos. Para o caso de escoamentos dispersos (bolhas, gotas ou intermitente), Ishii e Zuber (1979) propuseram a seguinte correlação para o atrito interfacial:

$$K_{lg} = \frac{1}{8} a_i C_D \rho_c |V_r| \quad (10)$$

onde:

a_i = área interfacial

C_D = coeficiente de arrasto

ρ_c = densidade da fase contínua

V_r = velocidade relativa

O coeficiente de arrasto foi desenvolvido por Ishii e Michima (1984) para diferentes padrões de escoamento bifásico em tubos verticais, como por exemplo: a bolhas ou gotas, pistonado e agitante.

O escoamento bifásico em uma caixa de retorno de um trocador de calor geralmente apresenta uma distribuição espacial das interfaces bem mais complexa comparada à distribuição das fases em um tubo reto. A existência de regiões muito ricas em líquido (filmes líquidos) e de regiões de grande concentração de gás dificulta a utilização dos modelos existentes para o coeficiente de arrasto de escoamentos dispersos (a bolha ou a gota) em tubos retos. Neste trabalho foi empregada uma forma alternativa da Eq. (10) do atrito interfacial.

Tendo em vista a necessidade de que a expressão para o atrito interfacial seja contínua e válida em toda a faixa de vazio, a densidade da fase contínua foi substituída pela densidade da mistura:

$$\rho_m = \alpha\rho_g + (1-\alpha)\rho_l \tag{11}$$

Foi também considerado que a área interfacial e o coeficiente de arrasto dependem somente da fração de vazio. Considerando que a área interfacial deve tender a zero quando a fração volumétrica de uma das fases tende para zero, adotamos a seguinte função:

$$\alpha_i C_D = C\alpha(1-\alpha) \tag{12}$$

Desta forma obtemos a seguinte expressão para o coeficiente de atrito interfacial:

$$K_{lg} = C\alpha(1-\alpha)\rho_m|V_r| \tag{13}$$

De acordo com os resultados de simulações numéricas de escoamentos bifásicos em entroncamentos (tês) de tubulações realizadas por Carneiro (1991), o valor da constante C, da Eq. (13) para o atrito interfacial, deve ser da ordem de 400 m^{-1}. Embora a geometria de caixa de retorno seja diferente da geometria dos tês, o mesmo valor da constante foi empregado neste trabalho como uma primeira aproximação. Espera-se, no futuro, realizar simulações numéricas com diferentes valores para esta constante e comparar os resultados com os resultados experimentais disponíveis.

Modelo Numérico

As equações que formam o modelo teórico descrito acima foram resolvidas pelo método de volumes finitos, utilizando-se o conceito de malhas entrelaçadas descrito por Patankar (1981). Esta técnica consiste em integrar as equações de balanço de massa em volumes de controle centrados nos pontos onde estão definidas as variáveis escalares (pressão, fração de vazio e densidade), e tendo as componentes da velocidade definidas nas faces deste volume de controle. As equações de balanço de quantidade de movimento são integradas ao longo de volumes de controle deslocados em relação aos volumes anteriores, de modo que a componente da velocidade encontra-se no centro e as variáveis escalares estão localizadas nas faces deste volume de controle.

A principal dificuldade na solução simultânea das equações discretizadas resulta do acoplamento entre as equações de quantidade de movimento das duas fases, que ocorre devido ao termo de atrito interfacial. O algoritmo utilizado neste trabalho e semi-implícito, ou seja, o gradiente de

pressão e o atrito interfacial são calculados implicitamente e os termos convectivo e difusivo são calculados explicitamente. O problema é reduzido a um sistema de equações algébricas para os incrementos de pressão em cada volume.

Uma descrição detalhada do algoritmo numérico foi apresentada anteriormente, Moura (1991), de modo que apenas as principais etapas serão discutidas a seguir.

Inicialmente, as equações de quantidade de movimento são transformadas em uma forma não conservativa. A equação de balanço de massa do líquido é multiplicada pelas componentes da velocidade do líquido nas direções x e y, e as equações resultantes são subtraídas das equações de quantidade de movimento do líquido nas direções x e y, respectivamente. As equações de quantidade de movimento do gás, na forma não conservativa, são obtidas seguindo o mesmo procedimento.

As equações de balanço de massa do líquido e do gás são integradas ao longo dos volumes centrados nas variáveis escalares. Os valores das variáveis escalares nas faces do volume são avaliados pelo método donor-cell, que consiste em usar o valor da variável no centro do volume mais próximo da face seguindo a direção do escoamento.

As equações não conservativas de quantidade de movimento do líquido e do gás, em ambas direções, são integradas ao longo de volumes centrados nas componentes das velocidades.

Os termos convectivo e difusivo são calculados explicitamente, ou seja, a partir dos valores das variáveis no passo de tempo anterior. Este procedimento implica em uma limitação do passo de tempo determinada pela condição de Courant. De acordo com esta condição, a distância percorrida por uma partícula fluida em uma determinada direção, durante um passo de tempo, deve ser menor que o comprimento do volume de controle nesta mesma direção.

As equações discretizadas da quantidade de movimento do líquido são reescritas de modo a explicitar a velocidade do gás (termo de atrito interfacial). Seguindo o mesmo procedimento é possível isolar a velocidade do líquido nas equações de quantidade de movimento de gás. Em seguida, as velocidades do líquido e do gás são eliminadas das equações de quantidade de movimento do gás e do líquido, respectivamente.

Finalmente, as equações de balanço de massa e de quantidade de movimento do líquido são combinadas, resultando em uma equação para a pressão e a fração volumétrica do líquido. Do mesmo modo é obtida umaequação envolvendo a pressão e a fração volumétrica do gás (fração de vazio). Estas equações podem ser resolvidas pelo método iterativo de Newton, gerando equações para os incrementos de pressão e de fração volumétrica de cada fase. Como os incrementos de fração volumétrica das duas fases são iguais e de sinais opostos, torna-se possível combinar estas duas equações obtendo uma única equação para o incremento de pressão em cada malha.

O sistema de equações para os incrementos de pressão relaciona a variação da pressão em cada malha com as variações de pressão nas quatro malhas vizinhas. Este sistema matricial pode ser resolvido por um método iterativo para matrizes tri-diagonais (TDMA). Uma vez calculado o novo campo de pressão, é possível voltar às equações de balanço de massa e de quantidade de movimento para calcular a fração de vazio e as componentes da velocidade de cada fase. Caso os balanços de massa em todos os volumes de controle não satisfaçam um determinado valor (critério de convergência), resolve-se novamente o sistema de equações para os incrementos de pressão, com os coeficientes da matriz atualizados.

Resultados Numéricos

Os resultados das simulações numéricas do escoamento bifásico em uma caixa de retorno de um trocador de calor foram obtidos através do programa TOFLU-2D (Two-Dimensional Two-Fluid Computer Code), descrito detalhadamente em Moura e Rezkallah (1991).

A geometria estudada é apresentada na Fig. 1. Esta geometria representa o plano de simetria da caixa de retorno de um trocador de calor com placas planas. Foi utilizada uma malha uniforme (20x40) com 800 elementos de 1 cm x 1 cm.

O escoamento ar-água entra na caixa de retorno pela metade inferior da face esquerda do domínio discretizado e sai pela metade superior desta mesma face. As condições de contorno na entrada são valores especificados para a fração de vazio e para a velocidade de cada fase. Na saída, as

condições de contorno se resumem a um valor especificado da pressão. Nas outras faces, formadas por paredes impermeáveis, prevalece a condição de contorno de não deslizamento.

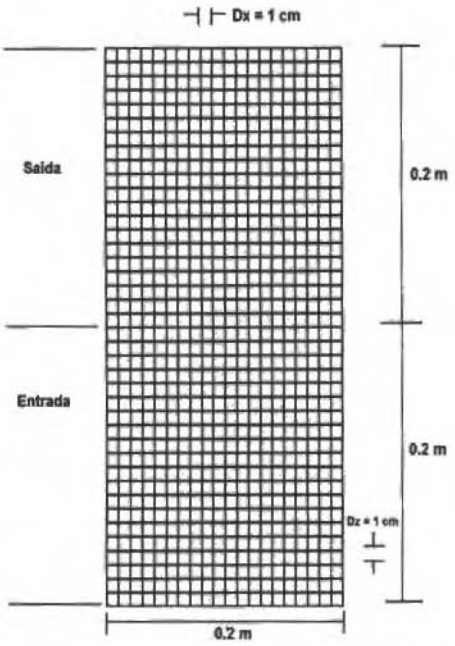

Fig. 1 Esquema da malha (20x40) utilizada

Foram estudadas nove condições de contorno na entrada da caixa de retorno, representando diferentes combinações de velocidade superficial do líquido e do gás. A Tabela 1 resume as condições de contorno utilizadas. Na saída da caixa de retorno foi especificada uma condição de contorno de pressão constante e igual à pressão atmosférica. A velocidade e a fração de vazio na entrada foram calculadas a partir dos valores especificados de velocidade superficial do líquido e do gás (distribuição uniforme), usando-se as relações do modelo homogêneo (Ishii, 1975).

$$V_m = J_l + J_g \tag{14}$$

$$\alpha = \frac{1}{1 + \frac{J_l}{J_g}} \tag{15}$$

Na última coluna da Tabela 1 foi incluído o número de Froude, determinado a partir da seguinte expressão:

$$Fr = \frac{V_m}{\sqrt{gl}} \tag{16}$$

onde l é a largura (0,2 m) da caixa de retorno.

Tabela 1 Condições de contorno na entrada

Cond. Cont	J_l	J_g	V_m	α	Fr
1	0,5	0,5	1,0	0,500	0,71
2	1,0	0,2	1,2	0,167	0,86
3	5,0	0,2	5,2	0,038	3,71
4	0,2	1,0	1,2	0,833	0,86
5	1,0	1,0	2,0	0,500	1,43
6	5,0	1,0	6,0	0,167	4,28
7	0,2	5,0	5,2	0,962	3,71
8	1,0	5,0	6,0	0,833	4,28
9	5,0	5,0	10,0	0,500	7,14

As condições de contorno descritas acima foram representadas no mapa de padrão de escoamento bifásico horizontal de Mandhane et al. (1974), de modo a facilitar a identificação de cada condição de escoamento na entrada da caixa de retorno. A Fig. 2 mostra este mapa com as condições de contorno.

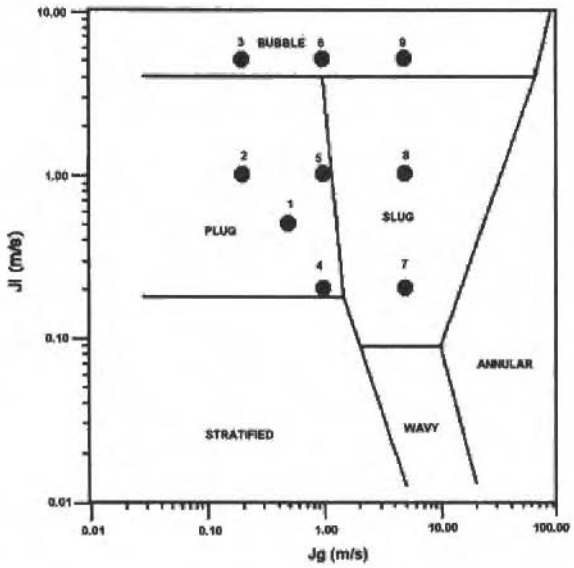

Fig. 2 Condições de contorno na entrada

As simulações numéricas foram realizadas a partir de condições iniciais arbitrárias, escolhidas com o único objetivo de diminuir o tempo necessário para atingir um estado de escoamento permanente.

Para cada condição de contorno foram calculados os campos de velocidade do líquido e do gás, de fração de vazio e de pressão. A partir dos perfis de velocidade e de fração de vazio foram determinadas as distribuições de vazão de líquido e de gás na secção de saída da caixa de retorno. Cabe lembrar que a distribuição de vazão na saída da caixa de retorno, ou na entrada do segundo passe do trocador de calor, é de fundamental importância para a avaliação do desempenho térmico do equipamento.

Nas Figs. 3 a 5 são apresentados, respectivamente, o campo de fração de vazio, o campo de velocidades do líquido e a distribuição de vazões na saída, para a condição de contorno 1. Pode-se observar uma forte tendência de acumulação da fase líquida na região próxima da parede vertical da caixa de retorno. Esta região apresenta também valores mais baixos de velocidade do líquido (e também do gás), indicando a existência de uma região preferencial do escoamento próxima do centro do domínio

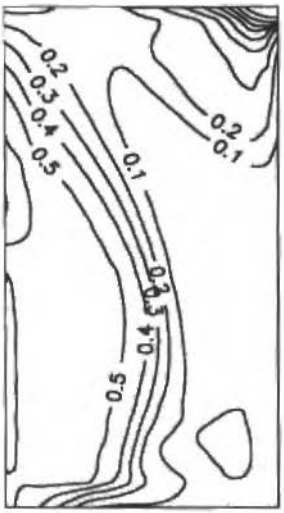

Fig. 3 Campo de fração de vazio para condição de entrada 1

A distribuição de vazões na saída mostra uma tendência do líquido em deixar a caixa de retorno pela parte superior da secção de saída. Esta tendência é mais ou menos pronunciada em função da relação entre as forças de inércia e gravitacional (número de Froude), conforme será discutido mais adiante. Cabe ainda destacar que a distribuição da vazão da mistura líquido-gás na saída não é uniforme, indicando uma influência da condição de contorno (pressão constante) na saída.

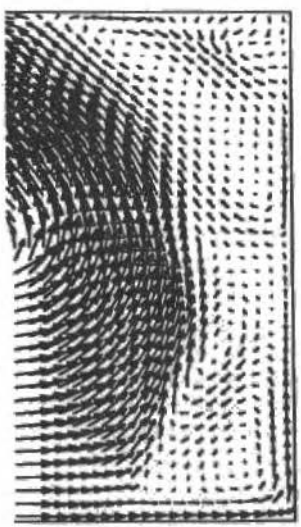

Fig. 4 Campo de velocidades de líquido para condição de entrada 1

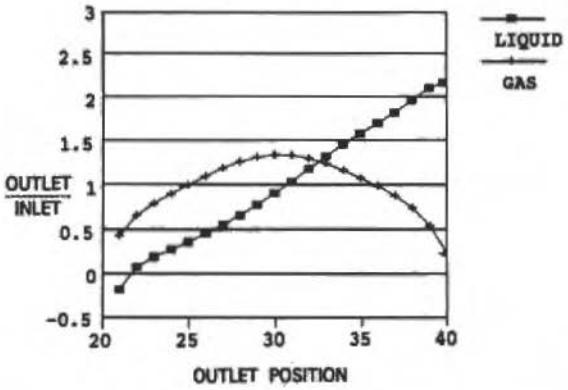

Fig. 5 Distribuição de vazões na saída para condição de entrada 1

A partir de uma análise cuidadosa dos resultados obtidos para as nove condições de contorno na entrada, descritas na Tabela 1, foi possível identificar algumas características comuns e definir três grupos distintos de escoamento bifásico em caixa de retorno de trocador de calor, conforme mostra a Tabela 2.

Tabela 2 Padrões de escoamento bifásico na caixa de retorno

Grupo	Cond. Cont.	Fr	J_L
A	3	3,71	5,0
	6	4,28	5,0
	9	7,14	5,0
B	1	0,71	0,5
	2	0,86	1,0
	4	0,86	0,2
	5	1,43	1,0
C	7	3,71	0,2
	8	4,28	1,0

A partir dos dados apresentados na Tabela 2 podemos caracterizar os três grupos da seguinte forma:

- Grupo A: número de Froude elevado (Fr > 3) e velocidade superficial do líquido elevada (J_L= 5m/s).
- Grupo B: número de Froude baixo (Fr < 2) e velocidade superficial do líquido baixa (J_L<1m/s).
- Grupo C: número de Froude elevado (Fr >3) e velocidade superficial do líquido baixa (J_L<1m/s).

Analisando-se o grupo A, observamos uma separação das fases logo após a entrada na caixa de retorno. Devido à diferença de inércia entre as fases, o líquido escoa principalmente na região mais externa da caixa de retorno, sendo que o gás ocupa quase toda a região central. As vazões tanto do líquido quanto do gás nas malhas de saída são relativamente próximas das vazões médias, com uma pequena tendência para uma maior vazão de líquido nas malhas localizadas na parte superior da secção de saída. Pode-se ainda observar que, apesar da relativa separação das fases, a distribuição de velocidades de ambas fases é bastante uniforme ao longo do domínio.

O grupo B pode ser caracterizado por uma influência maior da força gravitacional. A fase líquida continua sofrendo uma separação devido à diferença de inércia entre as fases. Porém, ao atingir a parte superior da caixa de retorno, a fração do escoamento mais rica em líquido apresenta uma tendência a descer em direção à região central da secção de saída (Fig. 3). Em conseqüência, ocorre uma maior vazão de líquido nas malhas centrais da secção de saída. O campo de velocidades também é

alterado devido à acumulação de líquido perto da parede vertical da caixa de retorno. Na Fig. 4 pode-se observar a existência de algumas regiões de recirculação ou de estagnação do escoamento, coincidindo com as regiões mais ricas em líquido.

Finalmente, o grupo C corresponde às condições de contorno com valores altos da velocidade da mistura e da fração de vazio. A pequena quantidade de líquido presente no escoamento é separada do gás, formando um filme líquido delgado que escoa junto à parede vertical. Devido à presença do escoamento do gás com alta velocidade na região central da caixa, este filme líquido continua escoando junto à parede superior e deixa a caixa de retorno ocupando apenas uma ou duas malhas da secção de saída. A distribuição de vazões na saída da caixa de retorno é muito irregular, sendo que praticamente toda a vazão de líquido escoa pelas últimas malhas de saída.

A Fig. 6 mostra o mapa de padrão de escoamento bifásico que contém os três grupos descritos anteriormente. As linhas separando os diferentes grupos foram traçadas apenas levando-se em conta as condições de contorno analisadas, sem a pretensão de identificar as transições entre os grupos.

Os resultados numéricos obtidos neste trabalho foram comparados qualitativamente com os resultados numéricos obtidos por Khan et al. (1992). Apesar dos resultados mencionados terem sido obtidos para uma caixa de retorno quadrada (40 cm x 40 cm) e com outra equação constitutiva para o atrito interfacial, observou-se que para uma mesma condição de entrada, os campos de fração de vazio e de velocidades são semelhantes. A Fig. 7 reproduz os resultados numéricos obtidos por Khan et al. (1992) para o campo de velocidades do líquido e de fração de vazio (condição de entrada igual à condição 1).

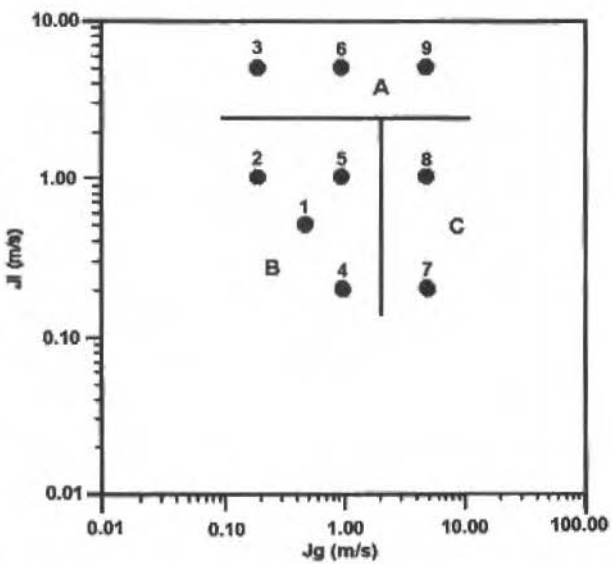

Fig. 6 Mapa de padrão de escoamento em caixa de retorno

Foram feitas também comparações com resultados experimentais obtidos por Moura (1989). Neste caso, apesar das dimensões da caixa de retorno serem iguais (20 cm x 40 cm), as condições de contorno são diferentes. Os resultados experimentais disponíveis correspondem às condições de entrada próximas do grupo B, porém com velocidades superficiais do líquido menores. Os resultados numéricos apresentam as mesmas tendências de separação das fases na caixa de retorno, apesar da distribuição de vazões na saída ser relativamente diferente. Para as condições de entrada impostas nos testes experimentais (velocidades superficiais mais baixas), observou-se uma tendência do líquido em escoar pela parte central da secção de saída, provavelmente devido à maior influência da força gravitacional.

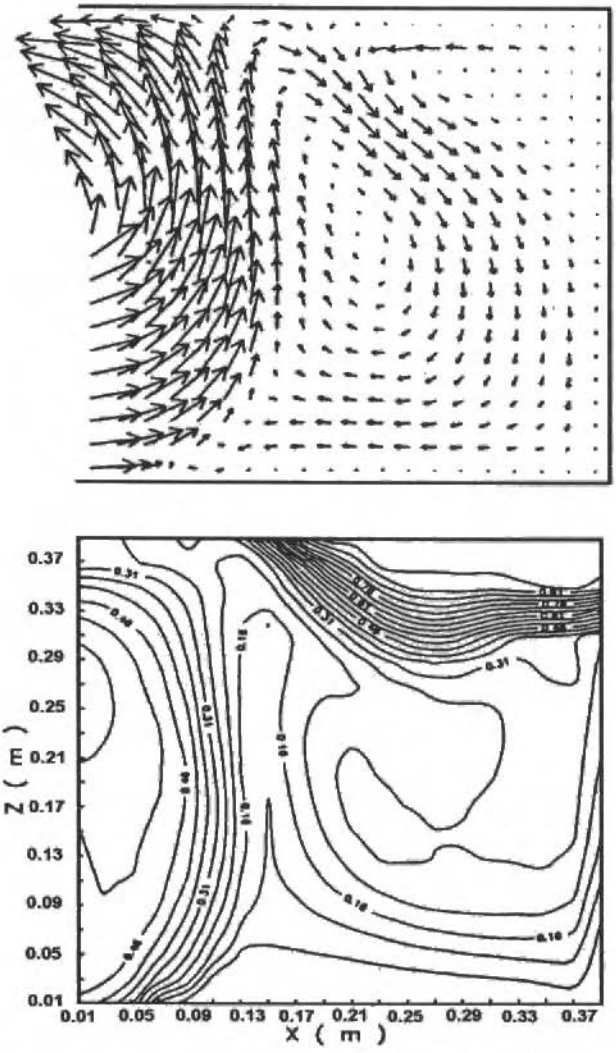

Fig. 7 Campo de velocidades do líquido e de fração de vazio obtidos por Khan et al. (1992)

Conclusões

A distribuição de escoamentos bifásicos gás-líquido em caixas de retorno de trocadores de calor pode ser estudada numericamente através do modelo de dois fluidos. A qualidade dos resultados numéricos depende, em grande parte, da equação constitutiva para o atrito interfacial. É de fundamental importância para a solução numérica que a expressão do coeficiente de atrito interfacial seja contínua e válida em toda a faixa de valores da fração de vazio. Neste trabalho foi proposta uma expressão que atende estas necessidades, mas que depende do ajuste de uma constante.

Foram estudadas diferentes condições de entrada do escoamento bifásico na caixa de retorno, de modo a investigar a influência das forças de inércia e gravitacional. A partir de uma análise dos resultados numéricos de distribuição de velocidade de cada fase, da fração de vazio e da vazão de cada fase na saída, foi possível dividir as condições de contorno em três grupos, gerando assim um mapa de padrao de escoamento bifásico em caixas de retorno de trocadores de calor.

Do ponto de vista do desempenho térmico de trocadores de calor do tipo casco e tubo com vários passes, é fortemente recomendável que a distribuição das fases, após cada caixa de retorno, seja a mais uniforme possível. Neste sentido, recomenda-se que as condições de entrada na caixa de retorno estejam situadas dentro do grupo B, conforme a Fig. 6. Isto seria possível, se o número de tubos de cada passe for calculado para garantir as velocidades superficiais desejadas.

Nomenclatura

a_i = Concentração de área interfacial - 1/m
C_D = Coeficiente de arrasto - adimensional
C = Constante - 1/m
Fr = Número de Froude - adimensional
g = Aceleração gravitacional - m/s^2
J = Velocidade superficial - m/s
K_{gl} = Coeficiente de atrito interfacial - $N.s/m^4$
ι = Largura da caixa de retorno - m
P = Pressão - N/m^2
u = Componente da velocidade na direção x m/s
v = Componente da velocidade na direção z m/s
V = Velocidade - m/s
α = Fração volumétrica - adimensional
ρ = Densidade - Kg/m^3
μ = Viscosidade - $N.s/m^2$

Indices

c = Fase contínua
g = Gás
l = Líquido
m = Mistura
r = Relativa entre as fases

Referências

Carneiro, F.A.S., 1991, "Simulação Numérica da Separação de um Escoamento Bifásico Gás-Líquido em um Tê", M.Sc. Thesis, Universidade Estadual de Campinas, Brazil.

Hwang, S.T., Soliman, H.M. and Lahey Jr., R.T., 1988, "Phase Separation in Dividing Two-Phase Flows", Int. J. Multiphase Flow, 14, pp. 439-458.

Ishii, M., 1975, "Thermo-Fluid Dynamic Theory of Two-Phase Flow", Eyrolles, Paris.

Ishii, M. and Zuber, N., 1979, "Drag Coefficient and Relative Velocity in Bubbly, droplet or particulate flows", AIChE Journal, 25, pp. 842-855.

Ishii, M. and Mishima, K., 1984, "Two-Fluid Model and Hydrodynamic Constitutive Relations", Nuclear Engng. Design, 82, pp. 107-126.

Khan, H.J., Wei, Y and Pertmer, G.A., 1992, "Numerical Calculation of Gas-Liquid Transient Flow in Channels and Bends", International Symposium on Multiphase Flow in Welles and Pipelines, ASME Winter Annual Meeting, Anaheim, USA, FED-Vol. 144, pp. 113-123.

Kubo, T. and Ueda, T., 1973, "On the Characteristics of Confluent Flow of Gas-Liquid Mixtures in Headers", Bull JSME, 16, No. 99, pp. 1373-1384.

Mandhane, J.M., Gregory, G.A. and Aziz, K., 1974, "A Flow Pattern Map for Gas-Liquid Flow in Horizontal Pipe", Int. J. Multiphase Flow, 1, pp. 537-553.

Moura, L.F.M., 1989, "Etude de la Redistribution d'un Écoulement Diphasique entre deux Passes d'un Échangeur de Chaleur", Ph.D. Thesis, Institut National Polytechnique de Grenoble, France.

Moura, L.F.M., 1991, "Desenvolvimento de um Modelo Numérico para a Simulação de Escoamentos Bifásicos no Modelo de Dois Fluidos", XI Congresso Brasileiro de Engenharia Mecânica, São Paulo, pp. 393-396.

Moura, L.F.M. and Rezkallah, K.S., 1991, "TOFLU-2D: A Two-Dimensional Two-Fluid Computer Code", Technical Report No. MRG-91-1, University of Saskatchewan, Canada.

Mueller, A.C. and Chiou, J.P., 1988, "Review of Various Types of Flow Maldistribution in Heat Exchangers", Heat Transfer Engineering, Vol. 9, No. 2.

Patankar, S.V., 1981, "Numerical Heat Transfer and Fluid Flow", Mc Graw-Hill, New York.

RBCM - J. of the Braz. Soc. Mechanical Sciences
Vol. XVII - nº1 - 1995 - pp. 26-34

ISSN 0100-7386
Printed in Brazil

Peculiarities of Two-Phase Flow in Coalbeds

Jakub Siemek, Jerzy Stopa, Czeslaw Rybicki
University of Mining and Metallurgy
Drilling and Petroleum Engineering Faculty
Al. Mickiewicza 30, 30 - 059 Kraków, Poland

Abstract

The theorical aspects of the two-phase gas-water flow, with sorption, in the coalbed treated as the double porosity system is presented and the equivalence of such model with the three phase flow model in classical porous medium is proved. Then, the results of computer simulation are presented and discussed to show the peculiarities of the flow in coalbeds.
Keywords: Degasification, Coalbeds, Porous Medium, Two-Phase Flow.

Introduction

Methane production from coalbeds, while originally a safety measure, has emerged as a major source of gas for a number of location world-wide. Gas desorption is the main production mechanism. This is accomplished currently by the hydraulic fracturing of the coalbeds, draining of water, which is always present in the limited pore structure, and reducing pressure to begin the desorption process. When a well is drilled in the coalbed and the pressure in the well is lowered to allow coalbed methane to desorb and flow to the well, two phase gas-water flow occurs and coalbed - water (usually brine) is also produced. This may cause the environmental problems with salt water disposal. It is shown, that gas and water production from coal deposit can be divided into three distinct stages. In the first, gas and water production rates decrease v.s. time. The second stage is characterized by a "negative decline" in gas production rate and a declining water rate. The third stage begins when the peak gas rate is reached. This final stage is similar to the first, but the slopes of the flow rates functions are smaller. The paper shows also the mathematical model of water infusion process into coalbed to point out the differences between flow mechanisms during water production and injection. The results of laboratory investigations using microwaves techniques are also reported.

The forecasting of the gas and water production is made using the relative permeability concept. Reservoir characteristic of coalbeds are quite complicated, which makes mathematical modelling a challenge. The coal matrix is heterogeneous and characterized by two distinct porosity systems: macropores (known also as cleat) and micropores. The micropore system consist of the primary-porosity matrix that exists between the cleat. The major portion of gas stored in coal exists in an adsorbed state, rather than in a free state. As water is removed from macropores, the reservoir pressure is lowered, causing gas to desorb from the matrix surfaces and to flow into the macropores. The free gas saturation in the macropore system increases until the critical saturation for flow is reached. On reaching this critical value, the gas becomes mobile and is transported simultaneously with water in the fractures of macropores. The primary - porosity system acts as a source of fluid to the macropore-system. The mathematical formulation of the gas-drainage problem is usually based on the Warren and Root model of the dual-porosity system (Remner, 1986). The gas transport from the coal-matrix into the macropores may be modelled as the diffusion process (Remner, 1986) or as the desorption process governed by the Langmuir's equation (Mjasnikov, 1977 and Seidle, 1993):

$$V = V_m\left(\frac{bp}{1+bp}\right)\rho_c \qquad (1)$$

In the literature, in both cases, the specially designed computer simulators are recommended for simulation of the degasification process. These programs are expensive and not in common use. However if the Equation (1) is used as the model of gas desorption, it is possible to use the ordinary black-oil type simulator.

The more complicated problem occurs when the water infusion into coalbed is to be modelled. For the gas-water flow in coal, water is usually the wetting phase. Hence, if the grain of coal (saturated with gas) contacts with the water (flowing in the macropores), the micro-flow of water and

Presented at the Fifth Brazilian Thermal Sciences Meeting - ENCIT, São Paulo, S.P., December 7-9, 1994. Technical Editorship: ENCIT Editorial Committee

gas in opposite directions through the surface of grain (block of coal matrix) may occur under the effect of capillary forces. For this reason, dry coal imbibes water. This process may be modelled by the parabolic-type equation with the "diffusion coefficient" depended on the micropore-system geometry and the interfacial tension.

Simulation of the Degasification Process

A mass balance was performed on an elemental volume of coal for both gas and water phases. This resulted in the continuity equation for each component:

water:

$$\nabla\left(\frac{k_{rw}k}{\mu_w B_w}\nabla p_g\right) - q_w = \frac{\partial}{\partial t}\left(\frac{\phi S_w}{B_w}\right) \tag{2}$$

gas:

$$-\nabla\left(\frac{k_{rg}k}{\mu_g}\frac{p_g}{z}\nabla p_g\right) - \frac{p_{sc}T}{T_{sc}}\frac{\partial V}{\partial t} - q_g\frac{p_{sc}T}{T_{sc}} = \frac{\partial}{\partial t}\left(\frac{\phi S_g p_g}{z}\right) \tag{3}$$

The number of unknowns was reduced by implementing two auxiliary Equations:

$$S_w + S_g = 1 \tag{4}$$

$$p_g - p_w = p_c(S_w) \tag{5}$$

Gas desorption was described by the quasisteady - state model developed in (Stopa, 1994).

$$q_{des} = \frac{\partial V}{\partial t} = \frac{V_E^{n+1} - V_E^n}{\Delta t}\left(1 - e^{-\Delta t/\tau}\right) \tag{6}$$

Having assumed that $\Delta t \gg \tau$ and incorporating the Langmuir equation we obtain the simplified model of gas sorption:

$$\frac{\partial V}{\partial t} = \frac{\partial V_g}{\partial t} = \frac{V_m b \rho_c}{(1+bp)^2}\frac{\partial p}{\partial t} \tag{7}$$

In the typical "black-oil" type simulator formulation the sorption term does not present but the solubility of gas in oil and water is incorporated. And moreover there is the 3-th, unused continuity equation for the oil phase. The continuity equations for oil gas phases are:

oil:

$$-\nabla\frac{u_o}{B_o} - q_{osc} = \frac{\partial}{\partial t}\left(\frac{\phi S_o}{B_o}\right) \tag{8}$$

gas:

$$-\nabla\left[\frac{u_g}{B_g} + \left(\frac{R_{so}}{B_o}\right)u_o + \left(\frac{R_{sw}}{B_w}\right)u_w\right] - q_{gsc} = \tag{9}$$

$$= \frac{\partial}{\partial t}\left(\phi\left[\frac{S_g}{B_g} + \left(\frac{R_{so}}{B_o}\right)S_o + \left(\frac{R_{sw}}{B_w}\right)S_w\right]\right)$$

where:

$$u_i = -k\frac{k_{ri}}{\mu_i}(\nabla p_i + \rho_i g) \tag{10}$$

Let S^o be the fictions saturations of coalbed with "oil" phase and $K_{ro}(S_o^o) = 0$.

This implies that $\partial S_o/\partial t = 0$ and $u_o = 0$. Then putting $B_o = 1, z_{sc} = 1, R_{sw} = 0$ and using Darcy's law and the gas formation volume factor definition:

$$B_g = \frac{p_{sc} z T}{p z_{sc} T_{sc}} \tag{11}$$

Equation (9) becomes:

$$\nabla\left(\frac{k_{rg} k p_g}{\mu_g z}\nabla p_g\right) - q_{gsc}\frac{p_{sc} T}{T_{sc}} = \\ = \frac{\partial}{\partial t}\left(\phi\frac{S_g p_g}{z}\right) + \frac{p_{sc} T}{T_{sc}} S_o \frac{\partial(R_{so}\phi)}{\partial t} \tag{12}$$

Putting

$$R_{so} = \frac{V}{\phi S_o} = \frac{V_m \rho_c}{\phi^* S_o}\frac{bp}{1+bp} \tag{13}$$

where $V=V_E$ is calculated using the formula (1) one may establish the formal analogy between the two-phase water-gas flow with sorption, and 3 - phase oil - water - gas flow is porous medium. For the calculations, the porosity and the saturations should be corrected according to formula:

$$\phi = \phi/(1 - S_o) \tag{14}$$

$$S_w = S_w/(1 - S_o) \tag{15}$$

$$S_g = S_g/(1 - S_o) \tag{16}$$

As an example we investigated the degasification process of the restangular coalbed (200x150x10m) using two vertcal wells W1, W2 working with the constant FBHP equal to 0.21 MPa. The additional parameters were: $S_{wo} = 0{,}6, k_x = 5\text{md}, k_y = 10\text{md}, \phi = 0{,}01, p_o = 10{,}33\text{MPa}$, $T = 300\text{K}, V_m = 35{,}4\text{nm}^3/\text{t}, b = 0{,}246\text{MPa}^{-1}, \rho_c = 1{,}3\text{t}/\text{m}^3$

The simulation was made using the "black-oil" type simulator BOAST II, (Stopa, 1994). The results of simulations are presented graphically in Figs. 1, 2 and 3.

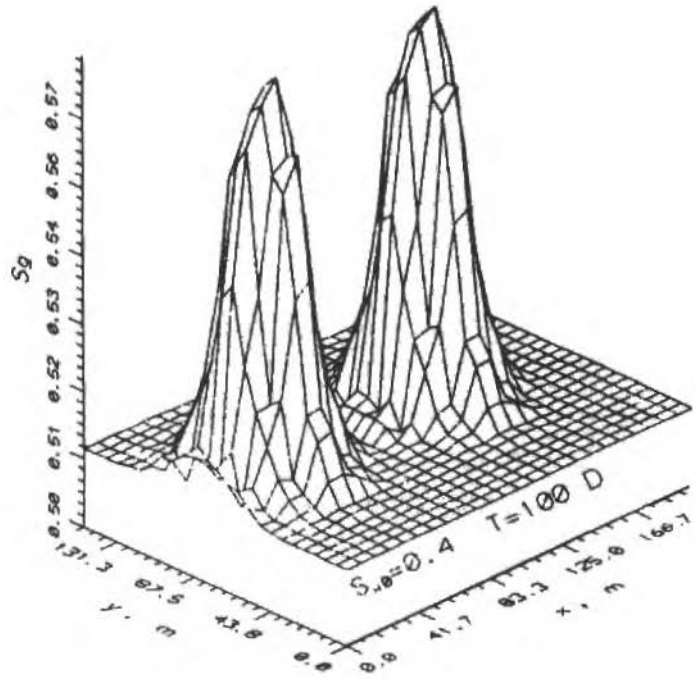

Fig. 1 Free gas distribution in coalbed (computer simulation results)

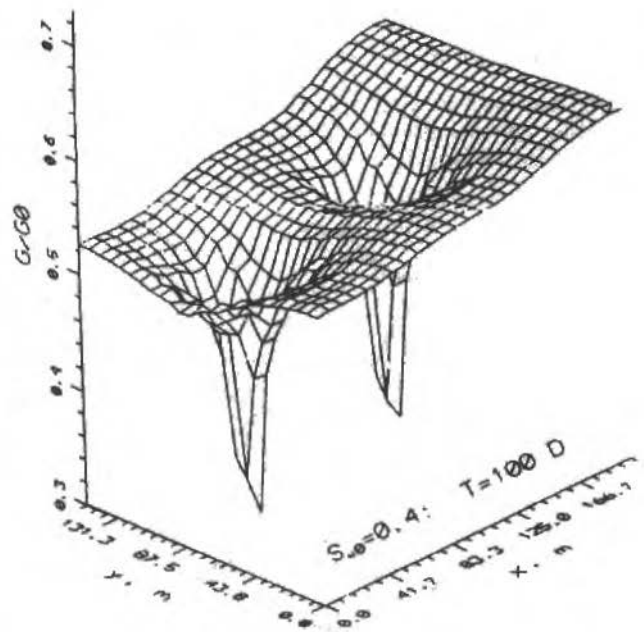

Fig. 2 Adsorbed gas contents in coalbed (computer simulation results)

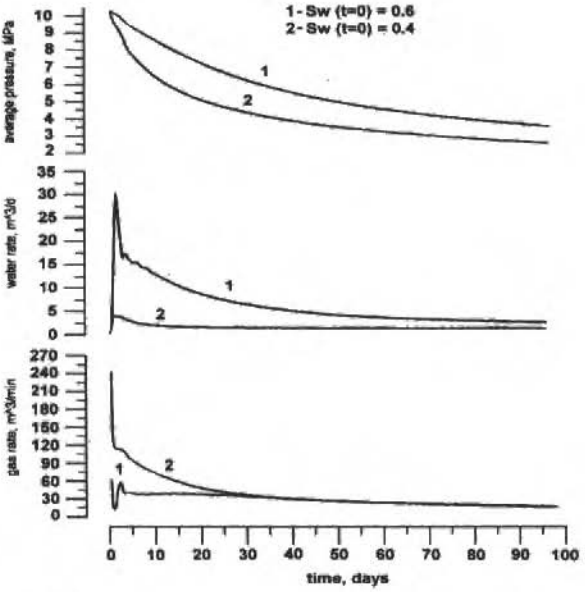

Fig. 3 Main characteristics of the degasification process (computer prognosis)

One may see that gas and water production from coal deposit can be divided into three distinct stages. In the first, gas and water production rates decrease v.s. time. The second stage is characterized by a "negative decline" in gas production rate and a declining water rate. The third stage begins when the peak gas rate is reached. This final stage is similar to the first, but the slopes of the flow rates functions are smaller.

Modelling of the Water Injection into Coalbeds

The most important mode of water transport in coalbeds is Darcy flow in the fractures and macropores. The micropore-system is also accessible to water because of imbibition and adsorption of water on the walls of capillary passages. The scheme of the flow is sketched in Fig. 4.

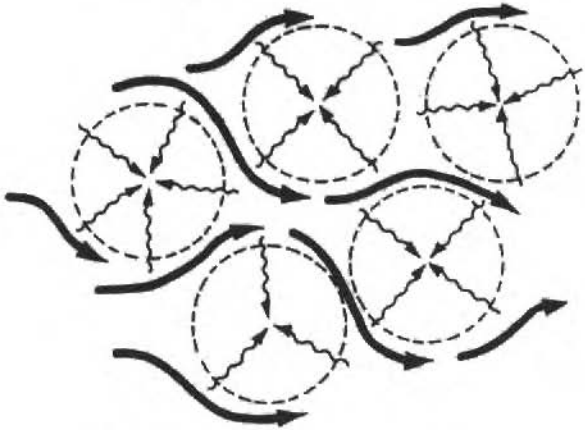

Fig. 4 The scheme of flow in the coal matrix

As the coal matrix acts as the negative source of water to the macropores-system, an additional "source" term Qw must be added to the water continuity Equation (2).

The mathematical model of this infusion process was developed in the previous work (Siemek, 1992 and Stopa, 1990).

The governing equation was developed in the local coordinate-system (x*, t) connected with individual grain of coal pressure. Assuming that the capillary pressure was the only driving force for the imbibition, it was found that the actual water content in the grain S* is described by the parabolic equation:

$$\frac{\partial S_w^*}{\partial t} + \mathrm{div}^* \left(D \,\mathrm{grad}\, S_w^*\right) = 0 \tag{17}$$

$$D = \frac{k^*}{\left(\frac{\mu_w}{k_w^*} + \frac{\mu_g}{k_g^*}\right)\phi^*} \frac{dp_c^*}{dS_w^*} \tag{18}$$

and "*" denotes that differential operators act in a local coordinate system connected with the grain or the parameters refer to the micropore-system.

Equation (17) is solved with the initial and boundary conditions:

$$S_w^* = S_o^*, t = 0$$

$$S_w^* = S_w(x, t), t > 0 \text{ on the grain surface.}$$

Determination of the Mass-Transfer Coefficient D

The average value of parameter D may by measured using the microwave techniques.

The experimental apparatus, microwave meter Wilmer 63 made it possible to measure the non-adsorbed fraction of moisture content in coal sample. The samples of crushed coal are first dried by evaporation, next saturated with water up to 10% (of weight) and inserted (in an air-tight box) into the microwave apparatus. The measurements are carried out in transmission geometry registering the sample attenuation A. The measured signal values were plotted against time. Typical plot is shown in Fig. 5.

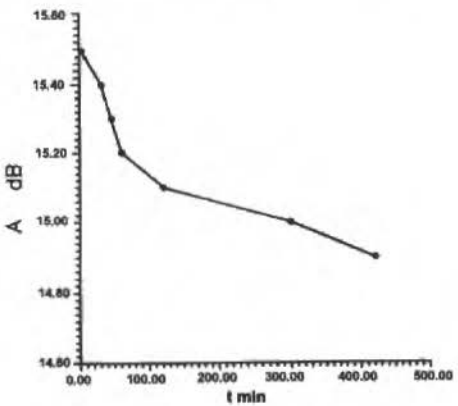

Fig. 5 Attenuation v.s. time. Sample A

The attenuation of a saturated sample is decreasing function of time and one may deduce that moisture is adsorbed on the internal surface of coal. When this process reaches equilibrium, the attenuation becomes steady.

In spite of the fact that the readings of microwaves attenuation A(1) are taken in decibels, due to linear characteristics of apparatus the following equality may be written:

$$\frac{A - A_0}{A_1 - A_0} = \frac{w - w_0}{w_1 - w_0} = \Sigma \tag{19}$$

where A_0 is the attenuation at $t = 0$, A_1 is the attenuation when imbibition reaches equilibrium, and w_0, w_1 are moisture contents (concentrations) at $t = 0$ and in equilibrium respectively. For this reason the relative measure of moisture content Σ may be used without calibrating of the apparatus (calibration curve depends on grain size variability). Referring to the geometry of the sample used in laboratory investigations, spherical particles of coal are assumed. Applying the spherical coordinates system, Equation (17) may be solved analytically.

The grain-volume arevaged solution defined by:

$$\langle S_w^* \rangle_R = \frac{1}{V_R} \int_{VR} S_w^* \, dV_R \tag{20}$$

where V_R is volume of grain, is:

$$\frac{\langle S_R^* \rangle_R - S_0}{S_1 - S_0} = 1 - \frac{6}{\pi^2} \sum_{k=1}^{\infty} \frac{1}{k^2} \exp\left(\frac{k^2 \pi^2 D}{R^2} t\right) \tag{21}$$

Because of linear dependence of S_w^* and w, and recalling Equation (19), expression (21) is equal to Σ. The following approximate Equation is also true.

$$\Sigma \approx 6 \left(\frac{D}{\pi R^2} t\right)^{0,5} \quad \text{for small t} \tag{22}$$

Matching of the curve (21) to the measured data points from Fig. 5 is presented in Fig. 6.

Having the attenuation at equilibrium w_1, the w_0 and D/R^2 were calculated using (22). Using these values for 50 terms of the series (21) the theoretical curve presented in Fig. 6 was obtained.

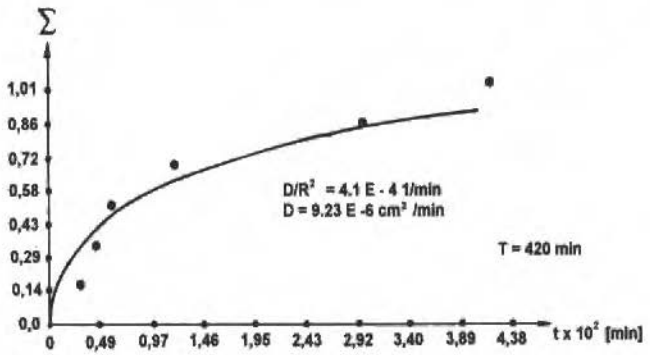

Fig. 6 Curve matching to the measured data

Conclusions

Two-phase gas-water flow with sorption is mathematically equivalent to 3 - phase flow without sorption. The "black-oil" type simulators can be used for modeling coalbeds degasification process, but the input data should be prepared in a specific manner.

Water can exist in coal both as flowing phase in macropores and as connate water, adsorbed in grains. The water sorption may be described mathematically by use of the diffusion type Equation. "Diffusion coefficient" may be determinated by use of the microwaves techniques.

Nomenclature

a = Attenuation, dB
S_g = Saturation with gas in macro-porosity system
S_w = Saturation with water in macro-porosity system
S_o = Saturation with oil in macro-porosity system
k_{ri} = Relative permeabilities, i=o, w, g
R_{si} = Gas solubility in phase i, i=o, w, nm^3/m^3
p_i = Pressure, i=o, w, g, bar
V_m = Constant in Langmuir Equation, nm^3/t
p_o = Initial pressure, MPa
b = Constant in Langmuir Equation, bar^{-1}
D = Diffusion coefficient, m^2/s
u_i = Darcy velocity, i=o, w, g, m/s
B_i = Formation volume factor, i=o, w, g
z = Gas compressibility
T = Temperature, K
V = Volume of gas actually sorbed in coal, nm^3/m^3
V_E = Volume of gas sorbed in coal in equilibrium, nm^3/m^3
q_{des} = Gas desorption rate per coal volume, nm^3/dm^3
q_i = External source rate per coal volume, i=w, g, m^3/dm^3
t = Time, d, sek
p_c = Capillary pressure, bar
k = Permeability, m^2, k = diag (kx, ky)
p_{wf} = Flowing bottom hole pressure, MPa
S_{wo} = Initial water saturation
ϕ = Porosity
ρ_c = Coal density, kg/m^3
ρ_i = Viscosity, Pa s
τ = Constant, d
w = Water contents
Σ = Relative water content, def. by (19)

Subscripts

sc = Normal conditions
o = Oil
g = Gas
w = Water
0 = Initial, t=0

Superscripts

* = Fictitious parameter (for calculations only) of referring to micropore-system
n = Time step number

References

Boyer, C.M. et al., 1981, "Methane Modelling - Prediction the Inflow of Methane Gas into Coal Mines", U.S. DOE, Contract DE-AC 22-80 PC 30123.

Durucan, S., Creedy, D.P. and Edwards, J.S., 1992, "Geological and geotechnical factors controlling the occurence and flow of methane in coal seams", Coalbed Methane Symposium, Townsville 19-21 Nov.

King, G.R. and Ertekin, T., 1988, Comparative Evaluation of Vertical and Horizontal Drainage Wells for the Degasification of Coal Seams, SPERE May.

Mjasnikov, A.A., Sadochin, W.P. and Zirnova, T.S., 1977, Primenienie EVM dla reenija zadae uprawlenija metanowydelenijem w szachtach, Nedra (in Russian).

Remner, D.J. et. al., 1986, "A Parametric Study of the Effects of Coal Seam Properties on Gas Drainage Efficiency", SPERE, Nov.

Seidle, J.P., 1993, "Long-Term Gas Deliverability of a Dewatered Coalbed", JPT vol. 45, No. 6 June.

Siemek, J. and Stopa, J., 1992, "Theoretical and laboratory investigations of the 2 - phase gas - water flow in coalbeds", Zesz. Nauk. Politechniki Slaskiej, Gornictwo z 195 (in Polish).

Stopa, J., 1990, "Experimental and Theoretical Studies of Imbibition of Water by Coal", Archives of Mining Sciences Vol 35,4.

Stopa, J. and Siemek, J., 1993, "Oil reservoirs simulators used in Poland" Proc. Conf. "Technology, Equipment and Services in Petroleum Industry, Jaremcza, Ukraine (in Polish).

Stopa, J., 1994, "Application of the "black-oil" type simulators for prediction of methane production from the water saturated coalbeds", Archives of Mining Sciences, 39,2 (in Polish).

RBCM - J. of the Braz. Soc. Mechanical Sciences
Vol. XVII - nº1 - 1995 - pp. 35-48

ISSN 0100-7386
Printed in Brazil

Information Integration in Computer Integrated Manufacturing (CIM)

Rosa Maria Scala Hernández-Vaquero
Universidad Politécnica de Madrid
Madrid - Spain

Abstract

One of the main problems when implementing the CIM concept concerns information integration. In order to support information integration an information system provided with suitable data models is required. In this paper, an information system is presented, which fulfils the requirements for an appropriate information management in CIM.
In order to make the information system transportable and worlwide accepted, it has been built on the basis of an international standard ISO 10303 (STEP). In this paper, an overview of STEP will be given as well as two of the most interesting aspects of STEP: the EXPRESS language and the neutral exchange file.
The EXPRESS language is used in the information system as data model. The users of the information system (CIM tool user) must establish their data models in EXPRESS and the information system will store them in the database. This makes the information system flexible because the implemented interface is independent of the database schema. Some access functions are provided by the information system for the storage and retrieval of instances of the model when the designer is working with the CIM tool. The data exchange format is the one used in STEP.
The information system was developed in the frame of the ESPRIT 2202 CIM-PLATO project of the European Community.
Keywords: CIM, Information Integration, STEP, EXPRESS.

Introduction

During the past 25 years, computers have been introduced in industry to perform technical tasks such as drafting, design, process planning, data acquisition, process control and quality assurance. Computer-based solutions, however, are still in most cases single isolated devices within a manufacturing plant.

Computer technology is evolving rapidly, and the life cycle products of today and production methods are shortening, with continously increasing requirements from customers, and a trend to market interrelations between companies at a national and international level. This forces a growing need for efficient storage, retrieval and exchange of information. Integration of information is urgent within companies to interconnect departments which used to work more or less on their own. On the other hand direct communication with outside customers, suppliers and partner institutions will often determine the position of an enterprise among its competitors. In the sense, Computer Integrated Manufactoring (CIM) is the key today for the competitiveness of tomorrow. But the realization of a future-oriented CIM concept is not possible without powerful, widely accepted and standardized interfaces. They are a vital issue on the way to CIM. They will contribute to harmonizing data structures and information flows and will play a major role in open CIM systems.

In addition, the designers and users of the CAD/CAM systems have witnessed, during the last decade, the appearance of several specifications as well as proposals for standards which either attempt to cover wider areas or to be more stable and reliable than the others. With the rapid evolution of hardware and software, the capabilities offered by CAD systems and CAD based application systems are far more advanced than they were only ten years ago. However, the situation with standards cannot be so. The standard has to be stable and should be general and flexible enough to accomodate present as well as expected future developments.

The ISO standard STEP has been developed to provide a neutral mechanism capable of describing product data throughout the life cicle of a product, independent from any particular system, and not only CAD data. This paper gives an overview of the ISO STEP standard, describing some

Manuscript received: October 1994. Technical Editor: Leonardo Goldstein Jr.

interesting aspects like the EXPRESS language and the neutral exchange file and presents an information system for CIM based in STEP. This information system was developed in the frame of the ESPRIT 2202 project of the European Community.

The STEP Normalization Effort

In 1984, ISO established a special committee to develop a standard for the exchange of product data (STEP), which would be the first international standard in CAD data exchange. The main reasons taken into account by ISO to start the development of STEP were:

- The international industrial community agreed that a standard for CAD data exchange requires a worlwide acceptance. ISO is the appropriate organization for this development;
- Theexisting standards focused on the exchange format. A different solution was needed in which the main point was the semantic specification (what to exchange) instead of the sintaxis (how to exchange), and
- In the area of solid models exchange, the IGES solution was not adequate. A new solution was needed.

STEP is an international standard ISO 10303 described in (ISO 10303-1, 1992) (Product Data Representation and Exchange) for the representation and exchange of product data between different computer systems. This standard has been developed by several groups of Subcommittee 4 (Industrial Data and Global Manufacturing Programming languages) of Technical Committee 184 (Industrial Automation System) in ISO.

The objective of STEP is to provide a mechanism capable of describing product data throughout the life cycle of a product, independent of any particular system. The goal of ISO 10303 is to support the creation of complete representations of products through the entire manufacturing process and not merely graphical representations, existing standards for which are already established. The product model in STEP must contain enough information to support advanced CAD/CAM applications. ISO 10303 provides a set of technical data elements which may be used to describe product data for:

- Communication of product data between activities or enterprises;
- Integration of activities involved in manufacturing within an enterprise, and
- Archiving of product data independent from the software system used to generate it.

STEP incorporates the experience gained in the development of several national standards IGES (NBS, 1984), VDAFS (DIN, 1986), SET (AFNOR, 1985) and the projects CAD*I (Beg Leuridan, 1988) and PDES (Gruttke, 1985).

Each International Standard in the ISO 10303 series is called a "part" and is published separately. The structure of the ISO 10303 family of standards provides a logical separation between the product data information which is common to many applications, the additional information that is required to support a particular application, and the implementation forms that may be used for storage or communication of that information. The independence of implementation forms means that the information content can be extended without changing the definition of the implementation form, and that new forms can be added to support existing information definitions. The product data description may be stored or communicated in a variety of implementation forms, such as a physical file, or through direct access to a database.

The STEP Structure

The ISO 10303 series of standards is divided into five logical groups of parts, each called a Class. Each Class has a unique function in ISO 10303.

Description Methods: The definition of information required for resource constructs and Application Protocols to support product models requires the use of a formal language to ensure consistency and avoid ambiguity. The language should be both human and computer processable to facilitate human understanding and the generation of applications and support tools. EXPRESS (ISO

10303-11, 1993) is the only formal language for data description used in STEP.

EXPRESS will be described in more detail in this paper:

- Information Content: The information content of the ISO 10303 series of International Standards is defined as a set of technical data elements known as integrated resources constructs.

  The integrated resources provide a neutral, complete and unambiguous representation of product model data, independent of the implementation forms used for storage or communication.

The set of integrated resource constructs used in the ISO 10303 series of International Standards have been assembled from information models representing different application domains. Similar ideas in different domains have been reduced to a single construct which is common to multiple domains, and may be used with extra constraints and relationships to support particular applications.

EXPRESS (ISO 10303-11, 1993) is used as the single standard data specification language for all constructs, constraints and functions in the integrated resources;

- Application protocols: The use of the ISO 10303 series of International Standards to support a particular application domain is based on the concept of the Application Protocol (AP). The AP provides a complete explicit statement of the product data description required to meet the specific needs of a particular application, and the implementation form or forms to be used. It is the basis of implementations of the ISO 10303 series.

The AP defines the scope and context of the application. This may include the use of an activity model (AAM) to clarify the process and the data flows involved. The AP describes the information requirements of the application in application specific terms, as a reference model (ARM) for establishing the necessary product data description;

The product data description (AIM) is based on constructs and schemas selected from the integrated resources and interpreted to meet the needs of the application;

- Implementation forms: The product data description may be stored or communicated in a variety of implementation forms, which are particular methods for storing, accessing or exchanging information. Possible alternative implementation forms which may be used for product data include physical file transfer and database access. Each implementation form is described as a mapping from the EXPRESS language onto the formal language used for the form, and is independent of the information to be transferred. The mapping is expressed in a formal notation, along with any additional syntax required for the particular implementation.

This series of International Standards provides for different forms of implementation. The exchange file implementation serves to exchange entire models or parts thereof between different systems. It is documented in (ISO 10303-21, 1992) and will be described in this paper, and

- Framework for Conformance Testing: The accreditation and certification procedures for ISO 10303 need to be common and consistently applied worldwide in order to ensure effective communication of product data. The Framework of Conformance Testing provides a general methodology, requirements and general guidance to test centers for testing conformance of a product which claims to implement an ISO 10303 AP against the relevant Part and normative references. The goal of the Framework is to ensure:
- Repeatability- Test results consistent wherever and whenever undertaken;
- Auditability- Procedures confirmed as correctly undertaken, subsequent to the process, and
- Comparability- Procedures are independent of test site.

The EXPRESS Language

The EXPRESS language (ISO 10303-11, 1993) provides a complete and unambiguous normative description of product data information for both resource constructs and Application Protocols, with supporting test.

The formal context free grammar of EXPRESS defines entities from data elements and constraints and other properties, which together define the valid forms of the product data information.

Other features of the language permit classification and structuring of constructs, and allow characteristics of constructs to be generalized or specialized. EXPRESS also facilitates the development of APs by allowing the addition of constraints and attributes to existing constructs. EXPRESS allows a more complete description of the data and constraints applicable to product data than is possible using conventional language.

EXPRESS is based on the following requirements:

- The size and complexity of this standard requires the language to be computer processable and not only by humans;
- The language is designed to allow the division of modelled data. The *SCHEMA* is the basis for this division, and
- The main language elements are the *ENTITIES* which are objets of interest. The definition is done based on data and behaviour.

The examples included here belong to the integrated resources of STEP.

SCHEMA: A SCHEMA corresponds to a part of the application "miniworld" and contains *ENTITY* and other declarations which maintain certain relationships. An *SCHEMA includes ENTITY* definitions, user defined types, functions, rules, *etc. SCHEMAS* can be nested, and can refer to elements defined in other *SCHEMA*

In Fig. 1 a header definition of an *SCHEMA* can be seen. It includes references to other elements defined in other *SCHEMAS*.

In this figure the graphical version can also be seen. The diagram is only in the *SCHEMA* level. The relation to other *SCHEMAS* must be stated in the clause *REFERENCE FROM*.

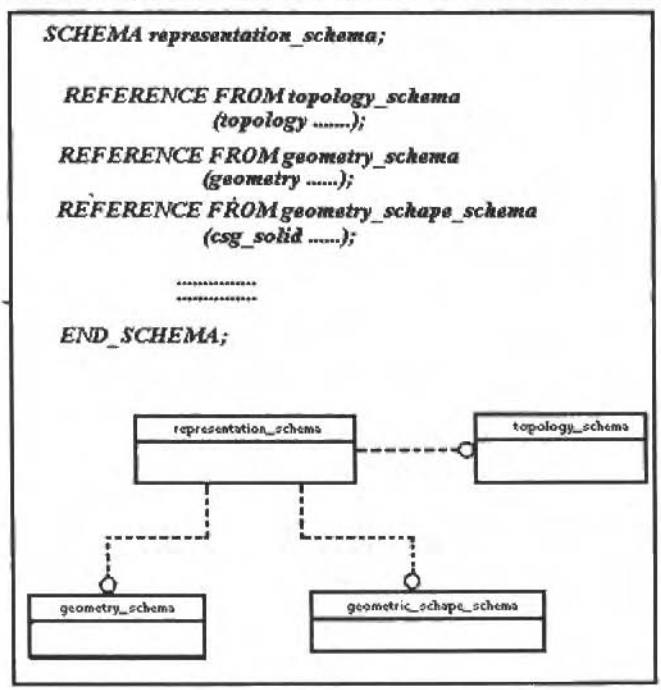

Fig. 1 Header definition for a *SCHEMA*

The elements referenced can be either types defined by the user or *ENTITIES* defined in *other SCHEMAS*.

TYPE: In EXPRESS there are some predefined types like *INTEGER, REAL, LOGICAL, STRING*, etc., which are simple types. There are as well aggregate types like *ARRAY, LIST, SET and BAG*. Aggregate types can be nested like *ARRAY [...] OF ARRAY [...] OF* .... Brackets include the limits for the number of elements.

In Fig. 2 some examples of *TYPE* definitions can be seen. The first definition is an aggregate which references an *ENTITY. The* graphical version of this type can also be seen. The second example is a type *ENUMERATION.* When an entity attribute is of that type, only the values in the list are valid.

ENTITY: An ENTITY represents an object or idea of interest for the application.

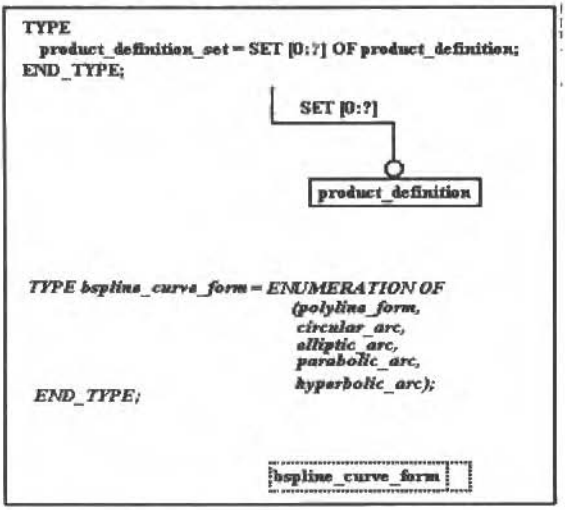

Fig. 2 Examples of user defined types

An ENTITY is characterized by a collection of attributes defined by the user. The types can be either predefined by EXPRESS or user types. An entity can belong to a hierarchy of entities with the relationship *SUPERTYPE OF / SUBTYPE OF.* An entity can be subtype of several entities and can have more than one subtype. The subtypes are related through different relationships and EXPRESS provides some operators to define the restrictions. These operators are: *ONEOF,* ANDOR, AND. An entity inherits the attributes of its supertype.

In Fig. 3 an entity definition can be seen. This definition belongs to the integrated resources of STEP. The definition is not complete due to its complexity. There are aggregate attributes as well as derived attributes (in the *DERIVE* clause) whose values are obtained through different functions.

Fig. 3 Example of an entity definition

It is also possible to define restrictions (in the WHERE clause) for some attributes.

The final part includes the header auxiliary definitions to which the entity references. These definitions include the supertype-subtype hierarchy in which the entity is included.

As mentioned before, the definition is not complete due to its complexity.

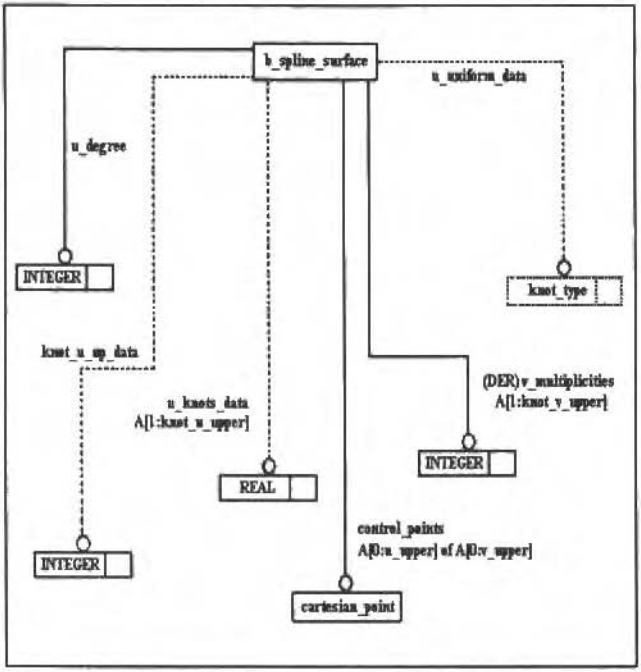

Fig. 4 EXPRESS-G representation for the entity defined in Fig. 3

STEP Neutral file Structure

General structure: The exchange file described in (ISO 10303-21, 1992) is sequential and the information contained is free format. The file is divided in modules with different sections containing one or more entities. It starts with the keyword "STEP" and ends with "ENDSTEP". There are two sections "HEADER" and "DATA".

The first section (Fig. 5) contains data common to all the exchange file.

```
STEP;
HEADER;
FILE_IDENTIFICATION('EXAMPLE STEP FILE-#1 ','19880211.153000',('JOHN DOE'
'ACME INC.' 'METROPOLIS USA'),('ACME INC. A SUBSIDIARY OF GIANT
INDUSTRIE''METROPOLISUSA'), STEP VERSION 1.0','CIM/STEP VERSION2','SUPER
CIM SYSTEM RELEASE 4.0');
FILE_DESCRIPTION('THIS FILE CONTAINS A SMALL SAMPLE STEP
MODEL'); IMP_LEVEL ('BREP_LEVEL 1.0');
ENDSEC;
```

Fig. 5 STEP file HEADER example

The second section (Fig. 6) contains the product data to be transferred. These data are instances of the entities defined in the conceptual model. The STEP exchange file can be considered as a sequence of characters belonging to the basic alphabet, grouped in recognizable chains called "tokens".

```
DATA
/* THE FOLLOWING ENTITIES REPRESENT A TRIANGLE                    */
@1 = PT(0.0,0.0,0.0);          /* IS AN ENTITY POINT*/
@2 = PT(0.0,1.0,0.0);
@11= VX(#1);          /* IS AN ENTITY VERTEX*/
@12 = VX(#2);
@16 = ED(#11,#12); /* IS AN ENTITY EDGE*/
@18 = ED(#13,#12);
@22 = ED_STRC(#18,0);
@23 = ED_STRC(#16,1);
@24= ED_LOOP((#21,#22,#23)); /* IS AN ENTITY EDGE_LOOP*/

/* ANOTHER WAY TO REPRESENT A TRIANGLE: */
@1100 = VX(PT(0.0,0.0,0.0));
@1200 = VX(PT(0.0,1.0,0.0));
@2400 = ED_LOOP
        SCOPE
        @1600 = ED(#1100,#1200);
        @1800 = ED(#1300,#1200);
        ENDSCOPE
        ((ED_STRC(#1700,0),ED_STRC(#1800,0),ED_STRC(#1600,1)));
ENDSEC;
ENDSTEP;
```

Fig. 6 STEP file DATA example

Correspondence between EXPRESS and the STEP neutral file: Given an entity modelled in EXPRESS, an instance is obtained assigning values to each attribute. These instances must be included in the STEP file following the format described above.

Figure 7 shows the mapping between an EXPRESS model and an instance as should be included in the neutral file. The attribute values are written sequentially, with the values separated by comas. References to other instances are preceded by #. An identifier must precede the instance, with the symbol @.

```
TYPE type1 = ENUMERATION OF (enum1, enum2, enum3);
END_TYPE;
ENTITY entity1
        SUPERTYPE OF (entity2);
        attribute11 = STRING;
        attribute12 = LIST [1:3] OF INTEGER;
END_ENTITY;
ENTITY entity2
        SUBTYPE OF (entity1);
        attribute21 = REAL;
        attribute22 = type1;
        attribute23 = ARRAY [1:3] OF ARRAY [1:2] OF
INTEGER;
        attribute24 = entity3;
END_ENTITY;
ENTITY entity3;
      .....
      .....
@763    =    ENTITY2        ('STRING', (23, 1, 790), 34.22,
.enum2., ((23,.5),(87,9),(7,102)),#112)
```

Fig. 7 Example of correspondence between EXPRESS and the STEP file

Frame for the Development of the Information System

As already mentioned, the information system presented in this paper was developed in the frame of the ESPRIT project nº 2202 CIM-PLATO "CIM System Planning Toolbox" of the European Community. The overall objective of the CIM-PLATO project is the development of an industrial toolbox prototype consisting of computer-based procedures and tools which support the design, planning and installation of FMS (Flexible Manufacturing Systems) and FAS (Flexible Assembly Systems) in a CIM environment. This concerns three closely interrelated fields of R&D: manufacturing systems planning, process execution planning and the provision of all necessary information to fulfill these tasks and integrate them into a factory information system. In order to ensure an effective cooperation within the project three subgroups were installed; two subgroups were for the configuration of exemplary toolboxes in different industrial areas. Beside the development of the tools, the tasks of these groups were to check the functionality and effectivity of the tools and evaluate them.

The third group (information integration) was established to address basic questions of common interest concerning the integration of tools. Furthermore tools were developed which were specially oriented to information acquisition, integration and management. Additionally, five demonstrator systems were defined, being one of them Flexible Assembly System Tools (FAST).

The information system was included in the FAST demonstrator (CIM-PLATO Consortium, 1992) system which configures tools realized by various project partners to a toolbox. The integration is reached via information management tools based on a relational database management system.

Although the design of a flexible assembly system (FAS) has been chosen as an application example, this does not signify a specific tool configuration for assembly.

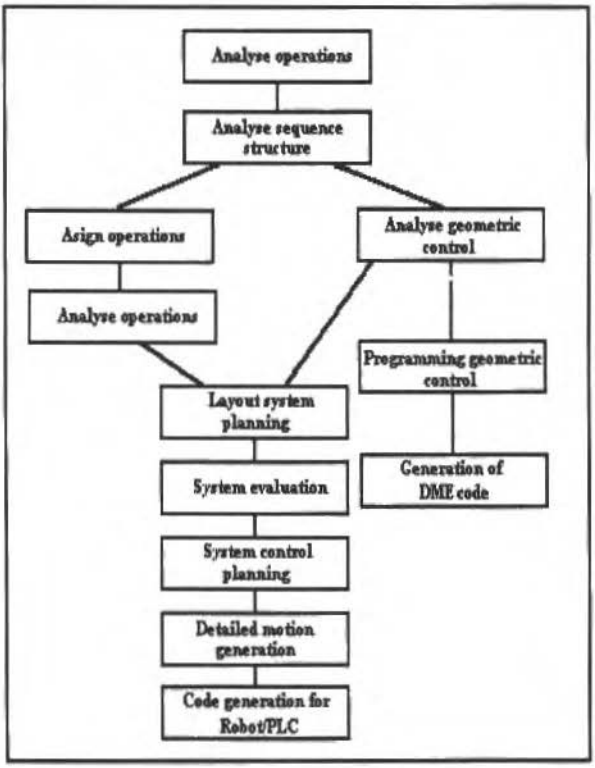

Fig. 8 CIM modules included in FAST demonstrator

Most of the tools are also applicable for the design of flexible manufacturing systems. The term "design" refers to the whole process starting with a product analysis and ending with the code generation for the target devices of an FAS. Fig. 8 shows the CIM tools included in the FAST demonstrator. The information system is used by the tools for the exchange of data between them. Every partner in the FAST demonstrator developed one or more tools. These partners were: UCG (University College Galway, Ireland), *IPK (Institut für Produktionsanlagen und Konstruktionstechnik,* Berlin, Germany), PSI *(Gesellschaft für Prozessteuerunngs-und Informationssysteme,* Berlin, Germany) and Renault Automation (Paris, France).

Requirements for the Information System

The users of the information system, CIM tools developers, had some requirements concerning the information system. The most important requirements were:

- Permanent information supplier. Once the tool is connected to the information system, it should be able to store or retrieve data at any moment;
- Flexibility. In this context, flexibility means that the information system should adapt in a quick and easy way to changes in data structures. The tool designer must transmit to the information system, before using it, the data structure in a conceptual model. If the designer changes this structure, the information system must store easily this new data model;
- The access functions provided by the information system to the tools should be invariable, and independent of the data model;
- The CIM modules need to manage complex data. The information system must store or retrieve these data;
- The information system must control concurrent accesses of different tools to the same data in order to avoid incompatible operations;
- The information system should control consistency of data. The tools store and retrieve instances of the data model. It must be checked that there is a correspondence between the instance and the model, and
- Once the information system architecture is described, it will be clear that it adapts to the requirements mentioned previously.

The Data Model and the Database

The first step in order to develop the information system, was to choose the data model. The first time the information system is used, the designer must store his data structure in the system. Only when the user wants to change the structure he must store it again. Several existing data models were analyzed: IDEF1X, NIAM and EXPRESS.

IDEF1X is near to relational databases, which was quite convenient due to the fact that the tool designers had worked previously with this kind of databases and had them installed in their computers. But IDEF1X has only graphical version, which makes it more difficult to be computerprocessable. NIAM allows to define complex models with great semantic content, but it has the same problem as IDEF1X, there is only graphical version.

EXPRESS has some advantages. It has both graphical and textual version. Mc. Donnell Douglas has developed various tools to process EXPRESS models. Also quite complex models can be defined in EXPRESS. Finally, the fact that is an ISO standard is a good reason to ease transportability for the information system.

The underlying database in the information system is a relational database, because most of the designers had these kind of databases installed. The access language is SQL.

Information System Architecture

The information system is an environment for information management based in EXPRESS. It contains facilities for the definition of conceptual models written in EXPRESS and facilities for the manipulation of the instances of the entities of the conceptual model.

The complete development of a database specifically designed for EXPRESS was discarded for budget reasons. Instead, the information system was built on top of a commercial relational DBMS using SQL.

The development therefore focused in the translation between EXPRESS and SQL at the data definition and data manipulation levels. The information system stores an explicit definition of the EXPRESS conceptual model and therefore can be easily configured to different applications.

The architecture can be seen in Fig. 9.

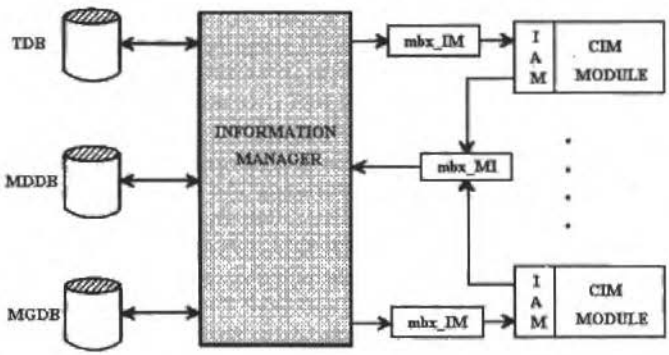

Fig. 9 Information System Architecture

The components of the architecture are:

Information Manager: The kernel element is the Information Manager which serves the requests of the clients. This component therefore acts as an intermediary between the EXPRESS-oriented world of the tools and the relational world of the DBMS used to physically store the information.

Information Access Methods (IAM): The information system provides to its clients an EXPRESS-oriented view of the information stored in a relational DBMS by means of an Information Access Interface. This interface consists of a set of functions for EXPRESS-oriented data retrieval, storing, updating and deletion. The communication is done via mailbox, a resource of VMS operating system.

Metadata Database (MDDB): In order to access the data stored in the relational DBMS, the Information Manager requires to resolve references and bind parameters. This can be done because the conceptual model of the application domain is stored in a database, named Metadata Database. It is a relational database containing data about the data, usually refered as metadata.

Technical Database: The conceptual model of the application domain is written in EXPRESS, and the instances are stored in a relational database, named Technical Database. The relational constructs of the Technical Database consists of a relational view of the EXPRESS data model.

Management Database (MGD): This table stores data operations done by every tool in order to control transactions and concurrent accesses.

The information system has the requirements mentioned previously:

- It is a permanent information supplier: once the tool is connected to the system (through the access function "Connect") it can store, retrieve or change data at any moment;
- Flexibility: the data structure, the EXPRESS data model, is stored in the Metedata Database. When the designer wants to change this structure, the new model is processed and stored again in the database. This operation is quickly done because there are tools to process EXPRESS models;

- The Information Access Methods (IAM) are provided by the information system in a library, and the user links it with his programs. These functions are independent of the data structure and never change;
- EXPRESS allows the definition of complex models. An entity can be as complex as the designer needs. The data stored or retrieved by the tool during its work are instances of EXPRESS entitles which are similar to objects of the application world (for example a cell a product, an assembly sequence, etc.);
- The information manager controls the concurrent accesses, and in the management database the locks over the entities are stored, and
- When the tool stores an entity instance, the information manager checks that the attributes in the instance correspond to the EXPRESS model stored in the Metadata Database.

Configuration Phase

The first time a CIM module will use the information system or if the designer changes his data structure (the EXPRESS model) a configuration phase is needed. Fig. 10 shows the operations done in this phase.

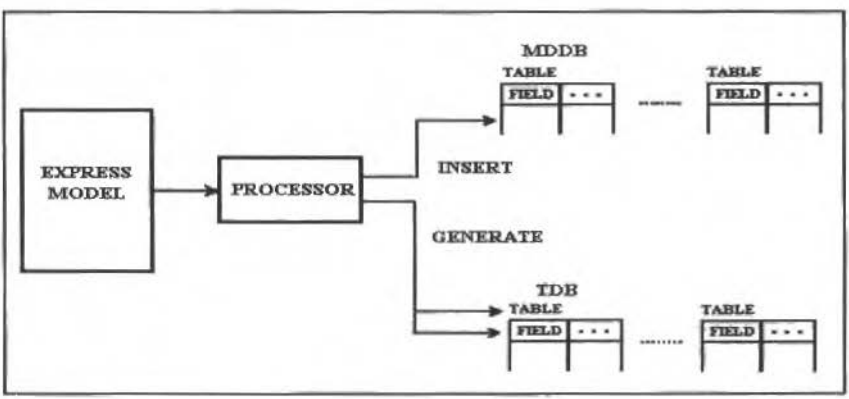

Fig. 10 Operations done during the configuration phase

The EXPRESS model is processed and stored in the Metadata Database. The technical database must be generated (tables and fields), because they depend on the data structure. This configuration phase is done in few seconds, and when it finishes the information system is ready for use.

The Metadata Database (MDDB)

As already mentioned, this database stores the data structure used by the designers.

The data exchanged between the CIM tools and the information system are the instances of the EXPRESS data model stored in this database. The information manager checks the consistency between the model and the instance. This database stores the entities in the model, the attributes of each entity, the entity hierarchy, etc. For consistency reasons, the database itself was designed using EXPRESS and then translated to tables and fields for implementation. In Fig. 11 two of the most significant entities are presented as well as the resulting tables. This correspondence between EXPRESS and SQL was developed according to some complex rules.

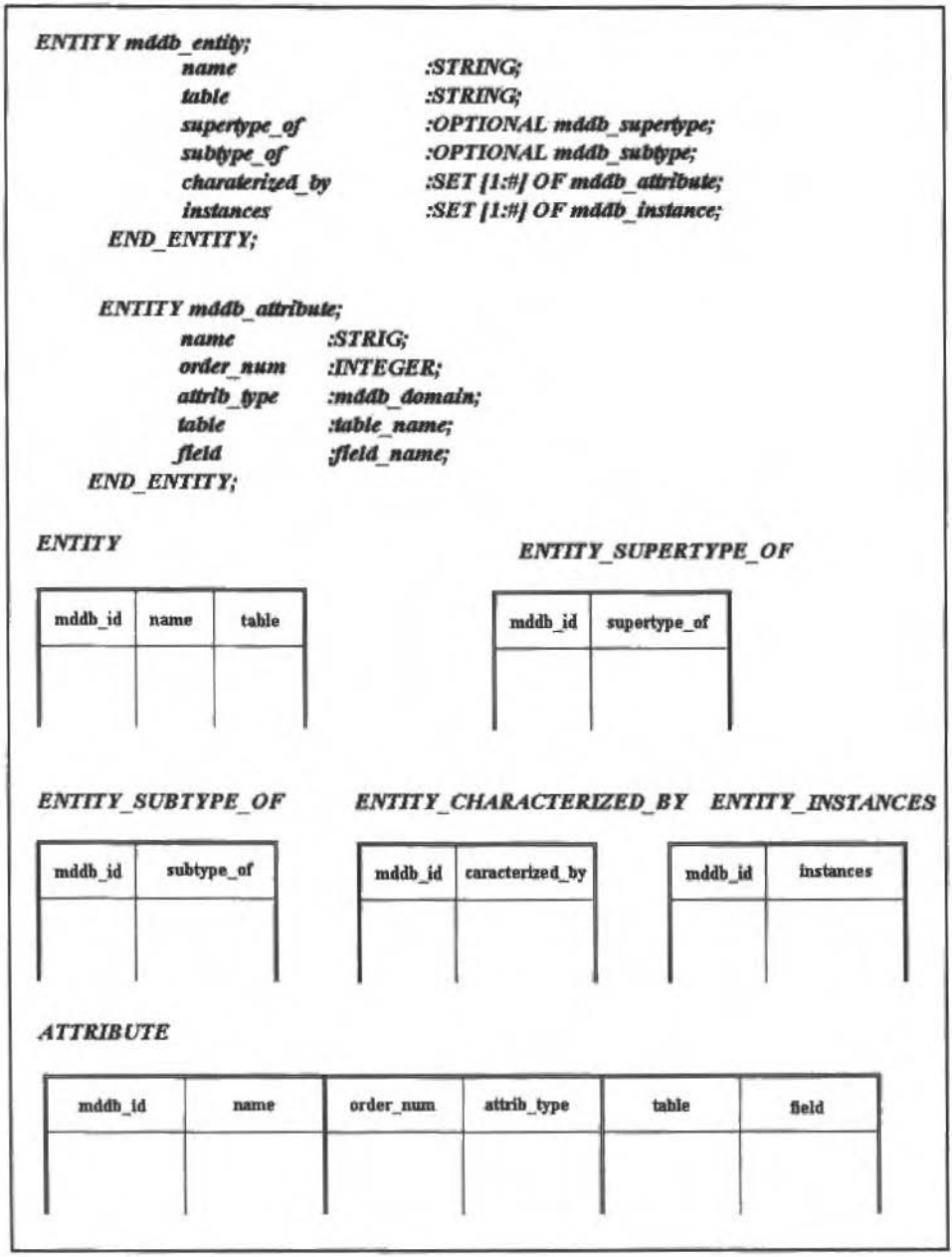

Fig. 11 Partial EXPRESS model for the Metadata Database and corresponding tables

The Information Access Methods

The following table presents the Information Access Methods provided to the designers.

Table 1 Information Access Methods

NAME	DESCRIPTION	INPUT	OUTPUT
ConnectTols	Starts a working session with the Information System	client	error_code
DisconnectFr oms	Finishes a working session with the Information System	client	error_code
StartLongTra nsaction	Starts a long transaction		error_code
EndLongTrans action	Finishes a long transaction	finish_mode (commit, rollback)	error_code
CreateObject Instance	Creates an EXPRESS entity instance and stores the values of its attributes	schema_name entity_name value (as ISO 10303-21)	instance_ id error_code
DeleteObject Instance	Deletes the specified entity	instance_ id	error_code
GetObjectIns tance	Retrieves the value of the attributes of an EXPRESS entity instance	instance_id	value (as ISO 10303-21) error_cod e
SelectObject Instance	Returns a list with the instance identifiers of a specified EXPRESS entity that fulfill a given condition.	schema_name entity_name condition (in EXPRESS)	instance_ id_list error_code
GetAttribute Value	Returns the value of an attribute of an EXPRESS entity instance	instance_id attribute_name	error_code
PutAttribute Value	Replaces the value of an attribute of an EXPRESS entity instance	instance_id attribut e_name value (as ISO 10303-21)	error_code

Conclusions

The CIM concept implies the integration of all the components (people, machines, information, etc.) of a manufacturing organization. One of the main goals of integration concerns information integration. This task requires the existence of means for data specification and widely accepted data models.

The ISO standard STEP (Standard for Exchange of Product Data Model, ISO 10303 Product Data Representation and Exchange) allows the exchange of data between CAD systems. For this purpose, there are other standards but STEP has the advantage of being an ISO standard and focus on the semantic specification of the exchanged information. In addition, STEP describes the product data through all its life cycle, and not just the product design information.

EXPRESS is the language used by STEP for the semantic specification of product data and the neutral file is the mechanism developed for the exchange of instances.

An EXPRESS-oriented information system has been presented in this paper. It has the basic tools taht are needed for information definition and management based on EXPRESS. The kernel of the environment consists of a database interface, supported by a relational DBMS, for EXPRESS-oriented manipulation of manufacturing information.

The expressive power of EXPRESS makes easier the modelling task and allows the creation of models with more semantic contents. The information system has the requirements needed by CIM tool users, like flexibility (store the EXPRESS schema in the Metadata Database), invariability for the access functions, concurrent access control, consistency control, manipulation of complex objects, etc.

The information system has been validated in the FAST demonstrator of the CIM-PLATO (ESPRIT 2202) project.

References

Afnor, 1985, Automatisation Industrielle, Representation Externe des Donnees de Definition de Produits. Specification du Standard d'éhange et de Tranfert (SET). Norme Expérimentale Z68-30.

Beg, I and Leuridan, J, (editors), 1988, ESPRIT Project 322. CAD*I, CAD Interfaces status report 4. PFT report 1392, Kernforschungszentrum, Karlsruhe GmbH.

CIM-PLATO Consortium, 1992, Presentation of the FAST Demonstrator at the CIM-PLATO Workshop. Karlsruhe.

DIN, 1986, VDA-FUßCHENSCHNITTSTELLE (VDAFS). Version 1.0. DIN 66301. Beuth Verlag, Berlin.

Gruttke, W.B., 1985, PDES file structure working draft version 3. Physical File Structure/Formal language committee. Internal notes.

ISO 10303 TC 184/SC4, 1992, Product Data Representation and Exchange. STEP. Part 1. Overview and Fundamental Principles. Document N154.

ISO 10303 TC 184/SC4, 1993, Product Data Representation and Exchange. STEP. Part 11. The EXPRESS language reference manual. Document N151.

ISO 10303 TC 184/SC4, 1991, Product Data Representation and Exchange. STEP. Part 21. Clear Text encoding of the Exchange Structure. Document N78.

NBS: US Department of commerce, 1984, IGES: Experimental Solids Proposal (ESP). Washington DC 20234.

RBCM - J. of the Braz. Soc. Mechanical Sciences
Vol. XV - nº 3 - 1993 - pp. 49-55

ISSN 0100-7386
Printed in Brazil

The Welding Arc Pressure

Américo Scotti
Universidade Federal de Uberlândia
Departamento de Engenharia Mecânica
38-400-902 - Uberlândia - MG

Abstract

The aim o the present article is to contribute for a best understanding of the phenomena which occur in an arc column during welding. The origin o pressure on the weld pool is described and discussed. Consensus and disagreement on the matter amongst author are also stated. Practical importance of the subject is conclusively pointed out.
Keywords: Welding, Physics of Arcs Plasma Jet, Arc Pressure.

Introduction

Arc pressure is an important and complex actor in welding Its action influences welding aspects such as metal transfer as well as penetration and bead shape. However, there very few work available from the literature on the subject. Some of them are even contradictory. It seems to exist some confusion on concepts and terminology.

When investigating the action of the arc pressure on the weld pool, most workers use non-consumable electrodes (GTAW, which stands for Gas Tungsten Arc Welding) as the cathode, owing to the "relative" simplicity of this process. Very few models have been established for GMAW (Gas Metal Arc Welding), where the electrode changes its geometry continuously. The characteristics of such arc columns are dominated by metal vapour and vaporisation may play a significant role in gas flow behaviour (Allum, 1981). Due to some similarities, however, most tendencies observed in GTAW can be expected in GMAW.

For didactic purposes, the arc column can be considered as a bell-shaped conductor. The current density within the arc column may assume a Gaussian-shaped radial distribution. The arc shape and the intensity and distribution of the current are claimed to be responsible for a pressure exerted by the arc on the molten metal. Considering the arc pressure as the resultant of forces acting on the weld pool, two main components can be identified, i.e., a dynamic component (plasma jet pressure) and a static component (electro-magnetic pressure), the former composed by two terms (mechanisms).

The first part of the dynamic component is an electromagnetically derived term; any current carrying conductor will have an associate magnetic field, which gives rise to the called Lorentz force ($\vec{I} \times \vec{B}$). The Lorentz force, directed radially toward the centre, is balanced by a radial pressure gradient in the arc. The gradient of this magnetic force along the arc length (Z axis), due to a divergence of the current at the electrode tip, is greatly responsible for the generation of a plasma flow (acceleration of hot "gases", actually plasma, from an area of high current density, the arc root, to an area of low current density, the body of the column). The plasma flow, in turn, induces pressure on the pool.

A second term of the dynamic component of the force is also due to the momentum flow (motion) of the plasma gas (Richardson, 1993) and originates from the expansion of the shielding gas as it is entrained into the arc core and heated. This force acts in the direction of least resistance, i.e., parallel to the arc axis and away from the cathode (as mentioned, in GTAW the electrode is usually the cathode and the plate the anode).

The magnetic field is, by itself, also able to exert a pressure on the pool axially, independently of the motion of the gas within the arc (although the magnitude of the force is dependent on the current density distribution and the axial variation of the arc shape). This is the static component (Lorentz term) referred above.

Savage et al. (1979) consider that the electron impingement force is an additional source of pressure. Choo and his colleagues, 1990, consider that since many investigators have neglected the gouge shear stress, this may be the reason why previous models have been unable to predict the surface depressions based on arc pressure alone. Savage et al. believe that the plasma jet is still the most powerful component of the arc.

Manuscript received: October 1994. Technical Editor: Leonardo Goldstein Jr.

Formulation of the Static Component

With regard to the static component, it can be demonstrated (Richardson, 1989) that the Electromagnetic Pressure (P_{em}) in any point of an infinite circular conductor may be calculated[1] as follows:

$$P_{em} = P_a + \frac{\mu_0 I^2}{4\pi^2 R^2} \quad (1)$$

where P_a is the atmospheric pressure (Nm^{-2}), μ_o the permeability of the free space ($4\pi \times 10^{-7} Hm^{-1}$), I the current (A), and R the arc column radius (m). This expression is only strictly valid for a conductor with uniform current density (Richardson, 1993). In the case of radial and axial current dependencies (a bell-shaped conductor, for instance), P_{em} can be expressed by:

$$P_{em} = P_a + \frac{\mu_0 I J_c}{4\pi^2 R^2} G(r, z) \quad (2)$$

where G may be regarded as a shape factor (function of r, radial position, and z, axial position) and J_c represents the current density at the cathode.

Figure 1 symbolises how a static component would appear in case of a diverging conductor. As pressure is an isotropic property (it does not depend on direction), the action of the pressure due to the static component on a given point of the pool surface leads to axial and radial components. The fact that the current line near the surface of the arc column are not perpendicular to the arc base (what could result in oblique electromagnetic forces), makes no change in the pressure on any point of the arc, as a consequence of the scalar nature of pressure.

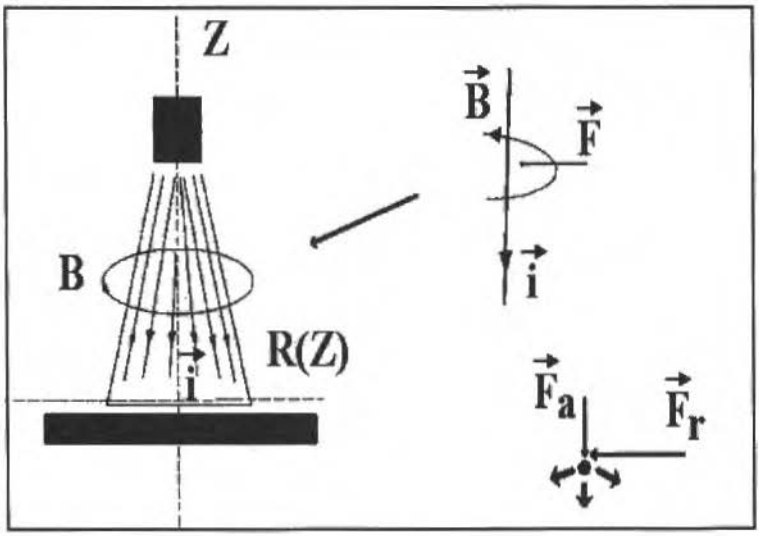

Fig. 1 Schematic representation of the electromagnetic force (F) and its radial (Fr) and axial (Fa) components, generated by the magnetic field (B) and the arc current lines (i)

1. The deduction of Eq. (and Further Eqs.) is negleted since enphasis is placed on welding aspects rather than mathematical ones. This deduction, however, is very familiar for those envolved with Magnetism and Fluid Mechanics.

These jets at the cathode and anode are supposed to be responsible for the stiffness of the arc column near the electrodes, since they tend to be nearly perpendicular to the electrode surfaces. The arc force, or pressure, is associate with the transfer of momentum from the plasma jet to the weld pool surface. Actually, the weld pool surface is a stagnation region, that is, the dynamic pressure is nil. However, one can still consider the dynamic component as the one which changes into static component on the surface, summing up to the original static component. The resultant pressure is known as **stagnation pressure**.

According to Ohara et al. (1986), the static component is considered to be the major part of the arc pressure at low arc voltage while the dynamic component plays the most important role in a high arc voltage level. Concerning the current influence, according to Allum's findings (1981), the magnetic static component of pressure of a 100 A, 3-mm long, argon arc is about 7 mmH_2O, which is significant (but not the major part) when compared to the respective measured manometer pressure value of 34 mmH_2O. The manometer pressure, or stagnation pressure (summation of both components), however increases remarkably with current.

Lancaster (1987) surveying the effects of variables on the arc pressure states that there is a general agreement that the gas kinetic pressure is affected by the electrode dimensions in GTAW. In practical terms, Lancaster (1986) states that for a given shielding gas the anode pressure tends to decrease as the diameter of the cathode arc root increases. In addition, the pressure is reduced, if all other parameter are the same, by using helium or helium-rich gas instead of argon as shielding agent, as illustrated in Fig. 2 (greater density and smaller viscosity of argon vs. helium, leading to a higher momentum).

Savage et al. (1979) found by measurement that the total arc force in GTAW acting against a plate surface is a function of the stand-off (distance from the end of electrode and test plate) and welding current (I_m) and it is not affected by travel speed (TS), shielding gas and electrode geometry. Adonyi et al (1992) demonstrated the influence of current and shielding gas on arc force, as seen in Fig. 3. Ohara et al. measured the GMAW arc pressure beneath an arc and observed an increase in the pressure for decreasing arc voltage (voltage is proportional to CTWD, contact tip-to-work distance, for a given condition). Adonyi et al. also found for GTAW an increase in maximum arc pressure with a decrease in electrode tip-to-workpiece distance, with the effect being most significant for helium shielding. The difference is attributed to the greater spreading of the helium plasma when compared with argon, and, correspondingly, the higher radial momentum dissipation in helium.

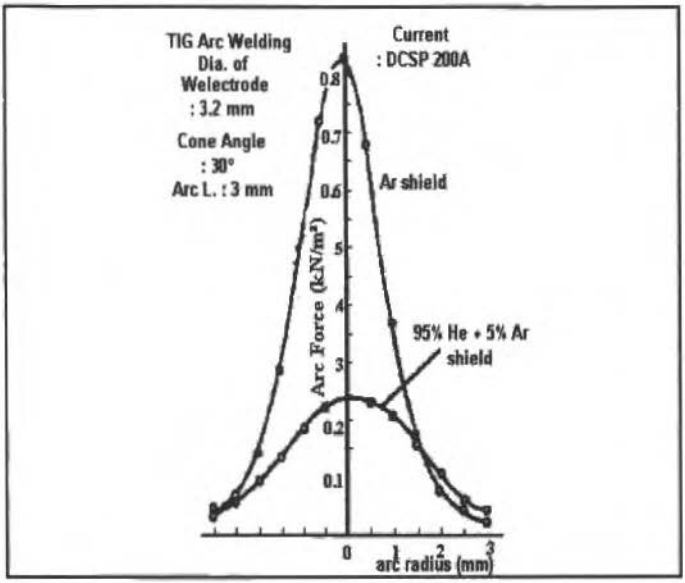

Fig. 2 The effect of shielding gas on arc force (from Lancaster, 1986)

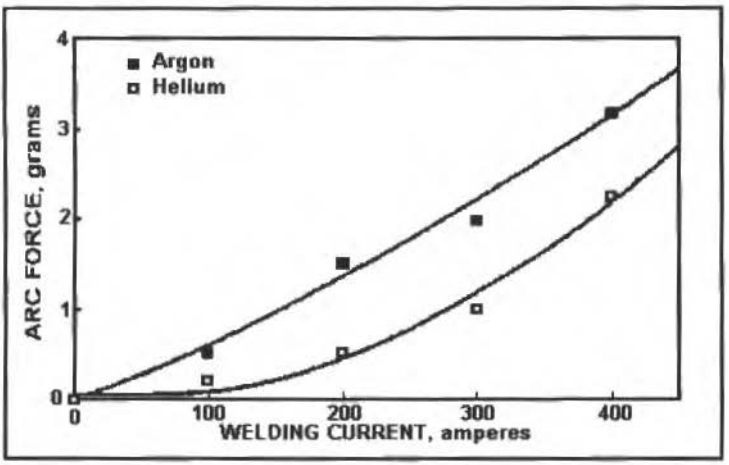

Fig. 3 Plot of arc force vs current for an arc produced between tungsten electrode and cooper anode. Contact tip-to-work distance = 6 mm; travel speed = 5.1 mm/s; argon and helium shielding (after Adonyi et al.)

Schoeck (1963) found that the radius R of the current conducting area of the anode surface increases with electrode spacing in argon arcs. This should indicate an increase of dynamic pressure as stand-off increases (Eqs. 3 or 5). The author, however, agrees with Ohara's and Adonyi et al.'s findings and explains it by the momentum exchange between the streamlines of high velocity near the axis and those of lower velocity further outside and by the mixing of the jet with the surrounding (the increase of the irreverstivity losses, Eq. 5). They do not mention it, but another reason for the relationship between pressure and CTWD might be a decrease in the static pressure as anode radius increases, Eq. 2, lessening the total pressure. Adomyi et al., on the other hand, observed that an increase in the electrode tip immersion depth below the top surface of the plate (while maintaining a constant distance from the electrode tip to the bottom of the groove constant) resulted in a continuous increase in arc force, as shown in Fig. 4.

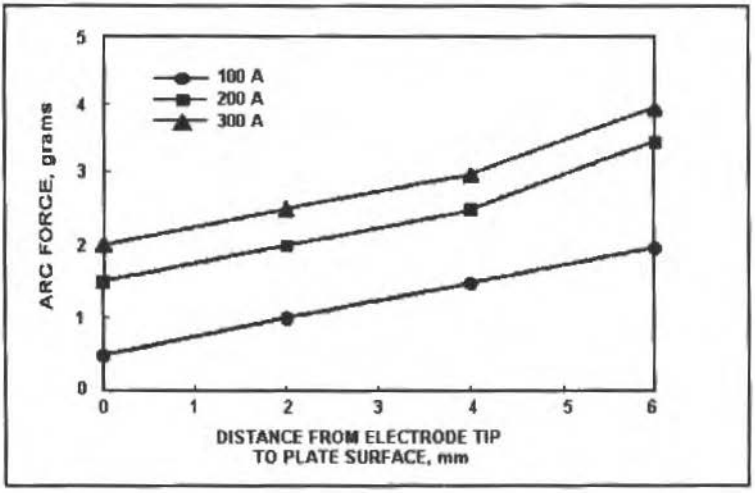

Fig. 4 Arc force vs. electrode to plate surface distance for TIG produced on water cooled anode. The distance between electrode tip and the bottom of the groove was 6 mm; argon shielding (after Adonyi et al.)

These jets at the cathode and anode are supposed to be responsible for the stiffness of the arc column near the electrodes, since they tend to be nearly perpendicular to the electrode surfaces. The arc force, or pressure, is associate with the transfer of momentum from the plasma jet to the weld pool surface. Actually, the weld pool surface is a stagnation region, that is, the dynamic pressure is nil. However, one can still consider the dynamic component as the one which changes into static component on the surface, summing up to the original static component. The resultant pressure is known as **stagnation pressure**.

According to Ohara et al. (1986), the static component is considered to be the major part of the arc pressure at low arc voltage while the dynamic component plays the most important role in a high arc voltage level. Concerning the current influence, according to Allum's findings (1981), the magnetic static component of pressure of a 100 A, 3-mm long, argon arc is about 7 mmH_2O, which is significant (but not the major part) when compared to the respective measured manometer pressure value of 34 mmH_2O. The manometer pressure, or stagnation pressure (summation of both components), however increases remarkably with current.

Lancaster (1987) surveying the effects of variables on the arc pressure states that there is a general agreement that the gas kinetic pressure is affected by the electrode dimensions in GTAW. In practical terms, Lancaster (1986) states that for a given shielding gas the anode pressure tends to decrease as the diameter of the cathode arc root increases. In addition, the pressure is reduced, if all other parameter are the same, by using helium or helium-rich gas instead of argon as shielding agent, as illustrated in Fig. 2 (greater density and smaller viscosity of argon vs. helium, leading to a higher momentum).

Savage et al. (1979) found by measurement that the total arc force in GTAW acting against a plate surface is a function of the stand-off (distance from the end of electrode and test plate) and welding current (I_m) and it is not affected by travel speed (TS), shielding gas and electrode geometry. Adonyi et al (1992) demonstrated the influence of current and shielding gas on arc force, as seen in Fig. 3. Ohara et al. measured the GMAW arc pressure beneath an arc and observed an increase in the pressure for decreasing arc voltage (voltage is proportional to CTWD, contact tip-to-work distance, for a given condition). Adonyi et al. also found for GTAW an increase in maximum arc pressure with a decrease in electrode tip-to-workpiece distance, with the effect being most significant for helium shielding. The difference is attributed to the greater spreading of the helium plasma when compared with argon, and, correspondingly, the higher radial momentum dissipation in helium.

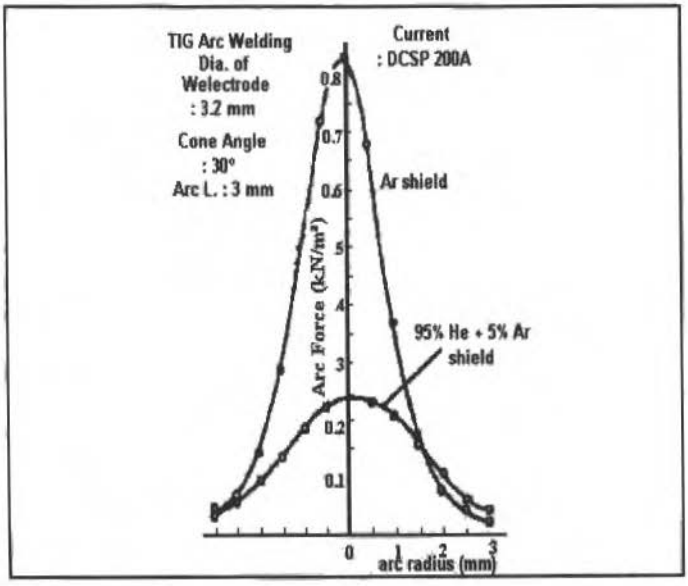

Fig. 2 The effect of shielding gas on arc force (from Lancaster, 1986)

Erokhin (1979) considers the relation P = KI2**, where P is the arc pressure, I the current and K a coefficient which depends on the length of the arc and on certain other factors. He found that K (and consequently P) drops as the arc is lengthened at low current level. This relationship becomes less definite at high current level (I > 200A). He also found that an increase in the diameter of the electrode is conducive to reduction in K and that the value of K is slightly higher for consumable electrodes than for tungsten. In the case of pulsed arc, pressure changes in phase with the pulsing was considered to be a characteristic of the process.

Final Considerations

The objective of studying arc pressure justifies from the effect of this pressure on the welding process performance, bead profile and associate defects. The arc force certainly plays a critical and dominant role in determining the formation and geometry of the weld pool and fusion zone (Adonyi et al.). However, to investigate the influence of arc force on weld-bead formation, it is necessary not only to account for the magnitude of arc force but also to note the deflection of the arc. According to Savage et al. (1979), the arc is deflected by the angling of the electrode and by electromagnetic forces (arc blow, residual magnetic field, and so on). Oscillation is not mentioned, but can certainly be considered as a deflector factor.

Choo et al. (1990) emphasise that most investigators have concentrated on representing weld pool behaviour on the one hand and modelling of welding arcs on the other with relatively little attention being paid to the interfacial regions. "Standard" postulates may represent and oversimplification in many instances. They believe that in case of deformed weld pools, which are observed for operation at high current levels, there may be an important two-way interaction between the welding arc and the molten metal in that the nature of the arc may be affected by the pool shape and vice-versa.

Calculations performed by Choo and his colleagues for deformed anode surfaces have shown that the current and heat flow distributions may be markedly affected by the shape of the free surface of the weld pool. Indeed, it has been shown that the generally postulated Guassian-type distribution may be transformed to a bimodal distribution curve. Savage et al.'s investigation, 1979, indicates that the pressure distribution rather that the total arc force may be the dominant factor in the formation of weld defects.

Adonyi et al's results on subsurfacing GTAW suggest an "arc containment" effect, such that an arc produced within a cavity surrounded by solid metal exerts a greater force than an arc produced (for the same welding parameters and electrode tip-to-work distance) on a flat, open surface. The difference results from the fact that the change in momentum of the fluid impinging the surface (and being reversed in direction) is greater for a convex than a flat surface.

Nomenclature

CTWD=Contact tip-to-work distance

GTAW=Gas Tungsten Arc Welding

GMAW=Gas Metal Arc Welding

μ_o = Permeability of free space (Hm^{-1})

ρ = Plasma density (Kgm^{-3})

A_c = Area cross-section near cathode (m^2)

B = Magnetic field strenght (Tesla)

c = Velocity of light (ms^{-1})

I = Current (A)

J_c = Current density at the cathode (Am^2)

P_a = Atmospheric Pressure (Nm^{-2})

P_{em} = Electromagnetic Pressure (Nm^{-2})

P_{max} = Maximum pressure (dynamic + static) (Nm^{-2})

P_z = Pressure at the arc base (anode) (Nm^{-2})

R = Arc column radius (m)

R_o = Radius of the arc next to the electrode (cathode) (m)

R_z = Radius of the arc base (anode) (m)

V_a = Maximum axial velocity near the anode (ms^{-1})

Conclusion

The use of mathematical and physics concepts on welding phenomena seems to help to understand the sources of pressure on weld pool and the facts related to it. For instance, the dependence of root radius, expressed in Eq. 3, can explain why changes in GTAW electrode vertex angle, damage or erosion result in changes in the observed arc properties. From the Welding Engineer point of view, it is believed that a better understanding of the matter can lead to a more efficient control of penetration and head shape.

References

Adony, Y. et al., 1992, "Investigation of Arc Force Effects in Subsurface GTA Welding", Welding Journal, 71, (9), pp. 321-330.

Allum, C.J., 1981, "Gas Flow in the Column of a TIG Welding Arc", J. Phys. D: Appl. Phys., 14, pp. 1041-1059.

Choo, R.T.C., Szekely, J. and Westhoff, R.C., 1990, "Modelling of High Current Arcs with Emphasis on Free Surface Phenomena in the Weld Pool", Welding Journal, 69, (9), pp. 346-361.

Erokhin, A.A., 1979, "The Force Exerted by the Arc on the Metal being Melted". Automatic Welding, 32 (7), pp. 17-23.

Lancaster, J.F., 1986, The Physics of Welding, Pergamon Press, 2nd edition, IIW/IIS.

Lancaster, J.F., 1987, "The Physics of Fusion Welding - Part I: The Electric Arc Welding", IEE Proceedings, Pt.B, 134, pp. 233-254.

Ohara, M., Fujita, H. and Nishi, T., 1986, "A New Approach to Avoid Undercut for High Speed Submerged Arc Welding", Transactions of ISIJ, 26, pp. 403-409.

Richardson, I.M., 1989, "Welding Technology; Introduction to Arc Physics". MSs course hand-out, Cranfield Institute of Technology, SIMS.

Richardson, I.M., 1993, Cranfield Institute of Technology, SIMS, personal communication.

Savage, W.F., Nippes, E.F., and Agusa, K., 1979, "Effect of Force on Defect Formation in GTA Welding", Welding Journal, AWS, pp. 212-224.

Schoeck, P., 1963. "An Investigation on Anode Energy Balance of High Intensity Arcs in Argon. In: Modern Development in Heat Transfer", IBELE, W.E., Academic Press, N. York, pp. 353-400.

RBCM - J. of the Braz. Soc. Mechanical Sciences
Vol. XVII - nº1 - 1995 - pp. 56-76

ISSN 0100-7386
Printed in Brazil

Thermal Contact Resistance of Wavy Surfaces

Kahoru Torii and Koichi Nishino
Department of Mechanical Engineering and Materials Science
Yokohama National University
Tokiwadai 156, Hodogaya-ku, Yokohama 240, Japan

Abstract

Experimental and analytical studies were made on the thermal contact resistance (TCR) of wavy surfaces. An emphasis was placed on the influence of the surface waviness on the overall TCR in a high vacuum. A nearly spherical waviness with a large radius of curvature was prepared on a metal surface made of copper, aluminum alloy or stainless steel. Heat transfer experiments performed at a high vacuum indicated a power law behavior of the TCR against the nominal contact pressure. The value of the exponent was, however, dependent on the material and the magnitude of surface roughness, and it was substantially smaller than those of the previous correlations. A technique for predicting TCR was developed by using a pressure-measuring film which was capable of visualizing a distribution of contact pressure. Predicted values of the overall TCR agreed reasonably well with the experimental values. It was shown that the macroscopic constriction resistance was predominant for the present wavy surfaces. Effects of the interstitial gas were also examined by varying the ambient air pressure from vacuum to atmospheric. As expected, the overall TCR decreased as the air pressure increased. Such behavior was analyzed by using a simple two-stage heat conduction model which took into account gas conductions through the waviness gap and the roughness gap. The model was shown to be adequate to explain quantitatively the effect of the interstitial gas on the overall TCR for wavy surfaces.
Keywords: Thermal Contact Resistance, Wavy Surface, Prediction Technique, Interstitial Gas.

Introduction

Thermal contact resistance (TCR) often plays a crucial role in heat transfer mechanisms when heat flow paths are interrupted by an interface formed by two contacting solid surfaces. This is because actual engineering surfaces are not perfectly smooth but consist of many peaks and valleys caused by the surface roughness and waviness. Hence, intimate solid-to-solid contacts occur only at discrete parts of the interface. Figure 1 depicts the contact geometry considered here, in which the heat flow is first constricted into a macroscopic contact area formed by the surface waviness, followed by a further constriction into a large number of microscopic contact areas formed by the surface roughness. Since these constrictions take place within a thin volume on both sides of the interface, the temperature profile inside the material will exhibit a sharp drop, ΔT, at the interface. For engineering purpose, it is customary to define the thermal contact resistance as $R\ (=h^{-1}) = \Delta T/q$, where q denotes the heat flux per unit area and h the thermal contact conductance. Comprehensive reviews on this subject can be found in, e.g., Madhusdana and Fletcher (1985), Snaith et al. (1986) and Fletcher (1988).

In general, the modes of heat transfer across the interface are:

- solid conduction through the real contact area,
- convection and conduction through the interstitial fluid, and
- radiation between the contacting surfaces.

Of these, the convection of the interstitial fluid is entirely suppressed for most practical contacts because of the narrowness of the interfacial gap (Snaith et al., 1986), and the contribution of the radiation heat transfer is also negligible at near the room temperatures (Fenech and Rohsenow, 1963). It has been shown that the contribution of the radiation heat transfer for metallic contacts seldom exceeds 2% of the overall heat transfer at temperatures below 900 K (Snaith et al., 1986). Consequently, two different kinds of heat conductions, one through the real contact area and the other through the interstitial fluid, become predominant modes of heat transfer in most practical situations.

Many of the previous studies on TCR were concerned with the microscopic constriction resistance, and hence small test surfaces of an order of one inch in diameter were used in the experiments. It was usually assumed that the real contact spots were distributed uniformly over the test surface. This was a necessary assumption for the use of some statistical approaches that are based on

Invited Lecture. Fifth Brazilian Thermal Sciences Meeting - ENCIT, S. Paulo, S.P., December 7-9, 1994

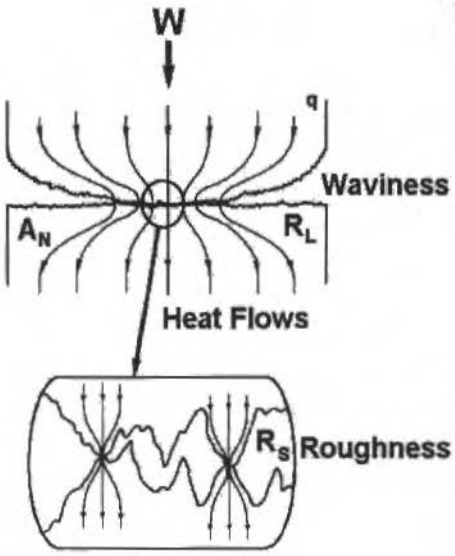

Fig. 1 Contact geometry and heat flow paths

simplified models describing shape, height and number density of the surface roughness. Such approaches as reported by Fenech and Rohsenow (1963), Cooper et al, (1969), Tsukizoe and Hisakado (1972a, 1972b), Mikić (1974) and Yanagi and Tsukada (1981a, 1981b) are useful in predicting the values of TCR, provided that the magnitude of surface waviness is negligibly small. However, no real engineering surfaces of practical size are perfectly flat, implying therefore that the influence of surface waviness may never be ignored. Moreover, the effect of the surface waviness becomes more significant if the contact pressure acting on the surfaces is low, as is often the case in spacecraft applications.

As a typical example of spacecraft applications, a photograph and a drawing of a cold-plate heat exchanger are shown in Fig. 2. It is designed to have a large contact surface (500x500 mm^2) and planned to be installed on an exposed facility of a Japanese experiment module (JEM) of a future space station. Since outer space is high vacuum, the heat transfer between the cold-plate heat exchanger and its payloads occurs only by the mode of pure solid conduction. As seen in this figure, payloads are to be bolted with the heat exchanger through the holes that are installed in a lattice pattern of about 70 mm interval. Since a honeycomb structure is employed, the heat-transfer surface will deform itself easily even for the lightest contact load. Influence of such deformation is clearly illustrated in Fig. 3, in which a distribution of real contact areas is made visible. This visualization is done with a pressure-measuring film that is capable of revealing a contact pressure distribution. It is indicated that the real contact areas are limited only around the bolts because of the localization of the contact pressure and the low rigidity of the contact surface. Since similar non-uniformity of contact may occur in many practical situations, its influence on the overall TCR must be understood sufficiently.

The importance of the macroscopic constriction resistance was noted in several previous studies as reviewed by Snaith et al. (1986). Clausing and Chao (1965) was the first to demonstrate that the macroscopic constriction had a commanding influence for many surfaces commonly encountered in engineering practice. They used cylindrical test pieces having a spherical cap as a surface waviness, and they proposed an expression for predicting the overall TCR. Their expression was based on the elastic deformation of the spherical caps, and good agreement was obtained between the predictions and the experiments for the surfaces having very small roughness. Yovanovich (1969) presented a

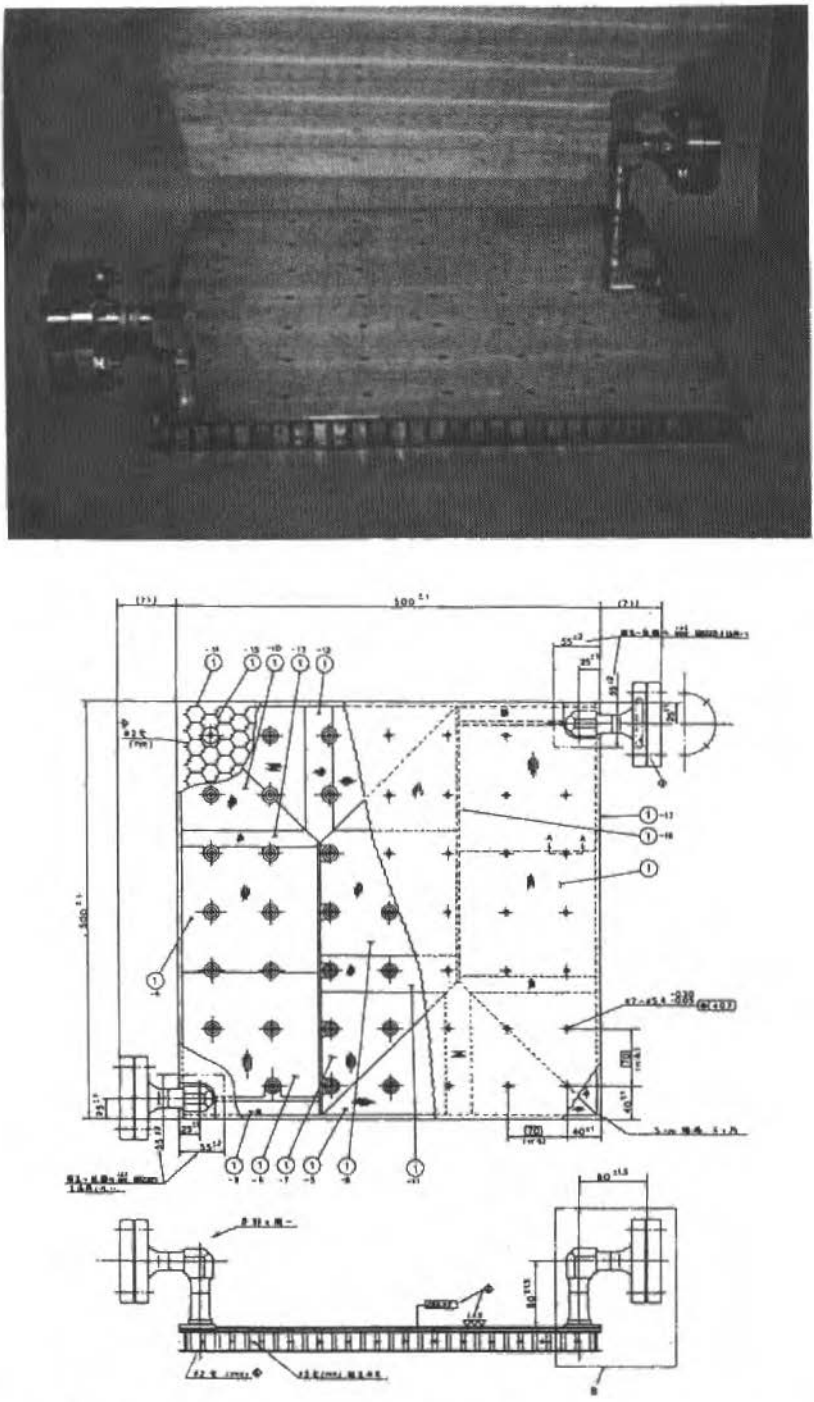

Fig. 2 A photograph and a drawing of a cold-plate heat exchanger for an exposed facility of the japanese experiment module (JEM)

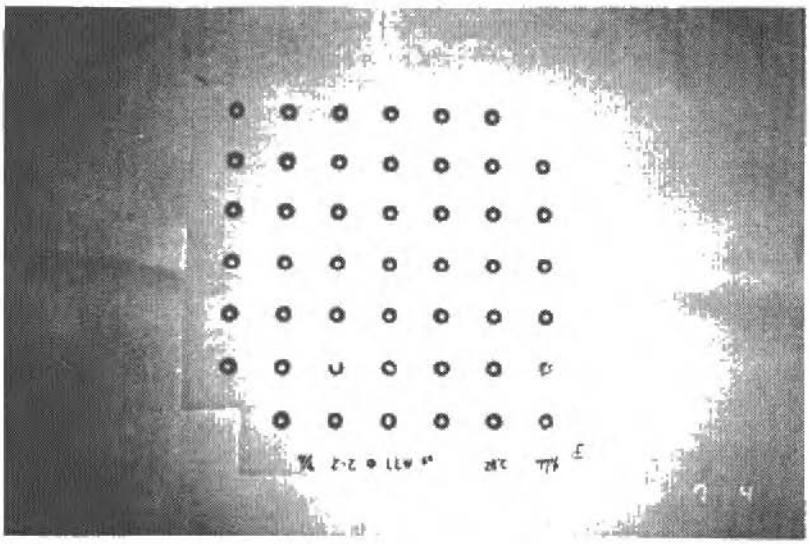

Fig. 3 Visualization of a contact pressure distribution on the cold-plate heat exchanger

that of Clausing and Chao (1965) was taken by Popov and Yanin (1972) to study the influence of surface roughness on the overall TCR for the contact between spherical and flat surfaces. More recently, the influence of surface roughness on the elastic surface deformation was studied by Tsukada and Anno (1979), and their result was used by Yanagi and Tsukada (1983) for the prediction of the overall TCR between spherical and flat surfaces both having various magnitudes of surface roughness.

The basic approach to treating the macroscopic constriction resistance relies on the theory for an electrical constriction resistance (Holm 1967), which can be expressed as follows:

$$R_L = g(x)/2r_L k \qquad (1)$$

Several functional forms of a constriction alleviation factor, g(x), are summarized by Snaith et al (1986). For the use of Eq. (1), the radius of the macroscopic contact area, r_L, must be assigned explicitly, whereas its evaluation is still intractable because of the case-by-case nature of the surface waviness. For this reason, most of the previous studies mentioned above considered only simple shapes of surface waviness such as sphere so that the Hertz theory of elastic surface deformation (e.g., refer to Timoshenko and Goodier, 1951) was applicable. However, there is a wide variation of the shape of surface waviness, and therefore it is desirable to develop an approach which can be applied to arbitrary shapes of surface waviness.

Instead of using Eq. (1), Mikić (1970) proposed a unique method for predicting TCR in vacuum. His method was based on the use of a contact pressure distribution, which was related to a distribution of heat transfer coefficient at the contacting surfaces through an expression derived by Cooper et al. (1969). The overall TCR was obtained by solving the governing Laplace equation. This method was used by Roca and Mikic (1972) who estimated a contact pressure distribution of a bolted joint.

To measure a contact pressure distribution, a stress-freezing technique and an autoradiographic technique were used by Bradley et al. (1971) and Gould and Mikić (1972), respectively.

In the present paper, recent efforts made by the authors (Nishino et al. 1993, Nishino and Torii, 1994) with a view to accumulating fundamental experimental data of TCR and developing a useful prediction technique are described. A special emphasis is placed on the influence of surface

waviness on the overall TCR both in the absence and in the presence of the interstitial gas. In the next section, experimental methods of the heat transfer measurements are described and results are compared with the previous correlations. A prediction technique for TCR and its performance are reported in section 3. In section 4, effects of an interstitial gas on the overall TCR are discussed by referring to the experimental data taken in a wide range of ambient air pressure. In addition, a simple two-stage heat conduction model was introduced to explain the dependency of TCR on the ambient air pressure.

Heat Transfer Experiment

Experimental Method

A test unit used in the present heat transfer measurements is shown in Fig. 4. The shape of the test plates was a square of 100x100 mm^2; this particular shape was chosen in order to simulate a unit cell of the cold-plate heat exchange mentioned in the previous section. The upper test plate with a thickness of 20 mm was heated by a silicone-rubber electrical heater with a heat flux of 5-10 kW/m^2, while the lower test plate of the same thickness was water-cooled by a cooler. An insulating plate made of Bakelite was placed on top of the heater. A copper block was inserted between the lower plate and the cooler to make the heat flow uniform, and silicone grease was used to reduce undesired TCR. The electrical power fed to the heater was measured and monitored with an alternating current power meter.

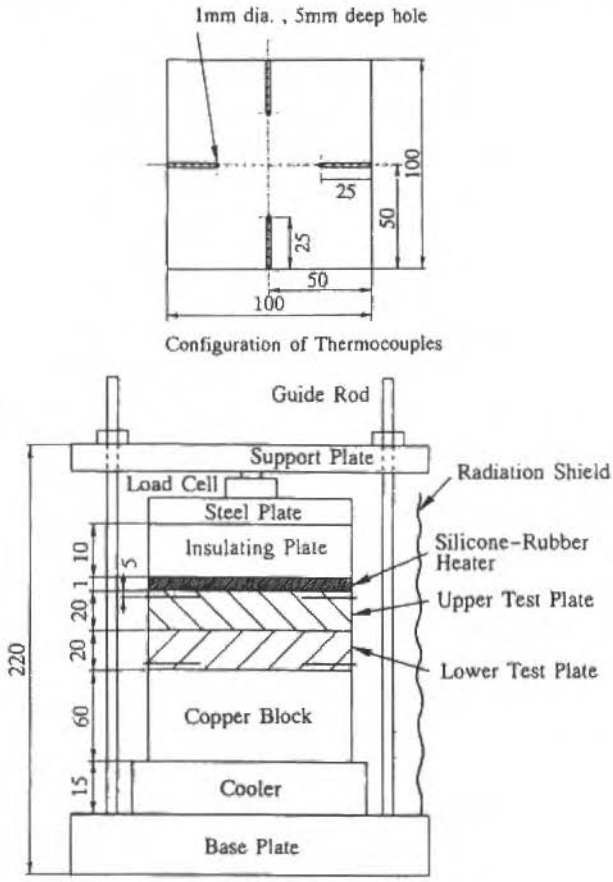

Fig. 4 Test section for the heat transfer experiment

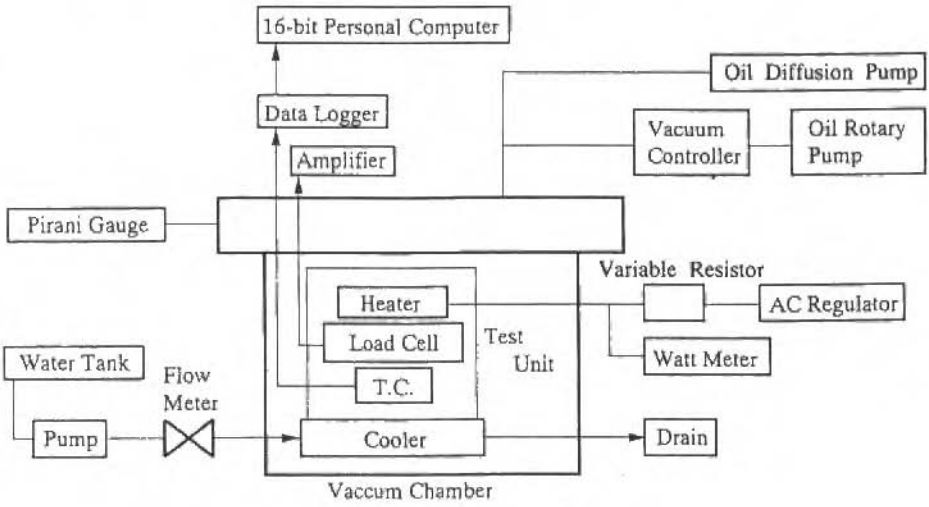

Fig. 5 Vacuum chamber and measurement system

The test plates were loaded by a compression force supplied by four bolts installed near the corner of a steel support plate. The nominal contact pressure which was defined as the total load divided by the nominal contact area, $P=W/A_N$, was in the range of 0.1-0.6 MPa. This low pressure range was selected here to conform to the specifications of the cold-plate heat exchanger which was designed to be used under low compression force. The applied load was measured with a load cell placed between the support plate and a top steel plate. It was confirmed that the applied force was maintained nearly constant throughout the measurement once a thermally steady state was achieved. Since the readings of the load cell included the effect of the material's thermal expansion due to heating, the actual load applied during the heat transfer experiment was measured accurately.

The test unit was surrounded by a radiation shield, and then placed in a vacuum chamber (Fig. 5), which could be evacuated to less than 1.3×10^{-2} Pa (10^{-4} torr) by an oil rotary pump and an oil diffusion pump. The degree of the vacuum was monitored with a vacuum gauge. The operation of the oil rotary pump was controlled by a vacuum controller, and an arbitrary air pressure in the range of 1.3-1.3×10^{5} Pa was achieved automatically. For lower air pressure, both vacuum pumps were controlled manually. Experiments were done either in a high vacuum environment or at a certain ambient air pressure ranging from atmospheric to vacuum.

Temperature measurements were made with a copperconstantan thermocouple 0.133 mm in diameter. The thermocouple was embedded in a hole 1 mm in diameter, located 5 mm below the surface and 25 mm from the side of the test plate. As shown in Fig. 4, a total of four pairs of thermocouple were used, and an average temperature was calculated from their readings. The temperature drop at the interface, ΔT, was calculated by extrapolating the average temperature to the interface. This extrapolation was done with the longitudinal temperature gradient which was evaluated from the heat flux and the thermal conductivity of the test plates. The heat flux measured by the power meter was corrected for the heat conduction loss through the insulating plate.

The material and surface parameters of the test plates are summarized in Table 1. Four different materials of engineering importance, i.e., stainless steel (SUS304), aluminum alloys (A6061 and A5052) and copper (C1020), were examined. Both upper and lower plates were made of the same material. Two different degrees of surface roughness were prepared on each material, i.e., the rough finishing ($\sigma_e \sim 10\mu m$) and the fine (or medium) finishing ($\sigma_e \sim 1\mu m$). For Cases #1-#6, the upper

test plate was given a large-scale waviness, while the lower plate was practically flat. This waviness was produced as a nearly spherical surface whose radius of curvature was approximately 15 m. This large radius of curvature resulted in only a 165\Im flatness deviation (FD), which was defined as a gap distance at the corner of the plates in contact. This amplitude of waviness was selected to simulate, to a realistic degree, the macroscopic non-uniformity of contact in practical situations. In contrast, both upper and lower surfaces were flat in Cases #7 and #8, having the flatness deviation of about 20 \Im. Although spherical surfaces were investigated previously by Clausing and Chao (1965), Kitscha and Yovanovich (1974) and Yanagi and Tsukada (1983), the present shape was unique in its extremely large radius of curvature. It should be mentioned that the test plates of Cases #1-#6 had a freshly prepared surface while those of Cases #7 and #8 did not. As shown later, the hysteresis effect of the loading cycle on the thermal contact conductance, which was known to appear for freshly prepared surfaces, was insignificant under the present range of contact pressure (0.1-0.6 Mpa).

Measurement uncertainties associated with the thermal contact conductance were estimated according to the procedure described in ANSI/ASME PTC 19.1-1985 (1986). The elemental error sources considered were the temperature measurement of the test plates, the reading of the power meter, the estimated conduction heat loss, the radiation heat loss and the thermal conductivity of the materials. Uncertainty intervals estimated thus are dependent on the material, the degree of the surface roughness, the contact pressure and the ambient air pressure. Typical uncertainty intervals estimated at 95 % converage for rough surfaces in high vacuum were 8.4%, 5.1% and 12.3% for SUS304, A6061 and C1020, respectively. At atmospheric pressure, these values respectively increased to 16.1%, 16.9% and 8.1% owing to the larger heat loss and the smaller temperature drop at the interface.

Tab. 1 Material properties and surface parameters of the test plates

Case	Material	k [W/mK]	Young's Modulus [GPa]	Poisson's ratio	$\frac{\sigma_1}{\sigma_2}\sigma_e$ [μm]	$\frac{\sigma_{max,1}}{\sigma_{max,2}}\sigma_{max,e}$ [μm	$\frac{\tan\theta_1}{\tan\theta_2}\tan\theta_e$	H [GPa]	$\frac{\rho_1}{\rho_2}\rho_e$ [μm]	ρ_L [M]	$\frac{FD_1}{FD_2}$ [μm]
#1	SUS304	21	188	0.27	$\frac{7,4}{5,3\,(rough)}\,9,10$	$\frac{31,0}{27,8}\,41,6$	$\frac{0,10}{0,06}\,0,12$	3.261 3.002	$\frac{945}{2850}\,710$	15.8 flat	$\frac{158}{22}$
#2	SUS304	21	188	0.27	$\frac{0,63}{2,14\,(fine)}\,2,23$	$\frac{4,68}{8,75}\,9,92$	$\frac{0,06}{0,11}\,0,13$	3.462 2.918	$\frac{507}{340}\,204$	16.0 flat	$\frac{156}{10}$
#3	A6061	180	69.4	0.33	$\frac{6,0}{9,5\,(rough)}\,11,2$	$\frac{24,4}{37,1}\,44,4$	$\frac{0,09}{0,26}\,0,27$	0.702 0.669	$\frac{945}{209}\,171$	14.9 flat	$\frac{168}{17}$
#4	A6061	180	69.4	0.33	$\frac{0,71}{0,21\,(fine)}\,0,74$	$\frac{6,48}{2,10}\,6,81$	$\frac{0,21}{0,06}\,0,13$	0.718 0.705	$\frac{131}{133}\,66$	15.5 flat	$\frac{161}{24}$
#5	C1020	393	130	0.34	$\frac{5,6}{9,5\,(rough)}\,11,0$	$\frac{24,1}{38,7}\,45,6$	$\frac{0,09}{0,40}\,0,41$	0.996 0.653	$\frac{979}{159}\,137$	15.4 flat	$\frac{163}{15}$
#6	C1020	393	130	0.34	$\frac{1,03}{0,32\,(fine)}\,1,08$	$\frac{6,40}{1,74}\,6,63$	$\frac{0,10}{0,07}\,0,12$	1.072 0.943	$\frac{204}{158}\,89$	15.3 flat	$\frac{164}{13}$
#7	A5052	140	69.7	0.33	$\frac{9,9}{9,9\,(rough)}\,14,0$	----------	$\frac{0,30}{0,30}\,0,42$	0.745 0.745	$\frac{300}{300}\,150$	flat flat	$\frac{20}{20}$
#8	A5052	140	69.7	0.33	$\frac{4,9}{4,9\,(medium)}\,6,9$	----------	$\frac{0,30}{0,30}\,0,42$	0.745 0.745	$\frac{130}{130}\,65$	flat flat	$\frac{20}{20}$

Thermal Contact Resistance in Vacuum

Variations of thermal contact resistance in high vacuum were measured as a function of the nominal contact pressure exerted on the test surfaces. In order to ensure the degree of vacuum, all the measurements were taken at an ambient air pressure lower than 1.3×10^{-2} Pa, except for the measurements with aluminum alloys (Cases #3, #4, #7 and #8) which were made at near 13.3 Pa (0.1 torr). It was, however, verified that if the ambient air pressure was lower than 13.3 Pa, the degree of vacuum had a negligible influence on the measured values of TCR for aluminum alloys (refer to Figs. 13(a) and 13(b)). This is in agreement with the findings of O'Callaghan and Probert (1974).

For freshly prepared surfaces (Cases #1-#6), several sequences of loading and unloading, i.e., loading cycles, were applied in order to observe the hysteresis effect of TCR. The measured results are shown in the form of the thermal contact conductance, $h=(R^{-1})$, in Figs. 6(a) and 6(b). The hysteresis effect was studied previously by Fenech and Rohsenow (1963) and Mikic (1971), and it was revealed that the first unloading (and in some cases subsequent loadings and unloadings) showed smaller values of TCR than the initial loading. Snaith et al. (1986) argued the hysteresis effect to be associated with the elastic relaxation of micro asperities and/or the cold welding for clean metal surfaces. Unlike those findings, the present results do not indicate any appreciable hysteresis, whereas Case #4 (A6061 with fine finishing) exhibits very slightly a trend similar to the previous one. The reason for this negligible hysteresis is likely due to the narrow range of contact pressure in the present experiments.

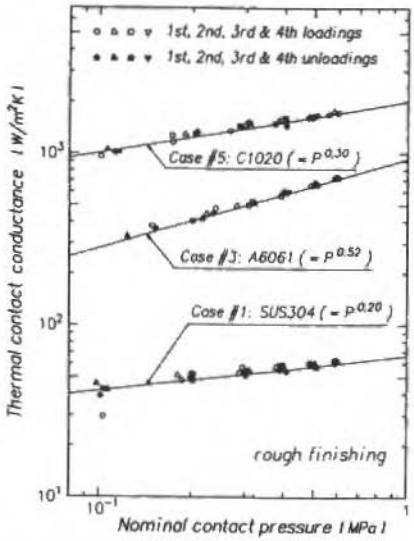

Fig. 6a Variations of thermal contct conductance against the nominal contact pressure: check of the hysteresis effect by the loading cycle for rough surface finishing

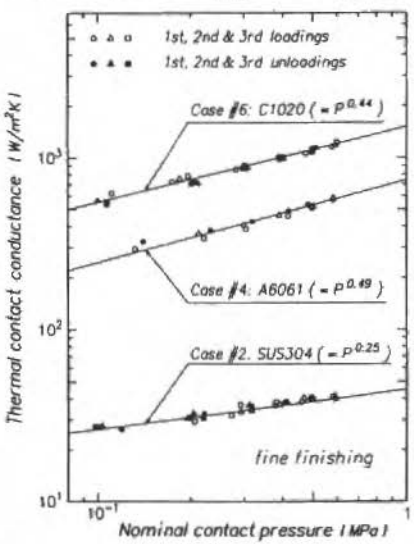

Fig. 6b Variations of thermal contact conductance against the nominal contact pressure: check of the hysteresis effect by the loading cycle for fine surface finishing

A noteworthy feature observed in Figs. 6(a) and 6(b) is the well-defined power-law behavior of the conductance against the nominal contact pressure. However, the value of the exponent varies from one case to the other, and no consistent explanation seems to be possible. This result supports the remark of Clausing and Chao (1965) that there is a region of nearly linear, increase of the conductance with load, but its exponent is dependent on the range of load as well as the material and the surface conditions. It may, therefore, be concluded that a universal power-law behavior between TCR and load can hardly be expected.

There have been many attempts to develop a simple correlation which can be used to predict the value of TCR as a function of some important controlling parameters such as the nominal contact pressure, the interface temperature, the properties of surface roughness and so on. Some of those correlations are summarized by Snaith et al. (1986) and Torii and Yanagihara (1989). Figures 7(a)-7(d) present comparison between the present results and some of the representative correlations. The correlations considered here were theoretical expressions of Clausing and Chao (1965) and Cooper et al. (1969), and laboratory correlations of Fletcher and Gyorog (1971) and Thomas and Probert (1972). Their expressions are as follows:

Clausing and Chao (1965):

$$h^{-1} = \frac{g(x_L)}{2r_L k_m} + \frac{g(x_S)}{2r_L k_m n_S}, \tag{2}$$

Cooper et al. (1969):

$$h = 1.45 \frac{k_m \tan\theta_e}{2r_L k_m} \left(\frac{P}{H}\right)^{0.985}, \tag{3}$$

Fletcher and Gyorog (1971):

$$h\delta/k_m = (5.22 \times 10^{-6} \delta_0^* + 0.036 P^* T_m^*)^{0.56}, \tag{4}$$

Thomas and Probert (1972):

$$hA_N/\sigma_e k_m = 9.58 (PA_N/\sigma_e^2 H)^{0.743} \quad : \text{stainless steel,} \tag{5a}$$

$$hA_N/\sigma_e k_m = 1.93 (PA_N/\sigma_e^2 H)^{0.720} \quad : \text{aluminum.} \tag{5b}$$

Since the theory of Cooper et al. is proposed for non-wavy surfaces, it may not be applicable to Cases #1-#6, in which a substantial surface waviness exists. On the other hand, the theory of Clausing and Chao is developed for the spherical surface waviness similar to Cases #1-#6. The laboratory correlations of Fletcher and Gyorog, and Thomas and Probert are determined from a compilation of available experimental data covering both wavy and non-wavy surfaces. Also included in the figures are the values given by the present prediction technique, which will be described in more detail in the next section.

From the comparison, it is obvious that the previous correlations are in a wide divergence, showing mutual disagreement of more than an order of magnitude. The measured values are roughly in the middle of the band specified by the previous correlations. The theory of Cooper et al. (1969) tends to overestimate the TCR except for Case #1 (stainless steel), while the correlation of Fletcher and Gyorog (1971) gives much lower values than the present measuremens. On the other hand, the theory of Clausing and Chao (1965) and the correlation of Thomas and Probert (1972) can provide reasonable, but not satisfactory, predictions, whereas the latter shows large discrepancy in Case #1 and no prediction is possible for copper plates. The present comparison demonstrates that a universal

correlation can hardly be achieved for a wavy surface, as argued before by Snaith et al. (1986). It is, therefore, desirable to develop a new approach for predicting TCR by taking into account the influence of the surface waviness. Such an attempt pursued by the authors will be presented in the next section.

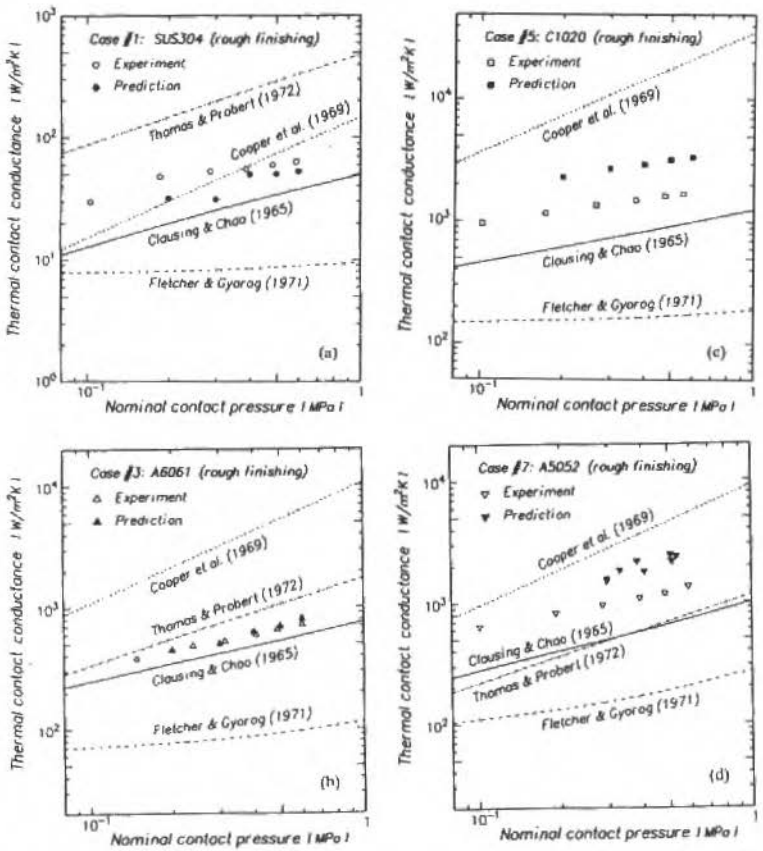

Fig. 7 Comparison of thermal contact conductance with previous correlations

Prediction of Thermal Contact Resistance

Theoretical Background

The existence of surface waviness produces a non-uniform distribution of contact pressure in a macroscopic sense, which leads to a large variation of TCR over the surfaces in contact. This variation is considered to be the main reason for most of the previous approaches to fail in predicting values of TCR with sufficient accuracy. This problem was previously noticed by Mikić (1970), and he proposed a remedy by taking into account explicitly a nonuniform distribution of contact pressure. Since the theoretical aspect of the present prediction is based on his consideration, it is outlined only briefly here. Readers should refer to his paper for full details.

Consider a heat conduction problem in a semi-infinitely long cylinder as depicted in Fig. 8. The upper end of the cylinder is a flat surface in contact with a wavy surface of mating material. Because of the surface waviness, there exists a variation of the local thermal conductance, $h(r)$. It is assumed to be related to the local contact pressure, $P(r)$, through the expression of Cooper et al. (1969), i.e., Eq. (3). The governing Laplace equation is solved for a temperature distribution inside the

cylinder with the appropriate boundary conditions. In order to get a first approximate solution, it is further assumed that the value of the local heat flux at the contact surface is proportional to the local value of thermal conductance. For an axisymmetric geometry, an analytical solution of temperature distribution is expressed by the Bessel functions, and the overall resistance, R, is given as follows:

$$R=(R_c)_S + (R_c)_L, \tag{6}$$

where

$$(R_c)_S = 0{,}345\frac{\sigma_s}{k_m \tan\theta}\left[\int_0^b \left(\frac{r}{b}\right)\left(\frac{P(r)}{H}\right)^{0.985} d\left(\frac{r}{b}\right)\right]^{-1}, \tag{7a}$$

$$(R_c)_L = \frac{8b}{k_m}\sum_{n=1}^{\infty}\left[\int_0^b \left(\frac{r}{b}\right)\left(\frac{P(r)}{P_m}\right)^{0.985} J_0\left(\frac{\nu_n r}{b}\right) d\left(\frac{r}{b}\right)\right]^2 / \nu_n J_0^2(\nu_n). \tag{7b}$$

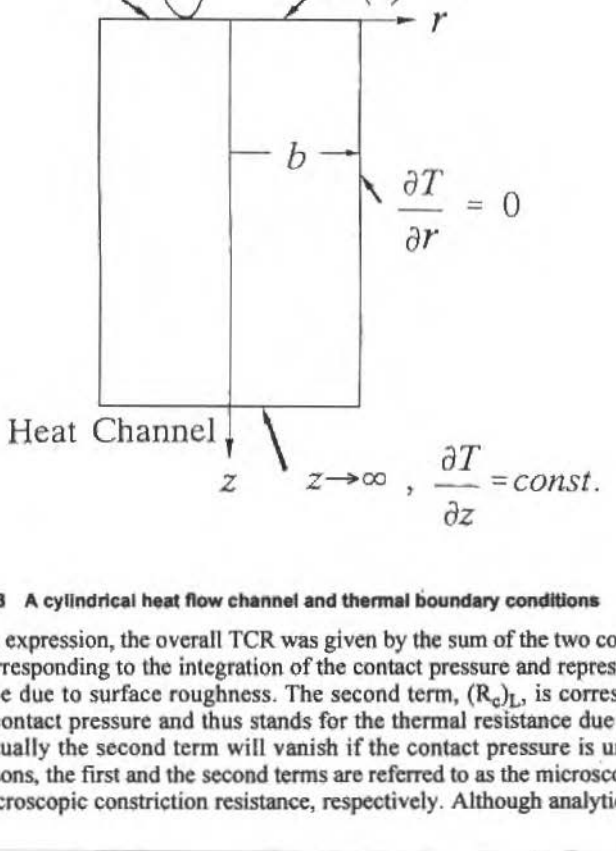

Fig. 8 A cylindrical heat flow channel and thermal boundary conditions

In the above expression, the overall TCR was given by the sum of the two contributions. The first term, $(R_c)_s$, is corresponding to the integration of the contact pressure and represents the thermal constriction resistance due to surface roughness. The second term, $(R_c)_L$, is corresponding to any spatial variations of contact pressure and thus stands for the thermal resistance due to non-uniform contact pressure. Actually the second term will vanish if the contact pressure is uniform over the surface. For these reasons, the first and the second terms are referred to as the microscopic constriction resistance and the macroscopic constriction resistance, respectively. Although analytical solutions are

limited to relatively simple cases such as axisymmetric and line-symmetric, more complicated geometries can readily be treated if a numerical calculation is employed. Such a procedure is now being undertaken by the authors and will be reported elsewhere.

In order to evaluate the microscopic TCR from Eq. (7b), a contact pressure distribution must be either theoretically predicted or experimentally measured. An analytical method can also be used in case of some simple contact geometries (Gould and Mikić , 1972, Roca and Mikić 1972). Although a stress-freezing technique (Bradley et al., 1971) and an autoradiographic technique (Gould and Mikić , 1972) are available to measure a contact pressure distribution, they are not easy to apply to complicated contact geometries. In the next subsection, a new measurement technique developed by the authors is described.

Measurement of Contact Pressure

A pressure-measuring film (Prescale) was used for the measurement of contact pressure distributions. The film, which is schematically shown in Fig. 9, consists of two polyester sheets of about 100 \Im in thickness. Micro capsules containing chromogenic substance are uniformly applied to one side of the top sheet while the opposing side of the bottom sheet is covered with base substance. When it is mixed with the chromogenic substance, the base substance changes its color from white to red. When pressure is exerted on these sheets in contact, rupture of the micro capsules takes place to result in a local mixture of the chromogenic and base substances. In consequence, the contact pressure distribution is visualized as a pattern of red color, whose density is a function of the local pressure.

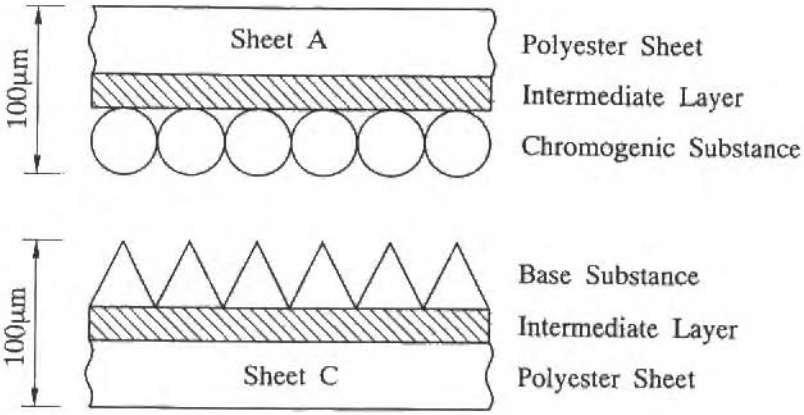

Fig. 9 Structure of a pressure-measuring film

To quantify the contact pressure, calibration relations between color density and pressure intensity are provided in the form of a chart by the manufacturer. Since the color density is affected by the ambient temperature and humidity during loading, several calibration curves according to these conditions are given in the chart. Six types of film covering the pressure range of 0.2-130 MPa are commercially available and one of the films having a sensitivity range of about 0.5 to 2.5 MPa was used presently.

Color density distributions visible in the film were analyzed with a digital image processing system shown in Fig. 10. It consisted of a monochromatic CCD camera, a high-frequency ring lamp, an image grabber (512 x 480 pixels) and a 16-bit personal computer. The TV signal from the CCD camera was digitized by the image grabber, which converted a color density into a monochromatic

brightness level having an 8-bit resolution. The analyzed size of the film was about 100x100 mm^2, resulting in a maximum spatial resolution of 0.2 mm. However, the effective spatial resolution was reduced to about 1 mm because of the moving averaging applied to the original image to reduce random noises in the brightness level. Since this effective spatial resolution was much larger than the length scale of the surface roughness, the measured variation of contact pressure was considered to be associated with the surface waviness. For example, a picture of the color density distribution is shown in Fig.11(a); it was obtained with the test plates of Case #4 (refer to Table 1) under the nominal contact pressure of 0.6 MPa. Note that the nearly circular pattern is due to a spherical waviness prepared on the test plate. At every measurement, a sheet of color standards prepared by the manufacturer was digitized in order to establish a relation between the brightness level and color density. This relation, as well as the color-pressure calibration curves described above, was used to calculate the local contact pressure from the brightness level (Yamashita et al., 1991). Figure 11(b) is a contact pressure distribution thus obtained from the color density pattern of Fig. 11(a).

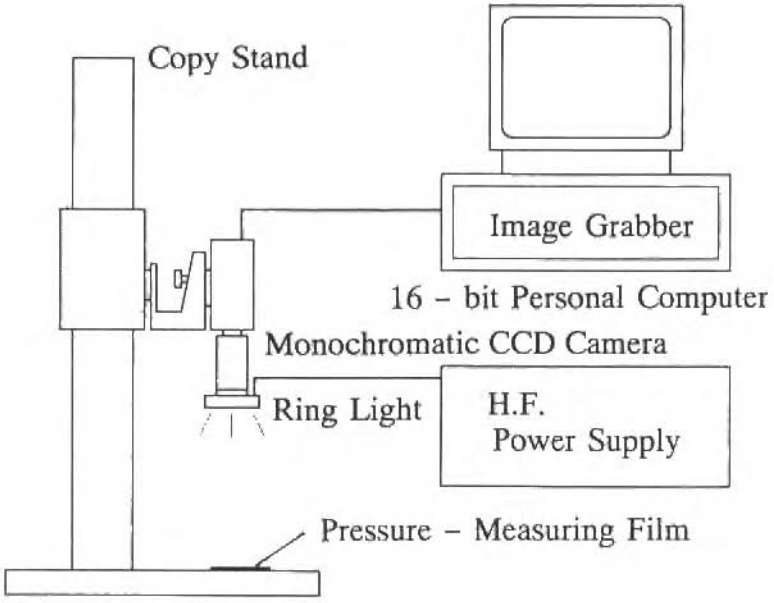

Fig. 10 Digital image processing system

To evaluate measurement uncertainties associated with the present technique, the total load measured by the pressure-measuring film was compared with the nominal load measured by the load cell. It was confirmed that there was reasonable agreement between them, though roughly 10-25 % difference was unavoidable (Nishino et al., 1994). This error was due to the narrow sensitivity range (0.5-2.5 MPa) of the pressure-measuring film. It was, however, anticipated that the uncertainties associated with $(R_c)_L$ be decreased because the quantity required for Eq. (7b) was not the local contact pressure but its ratio to the average contact pressure.

The pressure-measuring film was thick and soft, compared with the height and hardness of the micro asperities of the metal surfaces. This meant that the contact area that was formed in the presence of the film became larger than that formed under the direct metal-to-metal contact in the absence of the film. Therefore, the contact pressure distribution measured with the film should be more widespread than the real distribution. This biasing influence was corrected by using a simple model of elastic-plastic deformation of the micro asperities. The details of the correction, as well as its verification, were described in Nishino et al. (1994).

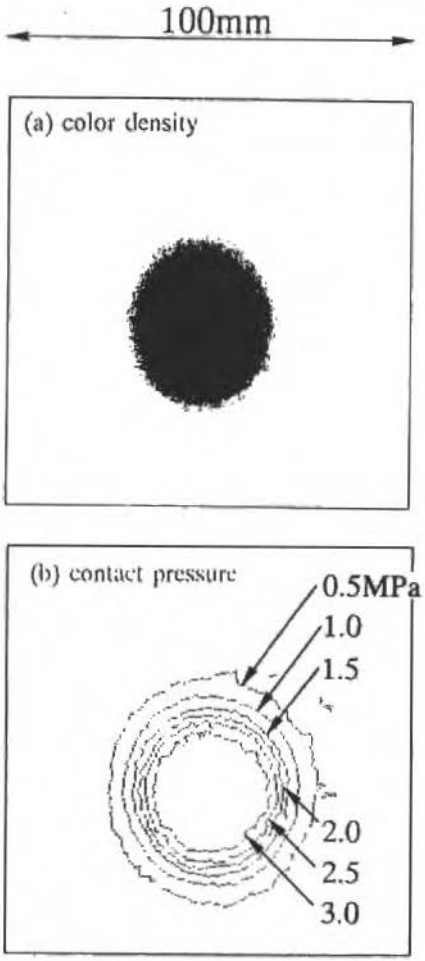

Fig. 11 An example of a color density distribution and corresponding contact pressure distribution

Performance of Prediction

Equations (7a) and (7b) were used to predict the TCR because the measured distribution of contact pressure was approximately axisymmetric for Cases #1-#6, as seen in Fig. 11(b). On the other hand, the measured distribution of contact pressure was roughly linesymmetric for Cases #7 and #8, and hence an alternative equation was used for the prediction. The predicted values are shown in Figs. 7(a)-7(d). An equivalent radius of the square test plate was defined as $[b = (l^2/\pi)]^{1/2}$, and a radial contact pressure profile, [P(r)], was obtained by taking a circumferential average around the center of the pressure distribution.

It is observed in these figures that the predicted values are in good agreement with those obtained by the heat transfer experiment over the entire range of contact pressure examined here. The dependency of the thermal contact conductance on the nominal contact pressure is also well captured in the predictions. Compared with the previous correlations, the present technique can provide further consistent predictions for all the materials. Although not shown here, similarly good agreement is also gained for the plates with fine finishing (Cases #2, #4, #6 and #8). It should be emphasized that the present approach is applicable to more complicated geometries of surface waviness with the help of a numerical procedure to solve the governing Laplace equation.

Figure 12 shows the ratio of the macroscopic constriction resistance to the microscopic one, $(R_c)_L$, $I(R_c)_S$.. It is found that $(R_c)_L$ is predominant for Cases #4 and #6 and larger than $(R_c)_S$ in other cases. The ratio generally increases with nominal contact pressure. This is because $(R_c)_S$ is inversely proportional to the nominal contact pressure whereas $(R_c)_L$ is comparatively insensitive to it. The predominance of $(R_c)_L$ implies that the overall thermal conductance, $((R_c)_L + (R_c)_S)^{-1}$ is essentially determined by the macroscopic part, and its evaluation, therefore, becomes a key factor for accurate prediction of the overall thermal resistance for wavy surfaces.

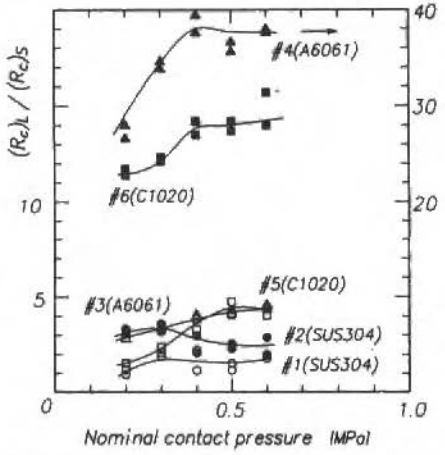

Fig. 12 Ratio of the macroscopic constriction resistance to the microscopic one as a function of the nominal contact pressure

Effects of Interstitial Gas

When the ambient gas is not perfect vacuum, heat conduction may occur through the interstitial gas between two contacting surfaces, and its contribution must be taken into account properly for estimating the overall TCR. A simple assumption that has been proposed in the literature (e.g., Holman, 1989) is that the gas conductance merely adds a new heat flow path which is parallel to the other paths due to the solid conduction. This assumption may be justified if the surface waviness is absent and only the surface roughness exists, as recognized intuitively from the roughness part of Fig. 1. However, the authors (Nishino and Torii, 1994) have reported that the existence of surface waviness requires a separate consideration of the gas conductance through the waviness gap in order for an accurate evaluation of the overall TCR. Their analysis has focused only on the air as an interstitial gas, whereas any change in the gas composition may be handled by the extrapolation of the their approach as long as the thermophysical properties of the gas composition are given properly. In the following, some of their results and analysis are described to show the effect of the interstitial gas on the overall TCR of wavy surfaces.

Variations of the overall TCR against the air pressure ranging from atmospheric to vacuum were measured with the same test plates summarized in Table 1. During the measurement, the nominal contact pressure was kept constant by adjusting an electrical input to the silicone-rubber heater, thus controlling the material's thermal expansion due to heating. The measured variations of the overall TCR in the form of conductance are presented in Figs. 13(a) and 13(b) as a function of ambient air pressure. The nominal contact pressure was 0.3 MPa. As expected, the overall conductance increased with the air pressure because of the enhancement of the gas conductance. If the air pressure is lower than about 10 Pa, the overall conductance almost became insensitive to the air pressure, finally showing a constant value. This tendency is in accord with the previous report (O'Callaghan and Probert, 1974) stating that the conductance is not appreciably affected by the degree of vacuum if it is lower than 13.3 Pa (0.1 torr). The air pressure has the largest effect on the stainless steel plates whose thermal conductivity are the lowest, whereas the air pressure has only a minor effect on the copper plates, particularly for rough finishing.

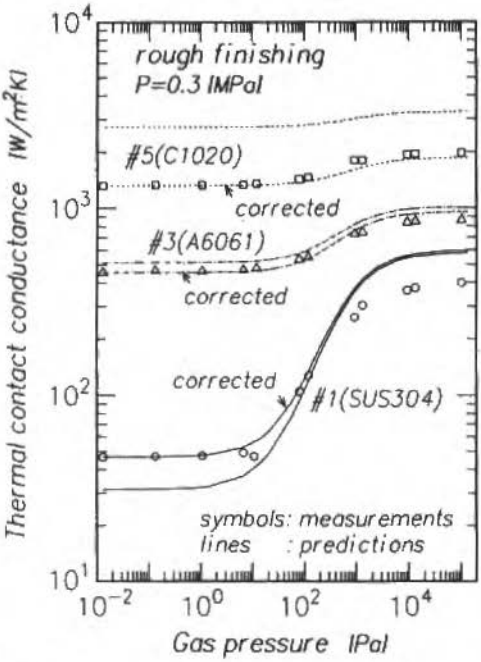

Fig. 13(a) Variation of thermal contact conductance against ambient air pressure for rough surface finishing.

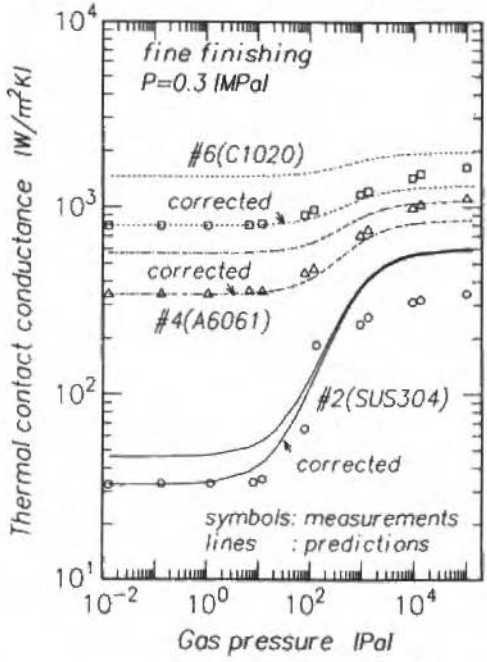

Fig. 13(b) Variation of thermal contact conductance against ambient air pressure for fine surface finishing.

To explain quantitatively such a behavior of TCR against the variation of the air pressure, a simple two-stage heat conduction model was proposed by taking into account the existence of the surface waviness. An electrical analog to the heat flow paths considered in the model is illustrated in Fig. 14. There are two different kinds of heat flow paths through the interstitial gas: one is a path through the waviness gap and the other is a path through the roughness gap. The thermal resistance of the former, $(R_g)_L$, is connected in parallel to the both constriction resistances, $(R_c)_S$, and $(R_c)_L$, while the thermal resistance of the latter, $(R_g)_S$, is connected in parallel to $(R_c)_S$ but in series with $(R_c)_L$. This electrical analog is conformed with the contacting geometry shown in Fig. 1 in the presence of the interstitial gas in the gaps between the two plates. As a result, the overall TCR is given as follows:

$$R^{-1} = (R_g)_L^{-1} + \left[(R_c)_L + \left[(R_g)_S^{-1} + (R_c)_S^{-1}\right]^{-1}\right]^{-1} , \tag{8a}$$

or

$$h = (1-\phi_L)(h_g)_L + \frac{(h_c)_L\left[(h_c)_S + (\phi_L - \phi_S)(h_g)_S\right]}{(h_c)_L + (h_c)_S + (\phi_L - \phi_S)(h_g)_S} , \tag{8b}$$

where the microscopic contact area ratio, $\phi_S (= A_S/A_N)$, is estimated by the ideal plastic flow assumption, i.e., $\phi_S = W/(A_N H)$, while the macroscopic contact area ratio, $\phi_S (= A_S/A_N)$ is evaluated from the measured contact pressure distribution. Their values are summarized in Table 2. If $(h_c)_L \ll (h_c)_S$ (or $(R_c)_L \gg (R_c)_S$) as in Cases #4 and #6 (refer to Fig.12), then $h=(1-\phi_L)(h_g)_L+(h_c)_L$ which means that the surface waviness dominates the whole heat transfer process. On the other hand, if $(h_c)_L = \infty$ and $\phi_L = 1$, as for the completely flat surfaces, then $h=(h_c)_S +(1-\phi_S)(h_g)_S$, indicating that only the terms concerning the surface roughness are involved. Although different mechanisms are involved, these two extremes are the same in the respect that the overall conductance can be evaluated by a simple addition of the gas conductance to the solid conduction. In general, however, such simplification is hardly justifiable because significant variations of $(h_c)_S/(h_c)_L$ exist as shown in Fig. 12.

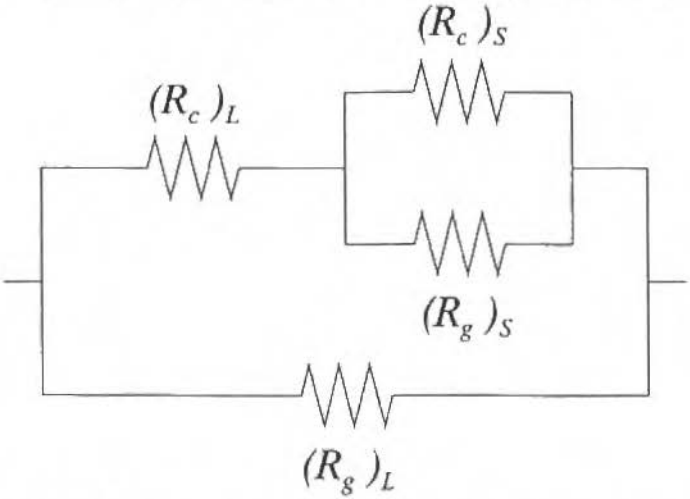

Fig. 14 An electrical analog to the overall heat flow path in the presence of interstitial gas

To predict the overall conductance from Eq. (8b), the gas conductance, h_g, is evaluated by using the thermal conductivity of the gas, k_g, and the characteristic thickness of the gaps, δ, as $h_g = k_g/\delta$. The thermal conductivity is given by the rarefied gas theory (e.g., Holman, 1989) for a wide range of gas pressures. Three flow regimes, i.e., the continuum, the slip and the free-molecule flows, are considered depending on the Knudsen number, $Kn=\lambda/\delta$:

$$k_g \begin{cases} (k_g)_a \text{ for kn} < 001, \\ (k_g)_a / \left(1 + 2\dfrac{2-\alpha}{\alpha}\dfrac{2\gamma_a}{\gamma_a+1}\dfrac{\lambda}{Pr_a\delta}\right) \text{for } 0{,}01 < kn < 3, \\ \delta\dfrac{\alpha}{2}\dfrac{\gamma_a+1}{\gamma_a-1}\left(\dfrac{R_0 P_g^2}{2\pi T_g M_g}\right)^{0.5} \text{ for } 3 < k3, \end{cases} \tag{9}$$

where the mean free path is given by $\lambda = 1.255(\mu_a/P_g)(R_g T_g/M_g)^{0.5}$ and the value of 0.9 is used for the accommodation coefficient, α.

The characteristic gap thickness due to the waviness, δ_L, is determined as the mean thickness of the gap created by the two plates. As for the gap thickness, δ_S, the equivalent rms roughness height, σ_e, is chosen for the rough finishing, while the equivalent maximum roughness height, $\sigma_{max,e}$, is chosen for the fine finishing (for their value, refer to Table 1). The latter is based on the consideration that the contact situation should be governed by some very high asperities if the roughness wave length is small. This is consistent with a previous finding (Cooper et al., 1969) that the total load is essentially supported by the highest asperities. Although the choice of δ_S, has only a minor influence under the present conditions, its importance increases as the surface waviness diminishes.

Table 2 Values of $\backslash l_S$, $\backslash l_L$, $(h_c)_S$ and $(h_c)_L$ for P=0.3 [Mpa].

	#1	#2	#3	#4	#5	#6
$\phi_S/10-4$	1.00	-1.03	4.45	4.34	4.60	3.18
$\phi_L/10-2$	4.52	4.91	8.66	9.07	28.8	7.55
$(h_c)_S$ [W/m^{2}K]	90.4	194	2440	20400	9200	19100
$(h_c)_L$ [W/m^{2}K]	47.8	60.7	651.4	585	3870	15800

The gas conductance as a function of the gas pressure is presented in Fig. 15, where the values of $(K_g)_a$, μ_a, γ_a, Pr_a are evaluated at the mean gas temperature, T_g, under the atmospheric pressure condition. In consequence, the variation of the overall thermal contact conductance is predicted by incorporating the estimated gas conductances (Figs. 13(a) and 13(b)). It is shown that the dependency of the overall conductance on the gas pressure is well reproduced by the prediction in all cases, whereas the agreement seems to be somewhat deteriorated by the difference seen at a perfect vacuum, particularly for copper plate (Cases #5 and #6). Hence included in these figures are the corrected predictions in which this difference at a perfect vacuum is compensated without changing the ratio of $(h_c)_S/(h_c)_L$. With this correction, the agreement becomes very satisfactory, except only for the stainless steel plates at around atmospheric pressure. This discrepancy would be improved if the estimated gap thickness due to the surface waviness is slightly modified. Nevertheless, the present results show that the two-stage heat conduction model is highly useful for understanding and predicting the behavior of TCR against the variation of ambient gas pressure.

Conclusions

The thermal contact resistance for wavy metal surfaces was studied with square test plates made of stainless steel (SUS304), aluminum alloys (A6061 and A5052) or copper (C1020). An emphasis was placed on the existence of surface waviness because it unavoidably appears in many practical situations involving a large heat transfer surface and/or a non-uniform contact pressure distribution. To simulate surface waviness in a reproducible manner, a spherical cap of very large radius of curvature (about 15 m) was given to the contacting surface. In addition, two different degrees of surface roughness, rough finishing and fine (or medium) finishing, were prepared on each material.

Heat transfer experiments performed in a perfect vacuum have revealed that the thermal contact resistance decreased with the nominal contact pressure, and that its behavior was expressed by a simple power-law whose exponent was, however, dependent on the material and surface finishing.

The values of the exponents were in the range of 0.20-0.52, which were substantially smaller than those of the previous findings. As a consequence, the experimental and theoretical correlations proposed in the literature were not capable of providing satisfactory predictions for the present cases.

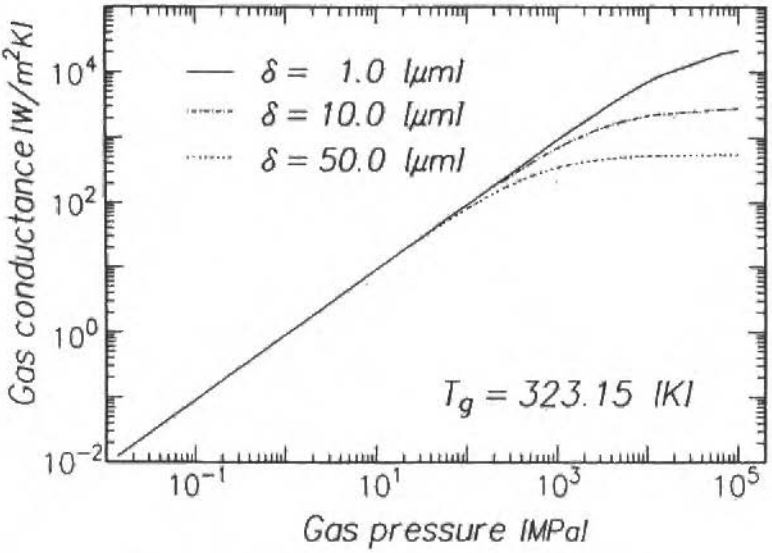

Fig. 15 Variations of air conductance against the air pressure

A novel approach developed by the authors for predicting the thermal contact resistance was described. This approach was based on a theoretical consideration of Mikić (1970) and a new measurement technique for a contact pressure distribution. It utilized a pressure-measuring film which was capable of visualizing a contact pressure distribution. Thermal contact resistance in a high vacuum was predicted by solving the governing Laplace equation with appropriate thermal boundary conditions including those evaluated from the measured distributions of contact pressure. It was demonstrated that the present predictions were in good agreement with the experiments for all the materials and surface finishings examined here. The prediction indicated that the macroscopic constriction resistance due to surface waviness was substantially larger than the microscopic constriction resistance due to surface roughenss. Hence, the consideration of the influence of the surface waviness was shown to become crucial for the accurate prediction of the overall thermal contact resistance.

The influence of the surface waviness was further taken into account for understanding the contribution of heat conduction through the interstitial gas between the contacting surfaces. Some results of the heat transfer experiments made at various ambient air pressure ranging from atmospheric to perfect vacuum were presented. As expected, the thermal contact resistance decreased as the ambient air pressure increased. A simple two-stage heat conduction model was described to exlain quantitatively such experimental results. It was demonstrated that the model reproduced fairly well the behavior of the thermal contact resistance against the variation of the ambient air pressure. In particular, agreement between the model predictions and the experiments became satisfactory if a small discrepancy seen at a perfect vacuum was corrected properly. This success of the two-stage heat conduction model supported the importance of the surface waviness for the prediction of the overall thermal contact resistance.

Acknowledgments

The authors gratefully acknowledge the valuable cooperation *extended by* Drs. M. Hori and R. Akiyoshi at the Technology Research Center, Ishikawajima-Harima Heavy Industires Co., Ldt. They also appreciate the permission by National Aerospace Development Agency (NASDA) of Japan

for the use of the drawing of the cold-plate heat exchanger (Fig. 2 in this paper). The financial supportby The Iwatani Naoji Foundation's Research Grant is gratefully acknowledged.

Nomenclature

A_N = Nominal contact area [m^2]
AL,AS = Macroscopic and microscopic contact areas [m^2]
b = Radius of the heat flow channel [m]
FD = Flatness deviation [m]
g(X) = Constriction alleviation factor
H = Micro Vickers hardness [Pa]
h = Thermal contact conductance per unit area [$W/m^2.K$]
J_n = Bessel function of order n
k = Thermal conductivity [W/m.K]
k_m = Harmonic mean thermal conductivity ($=2k_1.k_2.l(k_1,+k_2)$) [$W/m^2.K$]
ℓ = Side length of a test plate [m]
M = Molecular weight [kg/mol]
n_s = Number of micro-contacts
P,P_g = Contact pressure and gas pressure [Pa]
q = Heat flux per unit area [W/m^2]
R = Thermal contact resistance ($=h^{-1}$) [$m^2.K/W$]
R_0 = Universal gas constant [J/mol K]
$T, \Delta T$ = Temperature and temperature drop [K]
r = Radial coordinate [m]
W = Total load [N]
x = radius ration
α = Accommodation coefficient
γ = Ratio of specific heat
δ = Void or gap thickness [m]
θ = Slope of a micro asperity [rad]
λ = Mean free path of a gas molecule [m]
μ = Dynamic viscosity [Pa.s]
ν_n = Roots of $J_l(\nu_n)=0$
ρ = Radius of curvature [m]
σ = Root mean square value of the roughness height
σ_{max} = Maximum roughness height [m]
ϕ_L,ϕ_S = Macroscopic contact are ratio A_l/A_N and microscopic contact are ratio A_s/A_N

Subscripts

1,2 = Upper and lower plates
a = Atmospheric pressure
c = Constriction
e = Equivalent value
g = Gas
L,S = Macroscopic and microscopic quantities
m = Mean value

References

ANSI/ASME PTC 19.1-1985, 1986, Measurement Uncertainty, Supplement on Instruments and Apparatus, Part 1.

Bradley, T. L., Lardner, T. J. and Mikic, B. B., 1971, "Bolted Joint Interface Pressure for Thermal Contact Resistance", *Trans. ASME, J. Applied Mechanics,* Vol. 38, N°. 2, pp. 542-545.

Clausing, A. M. and Chao, B. T., 1965, "Thermal Contact Resistance in a Vacuum Environment", *Trans. ASME, J. Heat Transfer, Vol.* 87, N°. 2,pp-243-251.

Cooper, M. G., Mikic, B. B. and Yovanovich, M. M., 1969, "Thermal Contact Conductance"., *Int. J. Heat Transfer, Vol.* 12, pp. 279-300.

Fenech, H. and Rohsenow, W. M., 1963, "Prediction of Thermal Conductance of Metallic Surfaces in Contact", *Trans. ASME, J. Heat Transfer, Vol.* 85, N°. 1, pp. 15-24.

Fletcher, L. S. and Gyorog, D. A., 1971, "Prediction of Thermal Contact Conductance between Similar Metal Surfaces", AIAA Progress in Astronautics and Aeronautics, *Heat Transfer and Spacecraft Thermal Control,* J.W. Lucas, Ed., Vol. 24, pp. 273-288, MIT Press.

Fletcher, L S., 1988, "Recent Developments in Contact Conductance Heat Transfer", *Trans., ASME, J. Heat Transfer, Vol.* 110, N°. 4, pp. 1059-1070.

Gould, H. H. and Mikic, B. B., 1972, "Areas of Contact and Pressure Distribution in Bolted Joints", *Trans. ASME, J. Engineering for Industry,* Vol. 94, N°. 3, pp. 864-870.

Holm, R., 1967, *Electric Contacts - Theory and Application,* 4th Ed., Springer-Verlag, New York, p. 16.

Holman, J. P., 1989, *Heat Transfer* (SI Metric Edition.), McGraw-Hill.

Kitscha, W. W. and Yovanovich, M., 1974, "Experimental Investigation on the Overall Thermal Resistance of Sphere-Flat Contacts", Paper N°. 74-113 presented at the AIAA 12th Aerospace Science Meeting, Washington, D. C., pp. 93-110.

Madhusudana, C. V. and Fletcher L. S., 1985, "Contact Heat Transfer - The Last Decade", *AIAA Journal,* Vol. 24, N°. 3, pp. 519-523.

Mikić , B., 1970, "Thermal Constriction Resistance due to Non-Uniform Surface Conditions; Contact Resistance at Non-Uniform Interface Pressure", Int. *J. Heat Mass Transfer,* Vol. 13, pp. 1497-*1500.*

Mikić , B., 1971, "Analytical Studies of Contact of Nominally Flat Surfaces; Effect of Previous Loading", *Tans. ASME, J. Lubrication Technology,* Vol. 93, N°. 4, pp. 451-456.

Mikić, B. B., 1974, "Thermal Contact Conductance; Theoretical Considerations", *Int. J. Heat Mass Transfer*, Vol. 17, pp. 205-214.

Nishino, K., Yamashita, S. and Torii, K., 1993, "Thermal Contact Conductance under Low Applied Load in a Vacuum Environment", *Aerospace Heat Exchanger Technology 1993*, R. K. Shah and A. Hashemi Eds., Elsevier, pp. 763-788 (also to appear in Experimental Thermal and Fluid Science).

Nishino, K. and Torii, K., 1994, "Thermal Contact Conductance of Wavy Metal Surfaces under Arbitrary Ambient Pressure", *Proc. 10th Int. Heat Transfer Conf.*, Vol. 6, pp. 397-402, Bighton, UK.

O'Callaghan, P. W. and Probert, S. D., 1974, "Thermal Resistance and Directional Index of Pressed Contacts between Smooth Non-Wavy Surfaces", *J. Mech. Eng. Sci.*, Vol. 16, N°. 1, pp. 41-55.

Popov, V. M., and Yanin, L. F., 1972, "Heat Transfer during Contact of Machined Metal Surfaces with Waviness and Microroughnesses", *Heat Transfer - Soviet Research*, Vol. 4, N°. 2, pp. 162-167.

Roca, R. T. and Mikic, B. B., 1972, "Thermal Conductance in a Bolted Joint", AIAA *Paper N°. 72-282*.

Snaith, B., Probert, S. D. and O'Callaghan, P. W., 1986, Thermal Resistances of Pressed Contacts, *Applied Energy*, Vol. 22, pp. 31-84.

Thomas, T. R. and Probert, S. D., 1972, "Correlations for Thermal Contact Conductance in Vacuo", *Trans,. ASME, J. Heat Transfer, Vol.* 94, N°. 3, pp. 276-281.

Timoshenko., S. and Goodier, J. N., *1951, Theory of Elasticity, 2nd* Ed., McGraw-Hill, New York, pp. 372-377.

Torii, K. and Yanagihara, J. I., 1989, "Thermal Contact Resistance in Space Environment", *J. Heat Transfer Sciety of Japan.* Vol. 28, N°. 110,pp.79-99.

Tsukada, T. and Anno, Y., 1979, "On the Approach between a Sphere and a Rough Surfaces (lst Report, Analysis of Contact Radius and Interface Pressure), (in Japanese)", *J. Japan Soc. Precision Eng.*, Vol. 45,N°.4,pp.473-479.

Tsukizoe, T. and Hisakado, T., 1972a, "On the Mechanism of Heat Transfer between Metal Surfaces in Contact, Part I: Theoretical Analysis and Experimental Justification of Theory", *Heat Transfer-Japanese Research*, Vol. 1, N°. 1, pp. 104-112.

Tsukizoe, T. and Hisakado, T., 1972b, "On the Mechanism of Heat Transfer between Metal Surfaces in Contact (2nd Report, Thermal Contact Resistance between Metal Surfaces in Vacuum)", *Heat Transfer -Japanese Research, Vol.* 1, N°. 2, pp. 23-31.

Yamashita, S., Torii, K. and Nishino, K., 1991, "Evaluation of Thermal Contact Conductance between Metal Surfaces with Slight Waviness (Measurement of Real Contact Area Using Pressure Measuring Film)", (in Japanese), *JSME*, N°. 910-84, pp. 59-60.

Yanagi, K. and Tsukada, T., 1981a, "Thermal Resistance Caused by Machined Surface Asperities in Contact (lst Report, Theoretical Analysis of Thermal Contact Resistance at Plane Joints Making Their Lay Orientations of Asperities Parallel to Each Other)", (in Japanese), *J. Japan Soc. Precision Eng.*, Vol. 47, N°. 2, pp. 179-184.

Yanagi, K. and Tsukada, T., 1981b, "Thermal Resistance Caused by Machined Surface Asperities in Contact (2nd Report, Comparison between Calculated and Experimental Results of Thermal Contact Resistance in a Vacuum Environment)", (in Japanese), *J. Japan Soc. Precision Eng.*, Vol. 47, N°. 6, pp. 712-717.

Yanagi, K. and Tsukada, T., 1983, "Contact Heat Transfer between Spherical and Plane Surfaces with Microirregularities (Thermal Contact Resistance in Vacuum Environment)", (in Japanese), *J. Japan Soc. Lubrication Eng.*, Vol. 28, N°. 8, pp. 597-602.

Yovanovich, M. M., 1969, "Overall Constriction Resistance between Contacting Rough, Wavy Surfaces", *Int. J. Heat Mass Transfer. Vol.* 12,pp.1517-1520.

RBCM - J. of the Braz. Soc. Mechanical Sciences
Vol. XVII - nº1 - 1995 - pp. 77-88

ISSN 0100-7386
Printed in Brazil

Modelagem da Tensão de Escoamento de Materiais Metálicos em Função da Temperatura e Velocidade de Deformação

Modelling the Flow Stress in Metals as a Function of the Temperature and Strain-Rate

Ernani S. Palma
Depto. de Engenharia Mecânica - UFMG
Av. Antonio Carlos, 6627
CEP.: 31270.901 - B. Horizonte - MG

O. Vöhringer
Institut für Werkstoffkunde I
Universität Karlsruhe - RFA

Abstract

This work presents a mathematical model which describes the plastic deformation of metals. A constitutive equation, based on microstructural aspects of metal is derived. This equation establishes the dependence of the flow stress on the temperature and strain rate. The mathematical model results are then compared with experimental data produced by the authors, indicating the feasibility of the method.
Keywords: Modelling, Plastic strain, Sintered materials, Steel.

Resumo

Neste trabalho realiza-se uma modelagem matemática da deformação plástica de materiais metálicos. Para tanto utilizou-se uma equação constitutiva, a qual foi desenvolvida baseada em aspectos microestruturais destes materiais, que descreve a dependência da resistência mecânica em função da temperatura e velocidade de deformação. Posteriormente, foram comparados os resultados obtidos experimentalmente com aqueles resultantes da modelagem matemática.
Palavras chave: Modelagem, Deformação plástica, Materiais sinterizados.

Introdução

A resistência mecânica de materiais metálicos depende primordialmente da sua microestrutura. Outros fatores importantes são as condições externas de ensaio, como a velocidade e temperatura de deformação. A influência destes dois parâmetros sobre as propriedades mecânicas em ensaios de tração, e/ou compressão, uniaxiais tem um significado básico para a compreensão da deformação plástica dos metais e vem sendo motivo de pesquisas há bastante tempo (Seeger, 1981, e Sestak, 1978).

O aumento da resistência mecânica de materiais metálicos com a queda da temperatura de deformação em intervalo compreendido entre T=0 K e um valor crítico T_0, o qual é função do material e velocidade de deformação, é um fato bastante conhecido. Hoje em dia é amplamente aceito que, para ensaios com temperaturas inferiores a $T = 0{,}3\ T_F$ (T_F = temperatura de fusão em K) e velocidades de deformação menores que $10^4\ s^{-1}$, este acréscimo da resistência mecânica é devido ao movimento de discordâncias sobre obstáculos, cujos campos de tensões são de curto alcance, os quais podem ser vencidos com auxílio de energia térmica.

Este trabalho tem por objetivo modelar a variação da tensão de deformação de materiais metálicos ccc em função da temperatura e velocidade de deformação e comparar posteriormente estes resultados com aqueles obtidos experimentalmente. Para tanto será usado uma equação constitutiva que descreve a interação entre as discordâncias móveis e os obstáculos de curto alcance.

Deformação plástica ativada termicamente

Considera-se normalmente que a tensão de deformação plástica de um metal consista de duas componentes básicas:

Manuscript received:October 1994 Technical Editor: Agenor de Toledo Fleury.

$$\sigma = \sigma^* (T, \varepsilon, \text{estrutura}) + \sigma_E (G(T), \text{estrutura}) \quad (1)$$

onde σ^* é a componente dependente da temperatura, denominada tensão de deformação térmica e σ_E é a componente que reflete o efeito da estrutura de discordância existente no metal, denominada tensão de deformação atérmica, indicando que, exceto pela dependência do módulo de cisalhamento, ela independe completamente da temperatura.

σ^* é determinada pela interação entre discordâncias móveis e os obstáculos com campos de tensões de curto alcance, os quais podem ser vencidos com auxílio da vibração térmica da rede cristalina. O processo dominante de ativação térmica em metais ccc é a superação da tensão de Peierls e em metais cfc é a interceptação de discordâncias na chamada floresta de discordâncias (Macherauch e Vöhringer, 1978, e Reed-Hill, 1982). A Fig. 1 mostra esquematicamente a variação da tensão de escoamento em função da temperatura e velocidade de deformação. Para T = 0 K a probabilidade de ativação térmica é nula e σ^* atinge seu valor máximo $\sigma^* = \sigma^*_0$. Para temperaturas superiores a T_0 a energia térmica é suficiente, sem qualquer auxílio de tensões externas, para superar a tensão de Peierls, ou seja, $\sigma^* = 0$. Os obstáculos de curto alcance são parcialmente ativos entre as temperaturas limites T = 0 K e $T = T_0$, onde σ^* é função da velocidade e temperatura de deformação.

A resistência oferecida pelos obstáculos, cujos campos de tensões são de curto alcance, pode ser descrita pela sua curva força-distância como mostra esquematicamente a Fig. 2a (Burgahn, 1991).

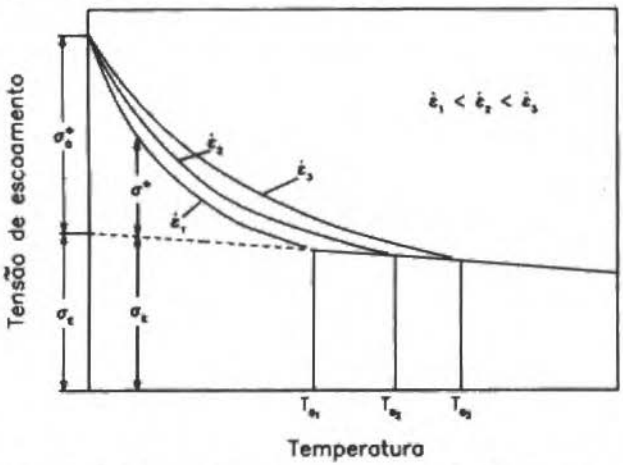

Fig. 1 Variação da tensão em função da temperatura e velocidade de deformação (esquematicamente)

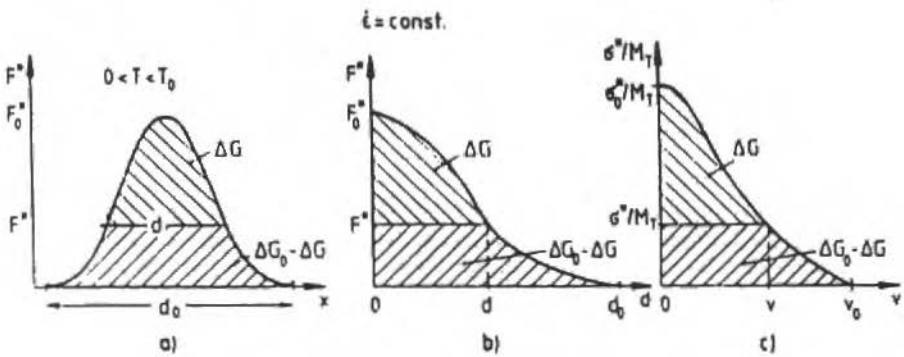

Fig. 2 Curva força-distância de um obstáculo, cujos campos de tensões são de curto alcance, e sua superação através de ativação térmica

Para temperatura T = 0 K é necessária uma força externa F_0^* para que o obstáculo seja vencido pela discordância, já que não existe qualquer vibração atômica nesta temperatura. Com o aumento de temperatura, necessita-se de forças externas F* menores, uma vez que uma parte do obstáculo é vencido somente pela vibração da rede cristalina. Para temperaturas $T \geq T_0$ (ver Fig. 1) todo o trabalho de superação do obstáculo é fornecido termicamente e a entalpia livre de ativação atinge o valor ΔG_0, o qual é um parâmetro característico do obstáculo, ou seja

$$\Delta G(T_0) = \Delta G_0 \tag{2}$$

Além disto, sabe-se que a velocidade de deformação de materiais metálicos pode ser escrito como (Vöhringer, 1987)

$$\dot{\varepsilon} = \dot{\varepsilon}_0 \exp\left[\frac{-\Delta G(T)}{kT}\right] \tag{3}$$

onde $\dot{\varepsilon}_0$ é a velocidade crítica de deformação e k é a constante de Boltzmann. Utilizando-se as Eqs. (2) e (3) pode-se determinar T_0:

$$T_0 = \frac{\Delta G_0}{k \ln(\dot{\varepsilon}_0/\dot{\varepsilon})} \tag{4}$$

Através de adequada transformação da Fig. 2a, chega-se à Fig. 2c, com $\tau^* = \sigma^* / M_T$ (M_T é o fator de Taylor e vale 2,75 para metais ccc). O volume de ativação v é definido por

$$v = bld \tag{5}$$

onde b é o vetor de Bürger, l é a distância entre dois obstáculos consecutivos e d é a largura do obstáculo.

A Fig. 2c acima mostra a parcela de energia necessária para vencer a resistência oferecida pelos obstáculos de curto alcance e fornece a base para sua determinação experimental. Além disso, através do conhecimento da largura do obstáculo d = f(σ^*), é possível modelar a variação da tensão de deformação térmica σ^* em função da temperatura.

A energia de ativação total do obstáculo ΔG_0 é determinada pela área sob a curva da Fig. 2c:

$$\Delta G_0 = \frac{1}{M_T} \int_0^{v_0} \sigma^*(v)\, dv \tag{6}$$

A parcela da entalpia que é fornecida termicamente ΔG (T pode ser calculada pela equação

$$\Delta G_0 = \frac{1}{M_T} \int_0^{v} \sigma^*(v)\, dv - \frac{1}{M_T} \sigma^* v \tag{7}$$

Das Eqs. (6) e (7) obtém-se a parcela da energia que deve ser fornecida externamente (mecanicamente) para temperaturas compreendidas entre T = 0 K e T = T_0:

$$\Delta G(T) - \Delta G(T) = \frac{1}{M_T} \int_v^{v_0} \sigma^*(v)\, dv + \frac{1}{M_T} \sigma^* v \tag{8}$$

Para determinação da energia de ativação, torna-se necessário o conhecimento do volume de ativação v e sua dependência da tensão de deformação, o qual é definido por (Macherauch, 1992):

$$v(T,\dot{\varepsilon}) = M_T kT \left.\frac{\partial \ln(\dot{\varepsilon})}{\partial \sigma^*}\right|_T \quad (9)$$

A variação de tensão de deformação plástica $\Delta\sigma^*$ causada por variações bruscas da velocidade de deformação em ensaios de tração ou compressão é devida à parcela da componente térmica da tensão, tornando-se assim possível a determinação experimental de $\Delta\sigma$ através de uma modificação da Eq. (9):

$$v(T,\dot{\varepsilon}) = M_T kT \left.\frac{\Delta \ln(\dot{\varepsilon})}{\Delta \sigma^*}\right|_T \quad (10)$$

Modelagem Matemática

A dependência existente entre a tensão e a temperatura de deformação pode ser descrita através de uma adequada modelagem matemática da curva força-distância de um obstáculo de curto alcance (Fig. 2), cuja superação é ativada termicamente. Para tanto procura-se determinar corretamente a forma desta curva através da seguinte equação constitutiva

$$\sigma^* = \sigma_0^* \left[1 - \left(\frac{\Delta G(T)}{\Delta G_0}\right)^n\right]^m \quad (11)$$

onde σ_o^* é a parcela de tensão térmica para T = 0 K, m e n são parâmetros dessa equação (Burgahn, 1991). Além disso assume-se que

$$\frac{\sigma_G(T)}{G(T)} = \frac{\sigma_{G0}}{G_0} = \text{const} \quad (12)$$

Usando-se as Eqs. (1) e (2), pode-se calcular a parcela da tensão de deformação térmica:

$$^*(T,\dot{\varepsilon}) = \sigma_x(T,\dot{\varepsilon}) - \left[\sigma_G\left((T_0)\frac{G(T)}{G_0}\right)\right] \quad (13)$$

A dependência do módulo de cisalhamento G(T) da temperatura é determinada experimentalmente e/ou através da equação (Wawra, 1978)

$$G(T) = K_1 + K_2 T + K_3 T^2 \quad (14)$$

com $K_1 = 87716{,}4$ N/mm^2, $K_2 = -19{,}0056$ N/K mm^2 e $K_3 = 8{,}056 \cdot 10^{-5}$ N/K^{2}mm^2.

O obstáculo de curto alcance é caracterizado pelo diagrama $\sigma^* / M_T - v$, o que permite a determinação da parcela de energia que deve ser fornecida mecanicamente ($\Delta G_0 - \Delta G(T)$, Eq. (8) através do ajuste da hipérbole

$$\sigma^*(v) = \frac{a}{(ev - c)^d} - b \quad (15)$$

aos pontos experimentais. Nesta equação a, b, c, d, e são parâmetros de ajuste.

O conhecimento da variação de $\Delta G_0 - \Delta G(T)$ com a temperatura permite a determinação de ΔG_0 e da temperatura T_0 através da extrapolação da curva obtida para T = 0 K e para $\Delta G =$, respectivamente. A determinação dos parâmetros constitutivos σ_o^*, m e n é possível usando-se as equações (Burgahn, 1991, e Palma, 1994)

$$\sigma^* = \sigma_o^* \left[1 - \left(\frac{T}{T_0}\right)^n\right]^m \quad (16)$$

$$\Delta\sigma^* = \sigma_o^* mn \frac{\Delta \ln \varepsilon}{\ln(\varepsilon_0/\varepsilon_1)} \left[1 - \left(\frac{T}{T_0}\right)^n\right]^{m-1} \left(\frac{T}{T_0}\right)^n \quad (17)$$

$$\sigma^*(\dot{\varepsilon}) = \sigma_o^* \left[1 - \left(\frac{kT \ln(\dot{\varepsilon}_0/\dot{\varepsilon})}{\Delta G_0}\right)^n\right]^m \quad (18)$$

Procedimento Experimental

Para os ensaios experimentais, foram usados aço 1045, com tamanho de grão igual a 5μm, ligas sinterizadas Fe-C-Cu com porosidade total P = 5,9% e 12,3%, Fe-P, Fe-Cu e Fe com porosidade total de 12,3%. Esses materiais apresentam um tamanho de grão de 20 μm. Os ensaios de tração foram realizados utilizando-se uma máquina de ensaios universal (Fábrica Roell e Korthaus, modelo SG, 300 KN) em um intervalo de temperatura compreendido entre 77 K e 370 K com velocidade de deformação $\dot{\varepsilon} = 2{,}10^{-4}\,s^{-1}$. Os ensaios de variação de velocidade de deformação foram realizados no mesmo equipamento e intervalo de temperatura acima. Nestes ensaios o corpo de prova é sujeito a vários ciclos em que a velocidade de deformação varia bruscamente de um fator 10, passando-se de $\dot{\varepsilon}_1 = 2{,}10^{-4}\,s^{-}$ para $\dot{\varepsilon}_2 = 2{,}10^{-3}\,s^{-}$ e vice-versa. O controle da velocidade de deformação foi feito automaticamente através do controle da velocidade de deslocamento do travessão da máquina. A rápida mudança da velocidade de deformação foi possível através de programação da máquina de ensaios, onde as velocidades desejadas eram armazenadas na sua memória e a mudança ocorria com um simples comando, via computador. A curva tensão-deformação apresenta o aspecto mostrado na Fig. 3.

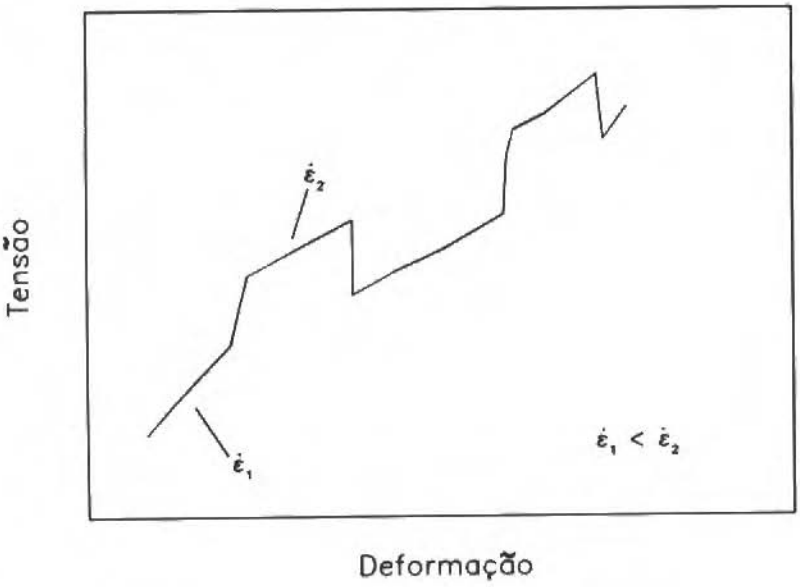

Fig. 3 Curva tensão-deformação com variação da velocidade de deformação

As dimensões dos corpos de prova utilizados nos ensaios experimentais, acima descritos, são mostrados na Fig. 4.

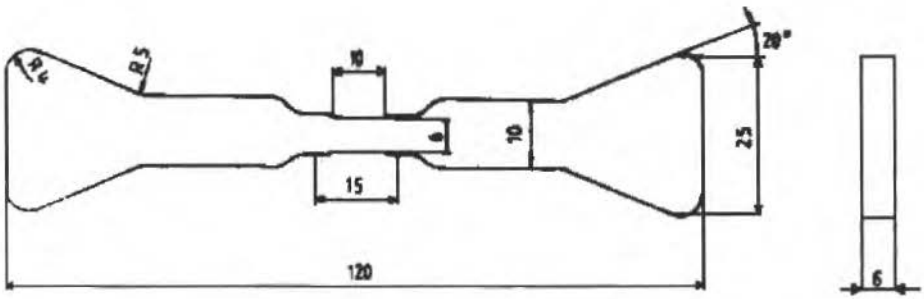

Fig. 4 Corpo de prova utilizado nos ensaios experimentais

A variação da tensão de deformação plástica Δ^*_σ causada pela mudança na velocidade de deformação foi determinada utilizando-se o método das tangentes como mostra esquematicamente a Fig. 5 (Munz e Macherauch, 1966).

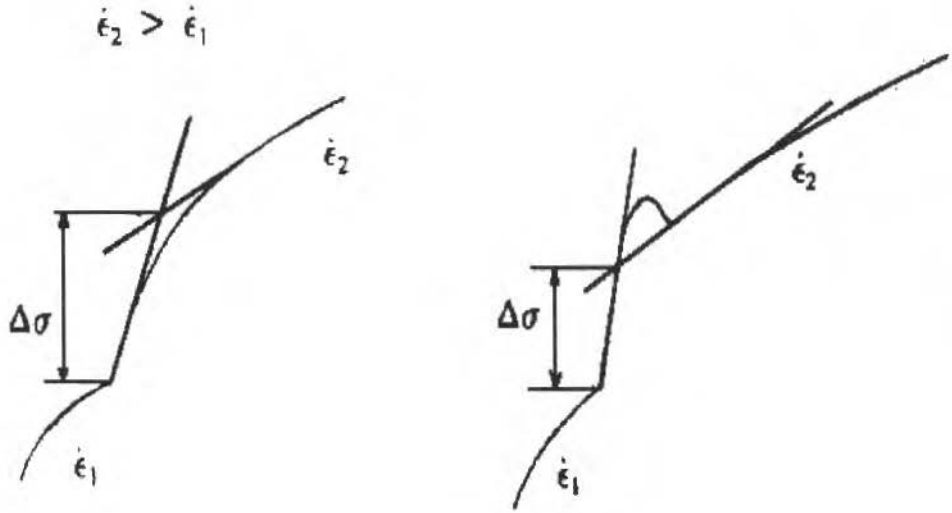

Fig. 5 Determinação da variação de tensão em ensaios com variação da velocidade de deformação

Para a modelagem da tensão de deformação em função da temperatura com a equação constitutiva (11), foi utilizado um programa desenvolvido por Schulze (1988), Burgahn (1991) e Palma (1994). Para rodar esse programa, são necessários os valores da tensão de deformação e do

módulo de cisalhamento em função da temperatura. Inicialmente, o valor de T_0 (Fig. 1) é determinado manual e grosseiramente pelo usuário. O volume de ativação v e a parcela da tensão de deformação térmica σ^* (T) são determinados pelas Eqs. (10) e (13) respectivamente, possibilitando assim traçar um diagrama σ^* (T) - v, o qual caracteriza o obstáculo de curto alcance. O cálculo de $\Delta G_0 - \Delta G$ (T) é feito pelo ajuste da hipérbole Eq. (15) aos pontos da curva σ^* / M_T - v. Este ajuste pode ser influenciado pelo usuário. Após algumas interações, os valores de T_0 e ΔG_0 são precisamente determinados. Quando a diferença entre o valor de T_0 (manual), previamente estimado pelo usuário, e T_0 calculado pelo programa for menor que 5 K considera-se o processo encerrado. Através das Eqs. (16) a (18), os parâmetros m, n e σ_o^* são determinados e a tensão de deformação plástica é calculada por

$$\sigma = \sigma_E + \sigma_o^* \left[1 - \left(\frac{T}{T_o} \right)^n \right]^m \qquad (19)$$

Para a solução desse sistema de equações, foi usado um processo iterativo, o qual está detalhadamente explicitado em Stoer (1983).

Análise dos Resultados

Para efeito de comparação da modelagem realizada, confrontaram-se nas Figs. 6, 7 e 8 os valores da tensão de escoamento a 0,2% das ligas Fe-C-Cu, os valores da tensão de escoamento a 1,5% de 1045 e da variação de tensão $\Delta\sigma^*$ em virtude da variação da velocidade de deformação obtidos experimentalmente (representados pelos símbolos) com as curvas obtidas respectivamente pela equação constitutiva (19) e pela Eq. (17). Observa-se que as curvas obtidas representam muito bem os valores experimentais.

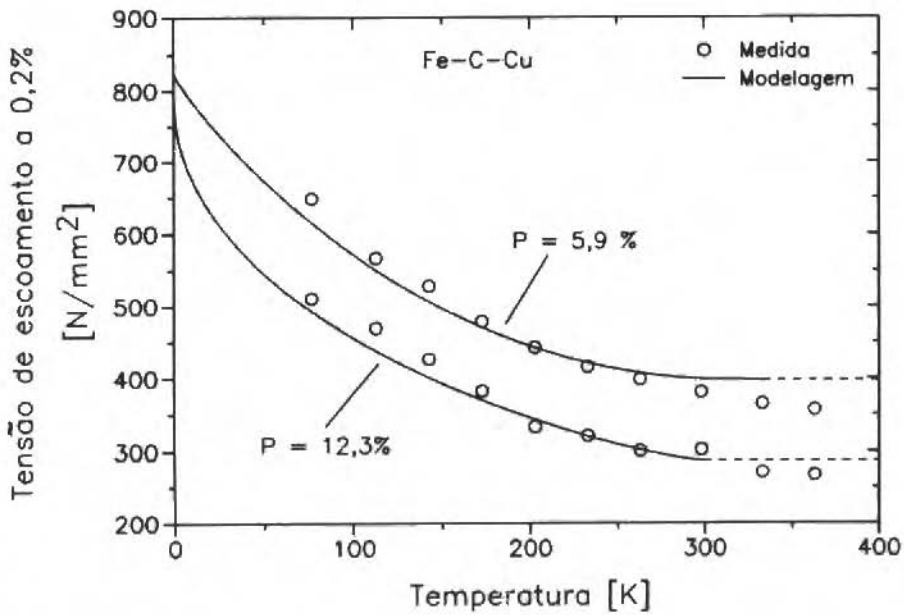

Fig. 6 Tensão de escoamento a 0,2% de deformação plástica das ligas Fe-C-Cu em função da temperatura e respectiva modelagem

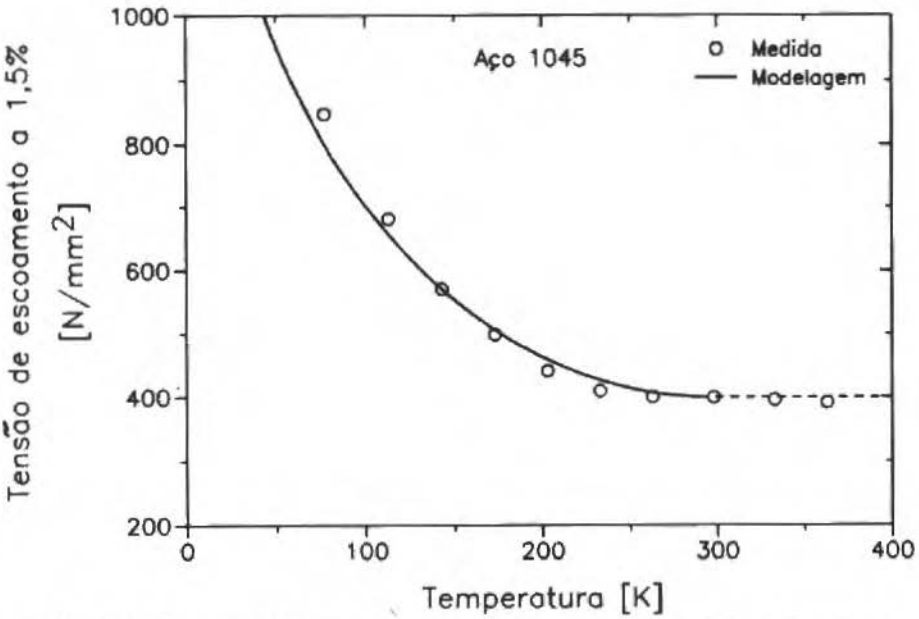

Fig. 7 Tensão de escoamento a 1,5% de deformação plástica do aço 1045 em função da temperatura e respectiva modelagem

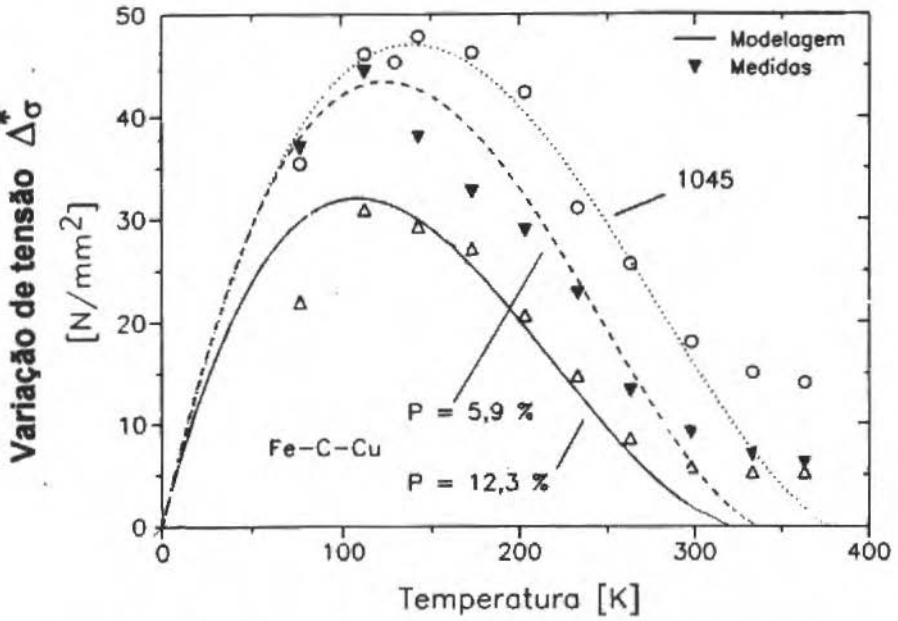

Fig. 8 Variação de tensão Δ_σ^* em virtude da alteração brusca da velocidade de deformação em função da temperatura e respectiva modelagem

Além disso, a tensão de escoamento a 1,5% do aço 1045 foi determinada através de ensaios de tração à temperatura ambiente (T = 298 K) com variação da velocidade de deformação (Fig. 9). A modelagem feita pela Eq. (18) consegue, também neste caso, descrever de maneira satisfatória os resultados obtidos experimentalmente.

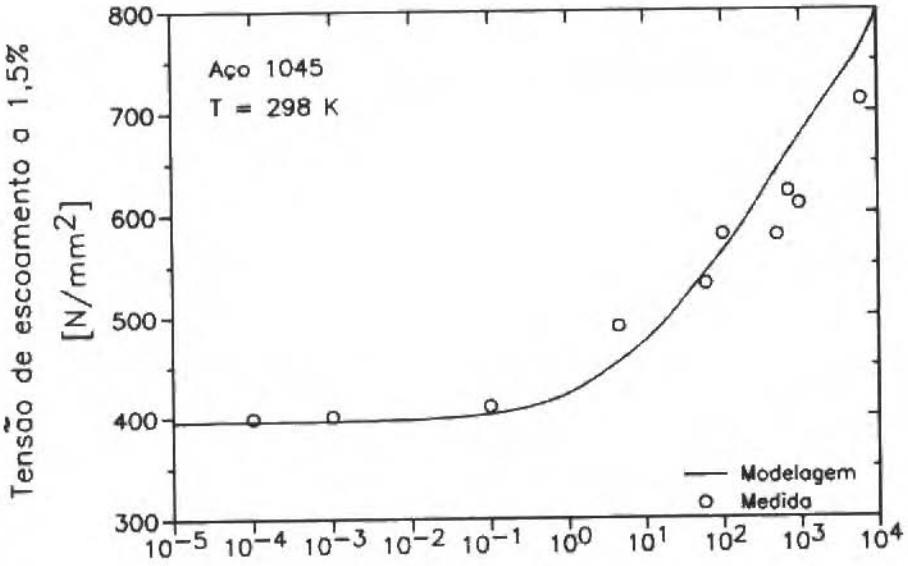

Fig. 9 Tensão de escoamento a 1,5% de deformação plástica do aço 1045 em função da velocidade de deformação e respectiva modelagem

A superação dos obstáculos com campos de tensões de curto alcance (tensão de Peierls) pelas discordâncias móveis, se dá em metais ccc pela formação de pregas, as quais se estendem posteriormente ao longo da linha da discordância sob a ação da tensão externa (Vöhringer e Macherauch, 1978). O efeito da energia térmica é auxiliar a formação da prega (Reed-Hill, 1982). Sendo este o mecanismo dominante de superação dos obstáculos de curto alcance nos materiais pesquisados, todos os parâmetros da Eq. (16) deveriam ser independentes da deformação plástica. Isto não ocorre entretanto com os resultados das ligas Fe-C-Cu (porosas), onde foi observado uma variação desses parâmetros com a deformação plástica, como mostram as Figs. 10 e 11.

Os poros influenciam a deformação plástica dos materiais sinterizados e provocam em conseqüência uma variação dos parâmetros σ_o^*, ΔG_0 e T_0. Para tais materiais, a deformação macroscópica permanente é dada pela equação

$$\varepsilon_{perm} = \varepsilon_p + \varepsilon^{poros} + \varepsilon^{trincas} \qquad (20)$$

com

ε_p = deformação plástica efetiva devido ao movimento de discordâncias;

ε^{poro} = contribuição dos poros através do aumento de tamanho e variação da forma e

ε^{trinca} = contribuição das trincas, as quais se iniciam em tensões inferiores à tensão de escoamento macroscópica.

A variação de Δ_σ^* em função da porosidade do material (Fig. 8) é expressão desta influência dos poros sobre a deformação permanente macroscópica. Variações de tensão em função da alteração brusca de velocidade de deformação ocorrem devido a alterações das componentes de tensões térmicas σ^*. O fator decisivo é que somente regiões onde ocorrem movimento de discordância, ativado termicamente, podem contribuir para os valores de Δ_σ^*. Em (Palma, 1994) foi mostrado que crescente porosidade inicial leva a grande heterogeneidade da deformação e que várias regiões do material deformam-se elasticamente até a ruptura final, sem qualquer contribuição para Δ_σ^*. Isto leva a uma

queda do valor de Δ^*_σ com o aumento da porosidade total quando da alteração brusca da velocidade de deformação, o que provoca uma certa dependência dos parâmetros da Eq. (16) com a deformação plástica.

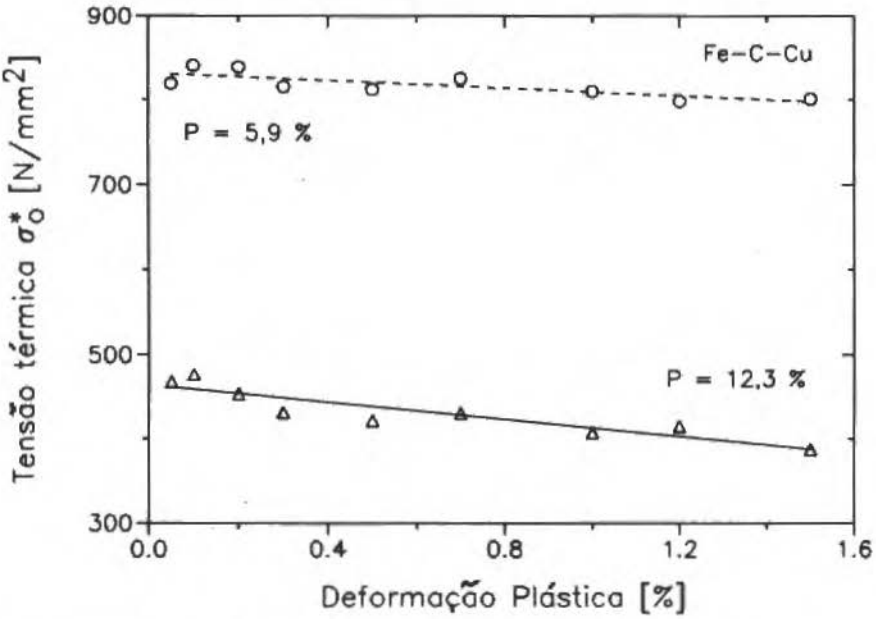

Fig. 10 Parâmetro σ^*_0 das ligas Fe-C-Cu com porosidade P = 5,9 e 12,3% em função da deformação plástica

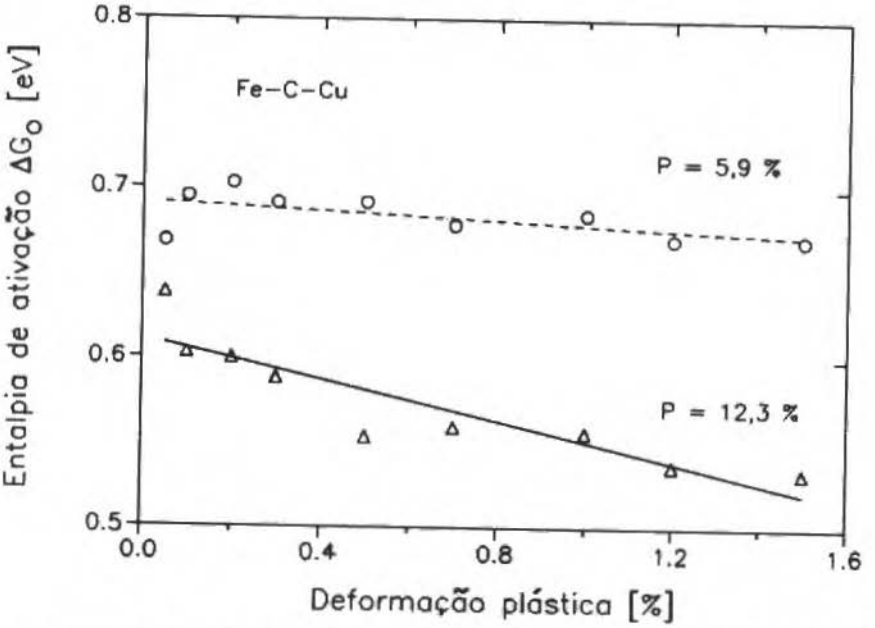

Fig. 11 Entalpia de ativação ΔG_0 das ligas Fe-C-Cu com porosidade P = 5,9 e 12,3% em função da deformação plástica

O uso de elementos de liga Cu, C e P provoca uma queda acentuada da parcela de tensão de deformação térmica e dos parâmetros σ^*_0, e conseqüente aumento da parcela atérmica σ_E, em comparação com ferro puro, como mostra a Fig. 12.

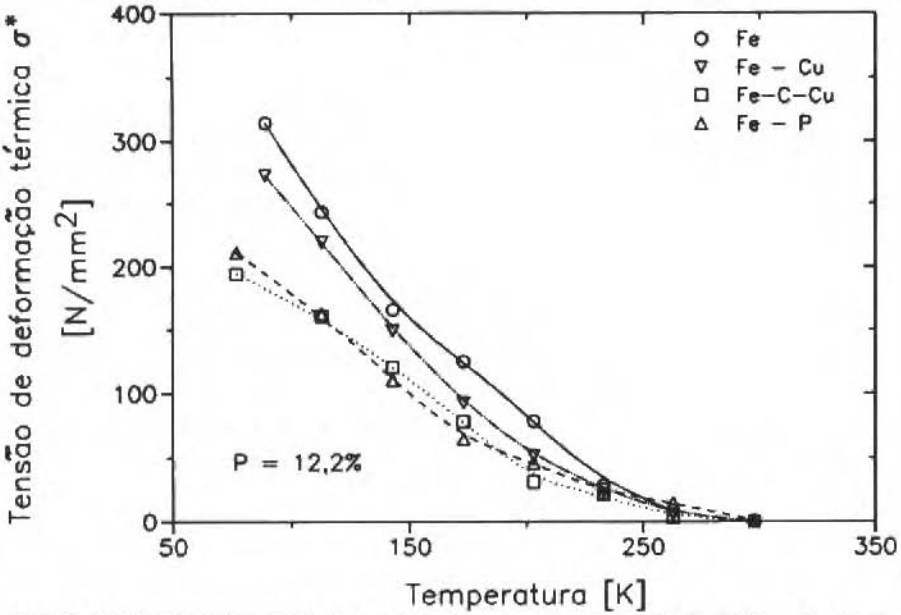

Fig. 12 Tensão de deformação térmica de ligas sinterizadas com porosidade total P = 12,3% em função da temperatura

As ligas possuem menores valores de Δ^*_σ e maiores do volume de ativação que ferro. Devido ao mecanismo dominante de ativação, a formação de pregas nas discordâncias, o volume de ativação é dado pela Eq. (5), onde o produto l.d representa a área de ativação. Considerando-se que o vetor de Bürger permanece praticamente inalterado, a área de ativação aumenta com o teor de elemento de liga dissolvido na matriz. Durante a superação dos obstáculos de curto alcance, a discordância abrange uma maior área, o que leva a uma queda da parcela de tensão térmica. Este fenômeno, amolecimento por elementos de liga, ainda não é totalmente compreendido (Pink, 197). A extensão da queda da tensão térmica depende da concentração e do tipo de elemento de liga usado. Para uma análise mais profunda da influência dos elementos de ligas sobre a tensão de deformação térmica, determinou-se os valores de σ^*_0 de materiais sinterizados com porosidade total P = 12,2%, os quais são apresentados na Tabela 1. Para tanto foi utilizada a Eq. (16) com m = 1,75 e n = 0,5, constantes, a fim de se evitar quaisquer influências destes parâmetros dobre o valor de σ^*_0. Fe possui o maior valor de σ^*_0. A queda do valor desse parâmetro, em relação ao Fe, devido ao uso de 0,45% de P na liga Fe-P é semelhante quando se utiliza simultaneamente 0,6% C e 1,55% Cu nas ligas Fe-C-Cu. Essa forte influência de P sobre a tensão de escoamento é conhecida há bastante tempo (Pink, 1976).

Tab. 1 Parcela de tensão de deformação térmica σ^*_0, com m = 1,75 e n = 0,5

σ^*_0 [N/mm²] (P=12,3%)			
Fe	FE-Cu	Fe-P	Fe-C-Cu
1192	1003	750	690

Conclusão

O aumento da resistência mecânica de materiais metálicos com a queda da temperatura de deformação em intervalo compreendido entre T = 0 K e T = T_0 é devido à redução do movimento de discordâncias ativadas termicamente sobre obstáculos de curto alcance.

Com a modelagem matemática realizada, utilizando-se a equação constitutiva (19) consegue-se descrever os resultados experimentais muito bem e serve de base para possíveis extrapolações desses resultados.

A dependência dos parâmetros da Eq. 19 (ΔG_0, m, n) da deformação plástica, ocorrida nas ligas sinterizadas, é conseqüência da heterogeneidade da deformação plástica desses materiais, a qual é conseqüência da porosidade residual existentes nesses materiais.

O uso de elementos de ligas leva a uma queda dos valores da parcela da tensão térmica de deformação plástica em relação aos valores de ferro puro. Neste caso, fósforo tem um efeito relativamente mais forte que o uso simultâneo de C e Cu.

Referências

Burgahn, F., 1991, "Einsinniges Verformungsverhalten und Mikrostruktur ausgewählter Stähle in Abhangigkeit von Temperatur und Verformungsgeschwindigkeit", Ph. D. Thesis, Universidade de Karlsruhe, RFA.

Macherauch, E., 1992, Praktikum im Werstoffkunde, Editora Vieweg & Sohn, Braunschweig, RFA.

Macherauch, E., Vöhringer, O., 1978, "Das Verhalten Metallischer Werstoff unter Mechanischer Beanspruchung", Z. Werkstofftechnik, No. 9, pp. 370-391.

Munz, D., Macherauch, E., 1966, "Geschwindigkeitswechselversuche an α-Messing", Z. Metalekunde, No. 6, pp. 442-451.

Palma, E.S., 1994, "Vervormungsverhalten von Sintereisenwerkstoffen bei Einachsig Homogenen und Inhomogenen Beanspruchungen", Ph. D. Thesis, Universidade de Karlsruhe, RFA.

Pink, E., 1976, "Legierungsentfestigung und der Spröd-Duktil-Übergang von krz Metallen", Z. Metallkunde, No. 67, pp. 564-567.

Reed-Hill, R.E., 1982, Princípios de Metalurgia Física, Editora Guanabara Dois, Rio de Janeiro, Brasil.

Schulze, V., 1988, "Optimiertes Verfahren zur Analysis thermisch Aktivierter Versetzungsbewegung und Anwendung am Beispiel des Edelstahls Ck 45", Trabalho de Graduação, Universidade de Karlsruhe, RFA.

Seeger, A., 1981, "The Temperature and Strain-Rate Dependence of the Flow Stress of bcc Metals: A Theory Based on Kink-Kink Interactions", Z. Metallkunde, No. 72, pp. 368-380.

Sestak, B., Seeger, A., 1978, "Gleitung und Verfestigung in krz Metallen und Legierungen", Z. Metallkunde, No. 6, pp. 195-432.

Stoer, J., 1983, "Einführung in die Numerische Mathematik I", Editora Springer, Berlin, RFA.

Vöhringer, O., 1987, "Neuere Ergebnisse der Plastizitäts- und Bruchforschung mit Praktischer Relevanz", Proceedings, Werkstoffverhalten und Bauteilbemessung, DGM Oberursel, pp. 25-47.

Wawra, H., 1978, "Die Kröner-Grenzen der Elastizitätsmoduln Technisch Wichtiger Werstoffe", Teile 1 und 2, Z. Metallkunde, No. 9, pp. 476-478 e 518-523.

RBCM - J. of the Braz. Soc. Mechanical Sciences
Vol. XV - nº1 - 1995 - pp. 89-101

ISSN 0100-7386
Printed in Brazil

Modelling, Simulation and Optimization of a Printer Sled Driving System

H. Springer and H. Ecker

Dept. of Meach. Engineering
TU-Vienna, Austria

F. Breitenecker

Dept. of Mathemathics
TU-Vienna, Austria

Abstract

An electromechanical system is considered that is composed of a sled, which is guided by two parallel guide rods and carrying a printer head elastically attached to the sled. The sled is driven by a two-phase step motor through an elastic belt and pulley system. The step motor torque characteristics are generated by frequency and amplitude modulated currents in the two phases controlled by a microprocessor. Nonlinear equations of motion for the system are established and numerically integrated by the simulation code ACSL. A new optimization routine GOMA is applied to the simulation model in order to optimize the current modulation parameters so that the dynamical position error of the printer head approaches a minimum.

Keywords: Printed Sled Driving System, Control of a Mechanical System.

Introduction and Definition of the Problem

Needle printers are still in use for specific applications as, for example, printing on multi-sheet commercial papers or documents. In order to generate the printing dots through several paper sheets relatively high needle forces are necessary, see Springer and Ullrich (1989). For the reason of vibration isolation, the needle printer head is elastically mounted to the sled, wich moves from left to right while the needles are in operation. During the start up period of the sled motion from standstill on the very left position (see Fig. 1) to the right, transient vibrations of the sled and the printer head are generated by the step motor. These vibrations, especially in the direction of the horizontal sled motion, may not have sufficiently died away at the moment of starting the printing process. This leads to a printer head position error that may cause a distortion of the characters to be printed. A remedial measure to avoid the printing character distortion right after the acceleration period of the sled might be introduced by increasing the damping in the printer head suspension system. However, this also increases the vibration transmissibility function between the printer head and the sled and deteriorates the vibation isolation. Another possibility to decrese the start-up vibration amplitudes of the printer head may be realized by an open loop control of the driving torque characteristic of the step motor during the start up period. In that way the acceleration excitation of the sled and the printer-head becomes less severe. This can be realized by minimizing a specific vibration-cost functional with respect to the step motor's current modulation parameters.

In this paper the complete system, that means the sled, the sled guiding system, the printer head, the belt-pulley driving arrangement and the two phase step motor is modelled, see Kreuth (1989). Nonlinear equations of motion are established including frictional effects in the guiding system and position dependent belt stiffness characteristics of the pulley system. The forwad integration in the time domain is done by using the simulation code ACSL, see ACSL Relevance Manual 1993). The optimization is applied with respect to specified current frequency and amplitude modulation parameters of the step motor and worked out by the new code GOMA, see Breitenecker, Ecker and Bausch-Gall (1993).

Manuscript received: July 1994. Technical Editor: Leonardo Goldstein Jr.

Description of the Electronichanical System

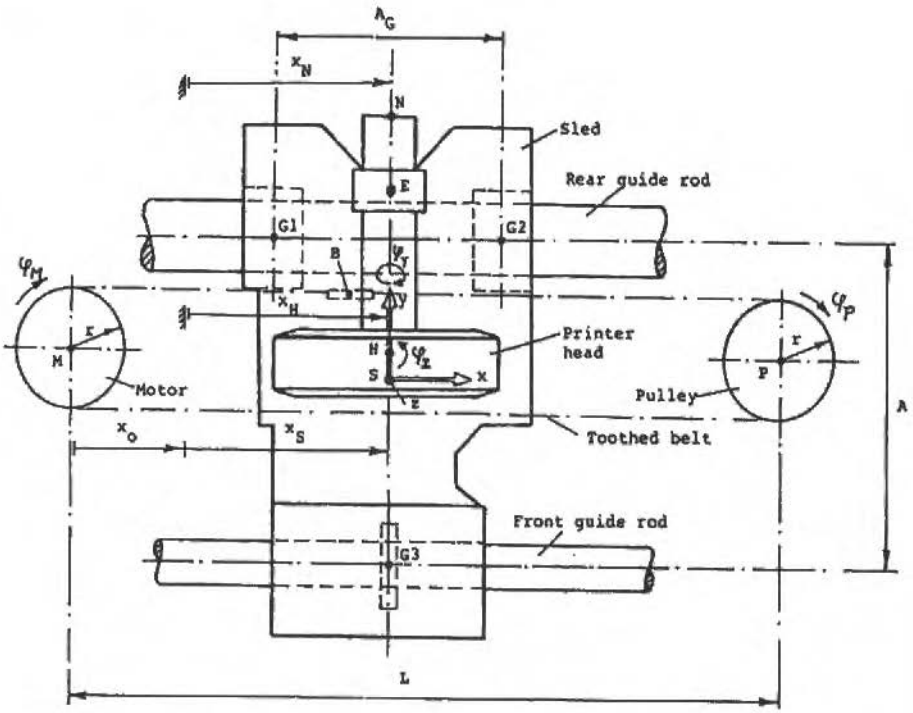

Fig. 1 Top view of the sled, printer head and driving system

Figure 1 shows a schematic diagram (top view) of the sled, the guide rod system, the printer head and the belt-pulley arrangement with the driving step motor. Figure 2 shows a corresponding photograph of the system mounted on a base frame.

The symbols as indicated in Fig. 1 have the following meaning.

Characteristic points in the system:

G1, G2 sled guiding points, located at the axis of the rear guide rod;

G3 sled guiding point, located at the axis of the front guide rod;

N needle exit point, located at the front of the printer head;

E elastic center of the printer head suspension system;

H center of mass of the printer head;

S center of mass of the sled;

M axis of rotation of the step motor;

P axis of rotation of the belt-pulley, and

B champing point between the sled and the toothed belt.

The reference frame x-y-z (x and y horizontal, z vertical) is connected with the rigid sled at its center of mass S.

The axes x-y-z are approximately parallel to the principle axes of inertia of the printer head with respect to its center of mass H. Both, the sled and the printer head are considered as rigid bodies aas well as the motor and the belt pulley. The front and rear guide rods are considered to be rigid.

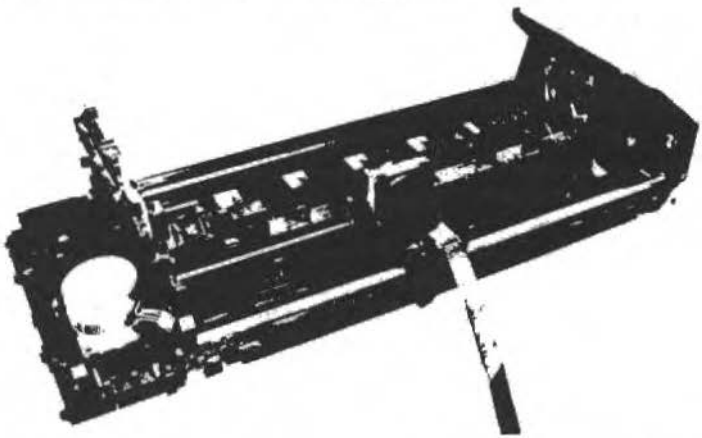

Fig. 2 Photograph of the printer sled driving system mounted on a base frame

The generalized displacement vector (degrees of freedom) is defined in the form

$$\mathbf{x} = [x_S, x_H, \varphi_y, \varphi_z, \varphi_P, \varphi_M] \tag{1}$$

x_S translation displacement of the sled in the horizontal x-direction;

x_H translation displacement of the printer head center of mass in the horizontal x-direction;

$\varphi_y << 1$ angular displacement of the printer head with respect to the horizontal y-axis;

$\varphi_z << 1$ angular displacement of the printer head with respect to the vertical z-axis, and

φ_P, φ_M angles of rotation of the pulley and the step motor armature, respectively.

The horizontal displacement X_N of the needle exit point of the printer head can be calculated from the components of the generalized displacement vector in the form $X_N = b^T x$, with b being a (6x1)-geometry vector. Angular displacements φ_X and translational displacements Y_H and Z_H of the printer head are not excited in the system during start up period. No excitation of the printer head due to the needle printing forces is considered here, i.e. the start up period is simulated without needle operation. The printer head is flexibly attached to the sled at point E with translational stiffness and damping coefficients K_X^E, C_X^E, respectively, in the horizontal x-direction and angular stiffness and damping coeficients ($K_{\varphi Y}^E$, $K_{\varphi z}^E$), ($C_{\varphi Y}^E$, $C_{\varphi z}^E$), respectively, with respect to the y-and z-axis. The toothed belt is considered massless with a translational stiffness EA_B per unit lenght and corresponding internal damping. Note that the front strand $\overline{MP}$, connecting the motor with the pulley, has a constant stiffness $K_{MP} = EA_B / L$ while the stiffness values of the rear strands $\overline{MB}$ and $\overline{PB}$ vary depending on the sled position X_S. Therefore, the stiffness and internal damping forces of the belt-pulley system are nonlinear in terms of the sled displacements X_S.

The front and rear guide rods for the sled cause constraint normal reaction forces, acting between the rods and the sled. Due to dry friction, adhesion forces or sliding friction forces are generated in the horizontal x-direction and are applied to the sled too. Both, adhesion and sliding friction forces are modelled and calculated together with the normal forces so that the sled inertia, constraint and applied forces and moments are in equilibrium at any time during the motion. In the sled stand-still position, the adhesion break-off friction force is calculated until the sled starts moving.

The driving motor is modelled as a two-phase hybrid-type step motor with 50 teeth of the armature and 200 steps per revolution. The current in the windings is voltage controlled by a microprocessor trhough a special program.

Equations of Motion

Corresponding to the generalized displacement vector of Eq. (1) the equations of motion can be established in the form

$$\ddot{x} + C(x)\dot{x} + k(x)x = f(x, \dot{x}, t) \tag{2}$$

where

$M=M^T$ is the constant mass - matrix of dimension (6x6),

$C(x) = C^T(x)$ is the damping matrix of the system depending on the sled position, see Description of the Eletromechanical System

$K(x) = K^T(x)$ is the stiffness matrix depending on the sled position, see Description of the Eletromechanical System, and

$$f(x, \dot{x}, t) = [F(x, \dot{x}), 0, 0, 0, 0, M(\varphi M, \varphi M\ i_1(t), i_2(t))]^T \tag{3}$$

is the applied force vector, with $F(x, \dot{x})$ representing the applied sled friction forces acting in the guide rods and $M(\varphi M, \varphi M\ i_1(t), i_2(t))$ representing the torque of the step motor, see Step Motor Driving Torque Characteristics.

Constraint Normal Forces and Applied Friction Forces Acting on the Guide Rods

If indices F and R, respectively, indicate the front and the rear guide rod (see Fig. 1), then the resulting friction force in the horizontal direction is

$$F = F^F + F^R \tag{4}$$

Further, if the front guide rod carries normal forces at point G 3 only in the vertical z-direction, (Fig. 1) then

$$N^{G3} = \begin{bmatrix} N_y \\ N_z \end{bmatrix}^{G3} = \begin{bmatrix} 0 \\ N_0^F \end{bmatrix} \tag{5}$$

holds. In Eq. (5) $N_0{}^F$ denotes the static normal force acting in the guiding point G 3 when the sled is in a stationary position (standstill). The normal reaction forces in the guiding points G 1 and G 2 of the rear rod, (Fig. 1), are given by

$$N^{Gj}(t) = \begin{bmatrix} Ny \\ Nz \end{bmatrix}^{Gj} = \begin{Bmatrix} (-1)^j \Delta N_y(t) \\ N_0^R + (-1)^j \Delta N_z(t) \end{Bmatrix} j = (1,2) \tag{6}$$

where $N_0{}^R$ denotes the static normal force (including weight and clamping effects) acting in G 1 and G 2 at the sled standstill position and $\Delta N_y(t), \Delta N_z(t)$ represent dynamic normal reaction forces to be calculated from

$$\begin{bmatrix} \Delta N_y \\ \Delta N_z \end{bmatrix} = A \begin{bmatrix} F^F \\ F^R \end{bmatrix} + K_N(x)x + C_N(x)\dot{x} \tag{7}$$

where A is a (2 x 2) geometry matrix and K_N, C_N are (2 x 6)- matrices containing stiffness and damping coefficients, respectively, of the system. The guide rods friction forces F^F, F^R applied to the sliding sled are calculated in the form

$$F^F = -\mathrm{sing}(x_s)\,\mu_s\left|N^{G3}\right| \tag{8}$$

for the front rod and

$$F^F = -\mathrm{sing}(x_s)\,\mu_s\left[\left|N^{G1}\right| + \left|N^{G2}\right|\right] \tag{9}$$

for the rear rod, where

$$\left|N^{Gj}\right| = \left[(N^{Gj})^T N^{Gj}\right]^{1/2} \quad (j = 1,2,3) \tag{10}$$

In Eqs. (8) and (9) μs is the sliding friction coefficient. Inserting Eq. (7) into (6) and Eq. (6) into (9) yelds a nonlinear relation for the sliding friction force F^R in the rear rod that has to be solved iteratively at any point in the time domain. A similar calculation can be carried out for the friction reaction forces at the sled's standstill position up to the break-off adhesion force before the sled starts moving.

Step Motor Driving Torque Characteristics

According to Kreuth (1989) the number of teeth of the rotor armature of a hybrid motor is given by.

$$z_R = z_{Ps}(2jz_{Ph} + 1) \quad (j = 1,2,\ldots) \tag{11}$$

where z_{Ps} is the number of pole pairs of the stator and z_{Ph} is the number of phases of the stator winding. In the present case j= 6, $z_{Ps} = 2$, $z_{Ph} = 2$ and therefore, the number of teeth is $z_R = 50$. The number of steps per revolution of the rotor is given by.

$$z_S = 2z_{Ph}z_R \tag{12}$$

In the present case $z_S = 200$ and therefore, the step angle is $\gamma = 2\pi/z_S = 1{,}8°$. The step motor torque is composed of a small remanence retaining moment,

$$M_R(\varphi_M) \cong M_P \cos(z_S\varphi_M + \pi/2) \tag{13}$$

corresponding to the DC-flux as generated by the permanent axial magnet in the rotor, and the applied moment (Kreuth, 1989)

$$M_I(\varphi_M,t) \cong \alpha\left[i_1(t)\cos(z_R\varphi_M + \pi/2) + i_2(t)\cos(z_R\varphi_M)\right] \tag{14}$$

corresponding to the AC-flux as generated by the applied currents $i_1(t)$, $i_2(t)$, in the two phases. The torque to current coefficient α (in Nm/A) can be calculated (Kreuth, 1989), or determined by measuring the retaining moment $M_{I=const}(\varphi_M$ for constant values of the currents. It is worth to note that in Eqs. (13) and (14) the periodic retaining moments $M_R(\varphi_M$ and $M_{I=const}(\varphi_M$ in terms of the motor angle φ_M are simply approximated by pure harmonic functions, i.e. higher harmonics are neglected, see Kreth (1989). Further more, magnetic damping due to eddy current for example, is neglected in this model, i.e. $\partial M/\partial\varphi_M \cong 0$, and α is kept constant, independent of the currents and the flux densities. Moreover, dry friction moments coming from the bearings of the step motor are neglected. From Eqs. (13) and (14) the total torque characteristic of the step motor has the form

$$M(\varphi_M, i_1(t), i_2(t)) = \alpha [i_2(t) \cos(z_R \varphi_M) - i_1(t) \sin(z_R \varphi_M)] - M_p \sin(z_S \varphi_M) \quad (15)$$

Control of the Applied Currents in the Step Motor

The applied currents in the step motor can be controlled by a microprocessor, for example in the form

$$i_j(t) = I_{j0}(t) \sin[\omega_j(t)(t - \tau_j)], (j = 1, 2) \quad (16)$$

where $\omega_j(t$ and $I_{j0}(t$ are time dependent (modulated) frequencies and current amplitudes, respectively. In the present case $I_{10}(t) = I_{20}(t) = I_0(t)$ is chosen and the frequencies are represented by a piecewise constant step function, see Fig. 3 and Fig. 4. According to Fig. 3, the following relations hold (T_n = time step interval)

Step number 1 = start up step ($0 \le t \le t_1 = T_1$)

	Angular frequency	Time delay
Phase 1	$\omega_1 = \pi/T_1$	$\tau_1 = 0$
Phase 2	$\omega_2 = \pi/2T_1$	$\tau_2 = 0$

Step number n $(t_{n-1} \le t \le t_n = \sum_{k=1}^{n} T_k)$

	Angular frequency	Time delay
Phase 1	$\omega_1 = \pi/2T_n$	$\tau_1 = t_{n-1} - nT_n$
Phase 2	$\omega_2 = \pi/2T_n$	$\tau_2 = t_{n-1} - (n-1)T_n$

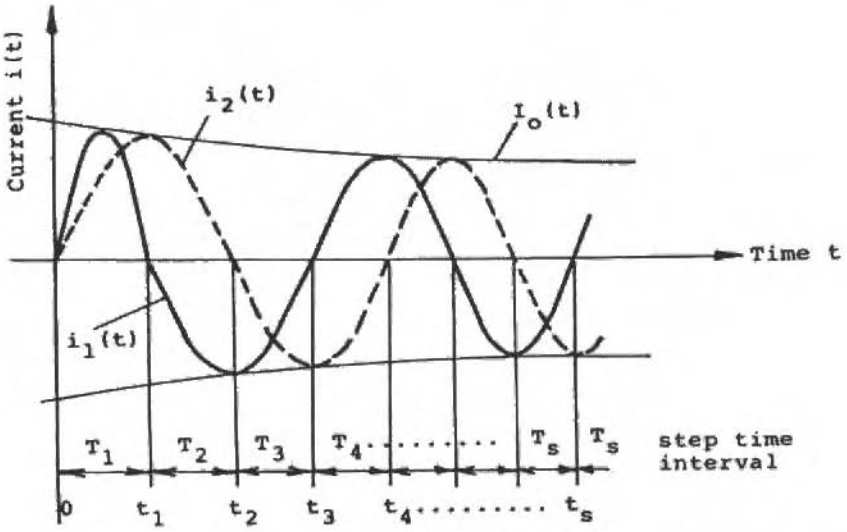

Fig. 3 Applied currents $i_1(t)$, $i_2(t)$, resp., during start up period of the step motor T_1, T_2, T_3, step time intervals, $_0(t)$ current amplitude modulation

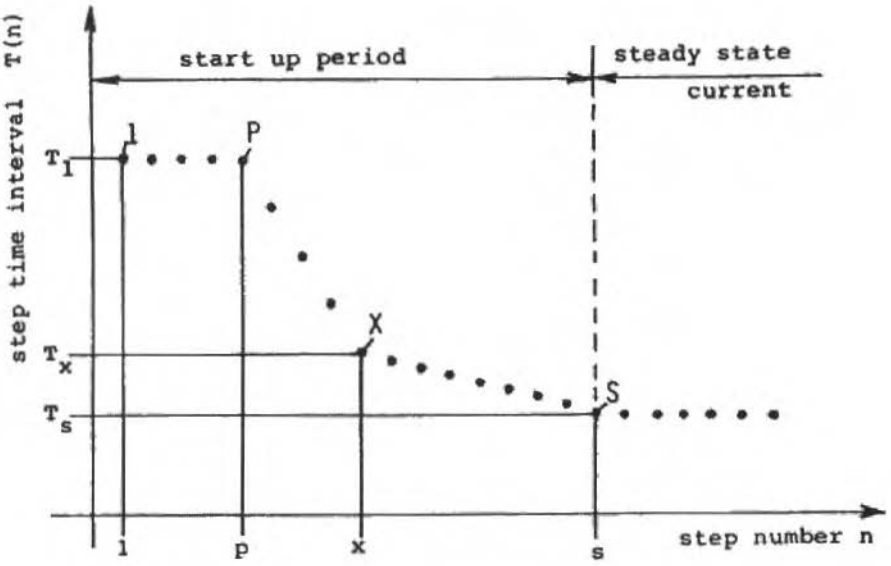

Fig. 4 Step time intervals T(n) in terms of the number of steps

Figure 4 shows a possible way of controlling the time intervals T_n as a function of the step number n. During the start up period of the step motor the step intervals T_n decrease in general with the step number n and approach the final value after step number s

$$T_s = \frac{2\pi}{z_S \Omega_{M\infty}} \tag{17}$$

Where $\Omega_{M\infty}$ is the requerid steady state angular speed of the step motor. After n = s steps or $t_s = \sum_{k=1}^{s} T_k$ the start up period is completed, and the corresponding sled displacement can be calculated from the step angle γ and the radius r by

$$x_s = s\gamma r \tag{18}$$

Opimization of the Current Modulation Parameters

Horizontal vibrations xn(t) of the printer head front end (see point N in Fig. 1) are generated by the step motor during the start up phase of the sled and may cause position errors of the printing needle and therefore affect the printing quality. Since the step motor is the source of the vibration excitation, a change in the control current parameters for the start up period might change the vibration level in the system. From this, an optmization problem can be established to minimize a cost functional for the vibration level xn(t) with respect to some adjustable control parameters of the step motor current. Possible optimization parameters are the current amplitude modulation function $I_{j0}(t)$, see Eq. (16) and Fig. 3 and/or the frequency modulation step function $\omega j(t)$, see Eq. (16) and Fig. 4. In this paper the amplitude functions $I_{j0}(t)$ are not varied. In the discrete time interval function of Fig. 4 the point S is determined from the required steady state speed and position of the sled after n = s steps, see Eqs. (17), (18). Therefore the parameters of point S are not adjustable. Changeable parameters are at point I with T_1 point P with (p, Tp) and point X with (x, Tx). Optimal values for these parameters can be determined from an optimization process so that the cost functional

$$CF = \int_{t_1}^{t_2} \left[\Phi (x_N, \dot{x}_N, \ddot{x}_N) \right]^2 dt \Rightarrow Min \tag{19}$$

becomes a minimum. The corresponding differential equation

$$\dot{CF} = \begin{cases} \Phi^2 (t) \; (t_1 \le t \le t_2) \\ 0 \qquad otherwise \end{cases} \tag{20}$$

can be integrated simultaneously with the equations of motion Eq. (2) and yields CF in terms of the adjustable current modulation parameters. The time interval (t_1, t_2) must be chosen properly, as for example

$$t_1 = t_s = \sum_{k=1}^{s} T \tag{21}$$
$$t_2 = t_{max}$$

Based on various optimization algorithms available in the program code GOMA, (Breitenecker, Ecker and Bausch, 1993), the minimization problem of Eq. (19) is solved numerically.

Numerical Simulation and Optimization Results

In this paper primarily the start up phase of the system between t = 0 and t = tmax including a short period of about 115 steady state steps between t = ts and t = tmax is investigated. In the following examples the standard start up version is run with the frequency modulation data T1 = Tp = 2623 µs, x = 7, Tx = 810 µs, see Fig. 4. For the optimization process the location of X = (x, Tx) in Fig. 4 is varied and the cost functional of Eq. (19) is calculated in terms of x and Tx in the form

$$F(x, T_x) = \int_{t_s}^{t_{max}} \left[\Phi (x_N, \dot{x}_N, \ddot{x}_N) \right]^2 \tag{22}$$

where Φ is chosen as

$$\Phi = \dot{x}_N - \upsilon\infty \tag{23}$$

In Eq. (23) $\dot{x}_N = b^T \dot{x}$ is the horizontal velocity of the printer head front end (see point N in Fig. 1, with b being a geometry vector) and $\upsilon\infty = r\Omega M\infty$ is the requerid steady state velocity of the sled, see Eq. (17)

Figure 5 shows the time responses of the applied currents i1(t), i2(t) in phase 1 and phase 2, respectively, of the step motor during the start up and steady period. The current amplitude modulation function I0(t) (=current envelope curve) is chosen as peicewise linear in this example and is not varied in the following optimization studies. Note, that after the first step the phase angle between i1 and i2 is 90 degress.

Corresponding to these applied currents, Fig. 6 shows the magnetic torque of the step motor. The superimposed high frequency component is caused by the magnetic remanence moment Mr in Eq. (13), its steady state frequency is $f_{R\infty} = 1/T_s$, seeEq. (17). The steady state effective moment is very small and is determined by the small sliding friction forces in the guide rods.

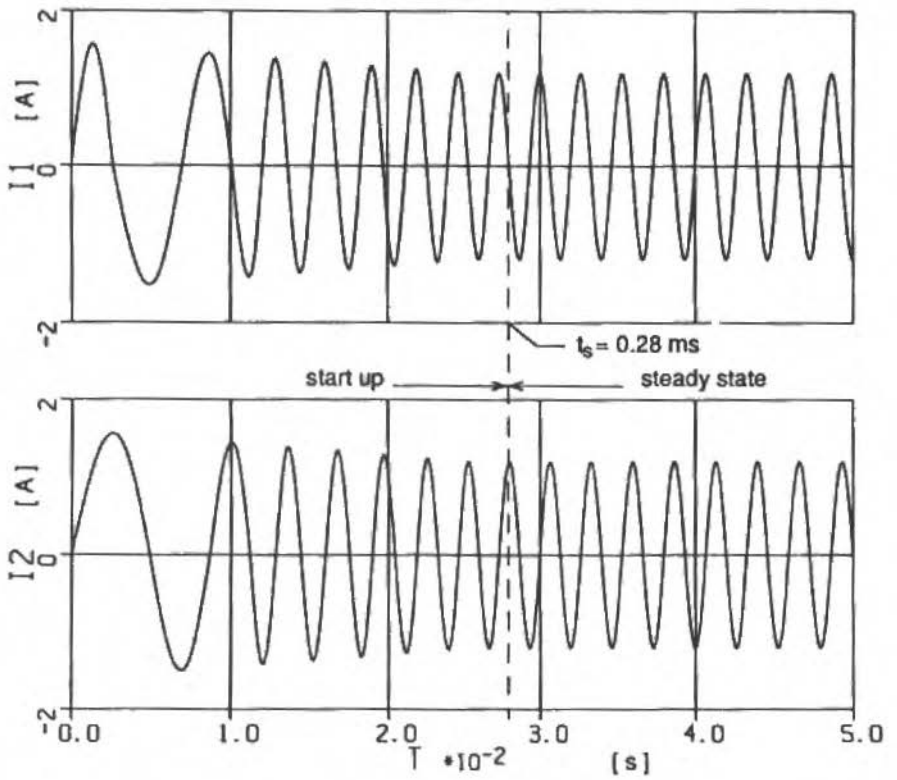

Fig. 5 Time responses of the applied currents in the stator windings of the step motor.
Phase 1:i1(t), top Phase 2: i2(t), bottom

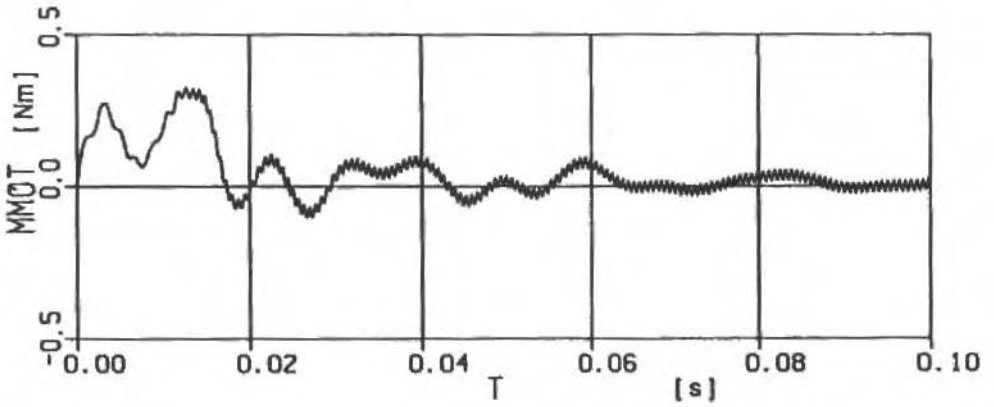

Fig. 6 Magnetic torque charcteristics of the step motor in terms of time

Figure 7 shows the time response of the sliding dry friction force F^R between the rear guide rod and the sled. The friction force approaches a constant value depending on the weight of the sled, the fit between the quide rod and the sled (generating a normal preload), and the coefficient of sliding friction. From the resulting steady state friction force (including rear and front guide rods) the effective torque and power of the step motor can be calculated.

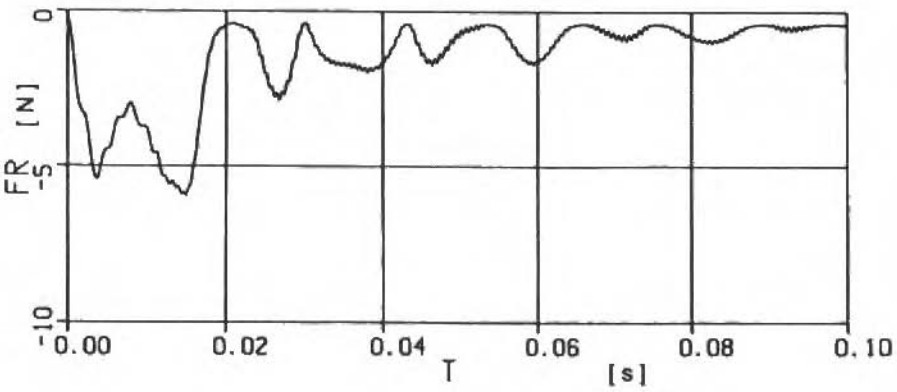

Fig. 7 Time response of the sliding friction force acting in the rear guide rod of the sled

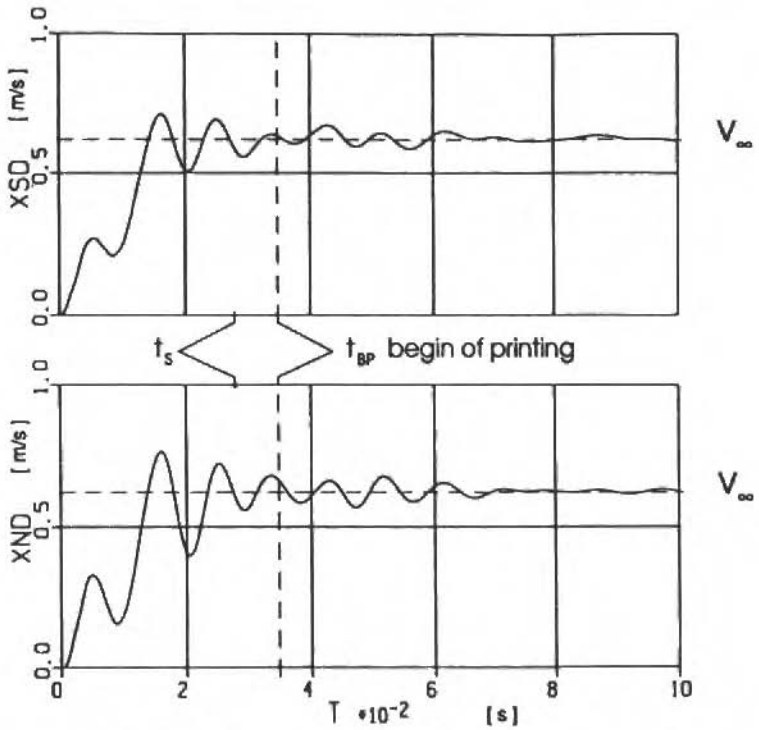

Fig. 8 Time responses of the sled velocity $\dot{x}_S$ (top) and the printer head front end velocity $\dot{x}_N$ (bottom)

Figure 8 shows a comparison between the horizontal x-velocities of the sled $\dot{x}_S$ (top) and the printer head front end $\dot{x}_N$ (bottom), see point N in Fig. 1. Both, $\dot{x}_S$ and $\dot{x}_N$ approach the same steady state value $\upsilon\infty = r\Omega_{M\infty}$, see Eq. (17). However, the vibration amplitudes of $\dot{x}_N$ are somewath higher than those of $\dot{x}_S$. This is due to the presence of printer head vibrations relative to the sled because of the visco-elastic head suspension system. Beside the belt damping the damping in the printer head suspension is responsible for the decay of the vibration level in the whole system.The time when the applied currents become steady state is marked by $t_s = \sum_{k=1}^{s} T_k$, and it can be seen, that there is still no constant speed $\dot{x}_{N,S} \Rightarrow \upsilon\infty$ approached at this moment. The required begin time of the printing process is marked in the figure at $= t_{BP} = \lambda t_s (\lambda \geq 1$. It can be seen that even at $t = t_{BP}$ the vibration level of the printer head front end is still too high, which leads to a distortion of the printed characters.

There are several posibilities to avoid a character distortion. First, the begin of printing could be delayed until the printer head vibrations have died out. However, in practice this is not possible, since the head position $_N(t_{BP})$ at t_B is fixed to the left paper margin and the final sled velocity υ_∞ would then become too small for high printing capacity requirements. Second, an increase of damping in the system would suppress the vibrations before the printing begins. However, in order to increase the critical damping of the printer head suspension, in general, its stiffness would decrease which is not acceptable from a design standpoint for high printing needle forces. A third possibility to reduce the start up vibration level in the system is an optimization of the appled current parameters so that the cost functional CF in Eq. (22) becomes a minimum. Figure 9 shows the cost functional CF in terms of the current frequency modulation parameters (x, T_x), see Fig.4. It can be seen, that there exists a minimum CF_{OPT} for the parameters (x_{OPT} = 8.4, T_{OPT}=911µs) whict guarantees a practicable start up procedure without violating start up time and sled position requirements at the begin of printing.

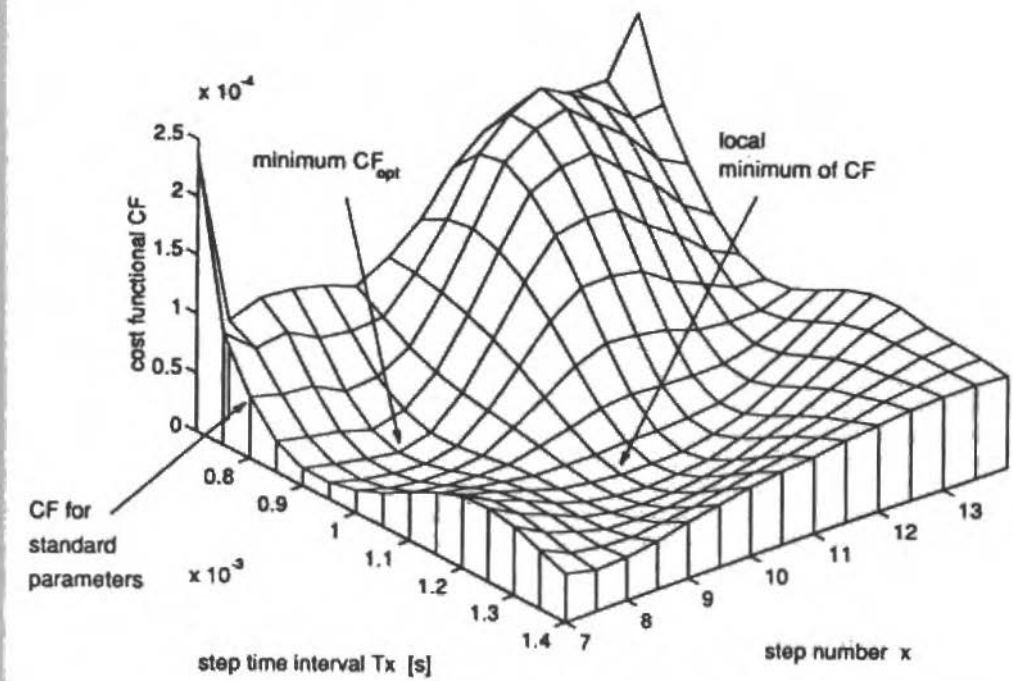

Fig. 9 Cost functional CF in terms of the two current modulation parameters step number X and step time interval T_x (see Fig. 4)

Figure 10 compares the time responses $\dot{x}_N$ (t) of the printer head front end for the current standard parameters x=7, $T_x = 810\mu s$ and the optimized parameters x_{OPT}, T_{OPT}. It can be seen, that in the optimum case the head vibrations have practically vanished when the printing starts at $t=t_{BP}$. This result is obtained by just changing the current control frequency modulation parameters without any change of damping and stiffness of the system.

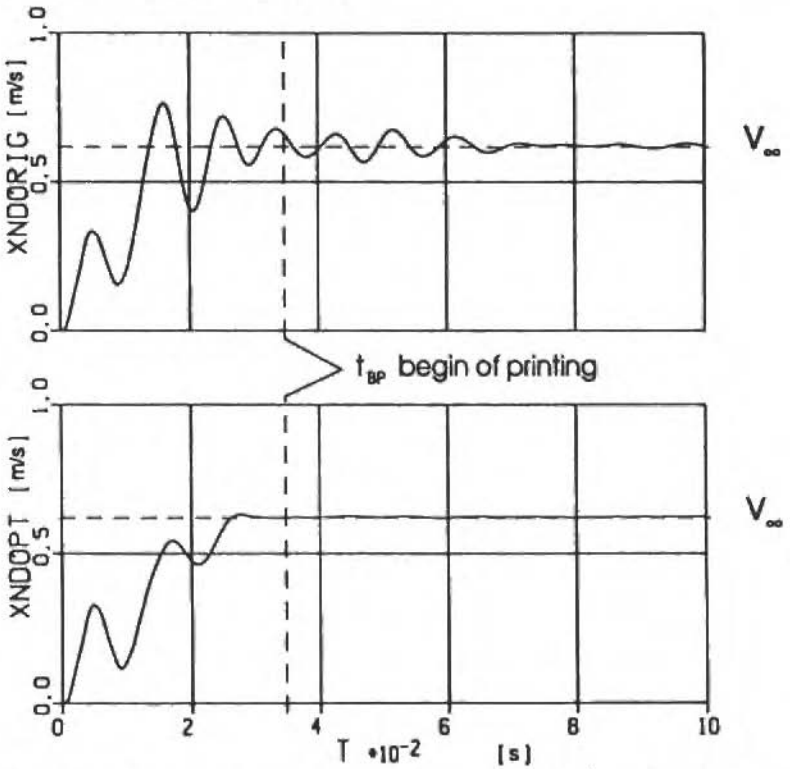

Fig. 10 Comparison between the standard startup velocity time response $\dot{x}_N$ (t) (top) and the optimized start up response of $\dot{x}_N$ (t) (bottom)

Conclusion

A highly nonlinear and complex electromechanical driving system of a needle printer sled has been modelled and numerically integrated by ACSL. The 6-degrees-of-freedom model includes nonlinear magnetic torque characteristics of the step motor, position dependent driving belt stiffness, constraint guide forces which generate dry friction forces, visco-elastic suspension systems, and a complex open loop voltage control of frequency and amplitude modulated currents in the step motor stator windings. An optimization with respect to the frequency modulation current parameters has been carried out in order to minimize the printer head vibrations during the start up period and therefore avoid a distortion of printed characters. In a future work the optimization will be extended to other adjustable parameters of the applied currents.

Acknowledgements

The authors gratefully acknowledge the support of Mannesmann Tally Company, Ulm, Germany. Thanks are due to Dr. J. Wassermann of the Institute for Machine Dynamics and Measurement Technology for carrying out torque measurements of the step motor.

References

Springer, H. and Ullrich, M., 1990, "Dynamics of Dot-Matrix Printers". Nonlinear Dymamics in Engineering Systems, IUTAM Symp. Stuttgart, Springer Verlag 1990, pp.297-304.
Kreuth, H. P., 1989, *Schrittmotoren*, Verlag Oldenburg, München.
ACSL Reference Manual, Edition 10.1, MGA Inc., Concorde MA 01742, 1989.
Breitenecker, F., Ecker, H. and Bausch-Gall, 1993, *Simulieren* mit ACSL, Verlag F. Vieweg & Sohn, Wiesbaden.

RBCM - J. of the Braz. Soc. Mechanical Sciences
Vol. XVII - nº 1 - 1995 - pp. 102-108

ISSN 0100-7386
Printed in Brazil

O Sistema de Fusão de Tecnologias e o Desenvolvimento de Novos Produtos

Technology Fusion System and New Product Development

Jarbas Lopes Cardoso Júnior
Fundação Centro Tecnológico para Informática
Instituto de Automação - Caixa Postal 6162
Campinas - SP - Brasil - 13089-500

Oswaldo Luiz Agostinho e Ettore Bresciani Filho
Universidade Estadual de Campinas
Faculdade de Engenharia Mecânica- Caixa Postal 6122
Campinas - SP - Brasil - 13083-970

Abstract

This article analysis the generation process of knowledge by technology fusion system as a self-organizing process and new product development catalyst. As a result of technology fusion the concept of adaptability of engineering system within an integrated product development enviroment is considered.
Keywords: Adaptability of Engineering Systems, Technology Fusion, Technology Innovation, Concurrent Engineering.

Resumo

Este trabalho analisa o processo de geração de conhecimento desencadeado pelo sistema de fusão de tecnologias como um processo de auto-organização, catalisador do desenvolvimento de novos produtos. Como conseqüência da fusão de tecnologias é discutido o conceito de adaptabilidade dos sistemas de engenharia aplicado a um ambiente de desenvolvimento integrado de produtos.
Palavras-chave: Adaptabilidade dos Sistemas de Engenharia, Fusão de Tecnologias, Diversificação Tecnológica, Inovação Tecnológica, Engenharia Simultânea.

Introdução

O mundo está vivendo uma época de transição nas organizações: da era industrial para a era da informação. Nos primórdios do capitalismo a principal fonte de riqueza era a posse da terra; no início do período industrial era o trabalho; atualmente, no que é considerado o fim do período industrial, a principal fonte de riqueza é o capital. Já no novo período que se inicia, o da organização ou da informação, a principal fonte de riqueza é o conhecimento (Drucker, 1992; Keys, 1991; Savage, 1990).

Na era da informação, apesar de o conhecimento ser a principal fonte de riqueza para os indivíduos ou para a economia de um modo geral, não quer dizer que terra, trabalho e capital, os tradicionais fatores de riqueza, desaparecerão. Eles continuarão importantes, porém, exercendo um papel secundário no processo produtivo (Drucker, 1992; Savage, 1990).

O conhecimento especializado por si só produz pouco. Ele torna-se produtivo quando integrado a outros conhecimentos especializados para realização de uma tarefa. Essa é uma das razões pela qual a era do conhecimento é também chamada de a era da organização, onde todas as unidades da empresa operam com objetivo de integrar especialistas na realização de tarefas comuns (Agostinho, 1993; Keys, 1991). Outros autores chamam esta integração de redes humanas ou de "times virtuais".

Esse conceito surge como conseqüência de as inovações tecnológicas ocorrerem em prazos cada vez mais curtos e exigirem um conteúdo tecno-científico cada vez mais complexo. A complexidade é de tamanha grandeza que as inovações não mais estão restritas às fronteiras de domínio tecnológico de uma única indústria.

Inovações nos produtos demandam inovações no processo produtivo. A transformação do modo de produção de bens é mais sentida nos chamados países desenvolvidos como Japão, Estados Unidos e países da Comunidade Européia. No entanto, no Brasil, apesar da defasagem tecnológica, já se notam sinais de mudanças através de iniciativas isoladas de empresas de padrão internacional (Kruglianskas, 1992).

Manuscript received: July 1994 - Technical Editor: Leonardo Goldstein Jr.

O sucesso das empresas devido às inovações caracteriza-se principalmente pelo modo como são definidas as diretrizes para a pesquisa e desenvolvimento (P&D) tecnológico e não apenas com o montante a ser investigado. Existem dois modos de estabelecer as diretrizes: substituição ou descontinuidade de tecnologias e combinação ou fusão de tecnologias, que estão intimamente relacionados ao modo de produção.

O enfoque de substituição das tecnologias convencionais por novas parte da definição de Schumpeter que define a inovação tecnológica como um processo de "destruição criativa" (Drucker, 1992). O processo de substituição é linear e segue uma estratégia de alterações tecnológicas incrementais até o ponto de descontinuidade: o transistor substitui a válvula, o "compact disk" substitui o disco de acetato.

A fusão de tecnologias procura combinar as tecnologias existentes e reuní-las no que se convencionou chamar de tecnologias híbridas. O processo de fusão é não linear, complementar e intensivamente cooperativo. O processo mistura desenvolvimentos técnicos incrementais a partir de diferentes tecnologias previamente escolhidas, para criar novos produtos que revolucionam o mercado: a optoeletrônica decorrente da combinação da óptica com a eletrônica, proporcionou o surgimento dos sistemas de comunicação baseados na fibra ótica; a mecatrônica decorrente da combinação da mecânica com a eletrônica que proporcionou grandes avanços em sensores muito utilizados na indústria automotiva e de bens de capital e, em particular, nas de máquinas-ferramenta e de robôs; a realidade virtual proporciona, através da combinação de recursos de multimídia (som, imagem, vídeo, informática), computação gráfica e simulação, possibilidades quase ilimitadas para as pessoas transformarem seus computadores em máquinas de criação de mundos.

Este trabalho analisa o processo de geração de conhecimento ou de diversificação tecnológica desencadeado pelo sistema de fusão de tecnologias como um processo de auto-organização e mostra como ele pode se tornar o principal elemento catalisador do desenvolvimento de novos produtos pelas empresas industriais inovadoras.

Num mercado competitivo onde o tempo é fundamental, obtém vantagens a indústria que mais rápido se adapta para primeiro chegar ao mercado oferecendo os produtos que os consumidores desejam. Este trabalho analisa também, como conseqüência da adoção da estratégia de fusão de tecnologias, a aplicação do conceito de adaptabilidade dos sistemas de engenharia para um ambiente facilitador das atividades de desenvolvimento integrado de produtos. Como conclusão, o trabalho mostra que as decisões por fusão de tecnologias, adaptabilidade dos sistemas de engenharia, flexibilidade dos sistemas de manufatura e desenvolvimento integrado de produtos são solidárias e complementares no processo de inovação tecnológica.

Desenvolvimento Tecnológico

O Processo de Inovação Tecnológica

A tecnologia é definida como a aplicação de conhecimentos à produção de bens e à prestação de serviços. Como o volume de conhecimentos é cada vez maior, é natural que as empresas e a sociedade estejam constantemente solicitando e produzindo inovações tecnológicas.

Inovação tecnológica pode ser definida como sendo as novas tecnologias que chegam ao mercado na forma de novos produtos e serviços de modo que a sociedade seja mais bem atendida.

Uma empresa domina a variável tecnológica quando ela internaliza o processo de inovação tecnológica, administra profissionalmente a função de pesquisa e desenvolvimento (P&D) e promove seu espírito empreendedor interna e externamente. Assim, a capacidade de obter ou produzir novos conhecimentos e com eles gerar inovações tecnológicas torna-se um fator determinante de competitividade - um meio pelo qual as organizações podem aumentar seus padrões de eficiência e eficácia (Kodama, 1992). Neste nível a preocupação das empresas se concentra nos temas relacionamento entre desenvolvimento tecnológico e planejamento estratégico, estudos mercadológicos, relações de trabalho e capacidade de inovação, adaptabilidade dos sistemas de manufatura e aspectos sócio-técnicos, isto é, o relacionamento entre a avançada tecnologia aplicada à

manufatura e a estrutura organizacional, já que não se pode implantar novas estratégias de desenvolvimento de produtos e de inovação tecnológica sem pensar na forma de organização mais adequada.

A Estratégia de Fusão de Tecnologias

A variável tecnológica é fundamental na definição da estratégia dos negócios de uma organização. Além disso, atualmente não se pode pensar em empresas com domínio de uma única tecnologia como faz supor o enfoque de substituição de tecnologias. A simples substituição não é mais suficiente. A organização deve enfatizar também a diversificação tecnológica para promover a combinação de tecnologias no desenvolvimento de novos produtos e serviços. Esse é o espírito da fusão de tecnologias.

Com o enfoque da fusão, as empresas adicionam novas tecnologias àquela inicialmente dominada. Combinam tecnologias de modo a ampliar a funcionalidade dos produtos, proporcionando soluções mais abrangentes que as decorrentes da soma de soluções oferecidas isoladamente por cada uma das partes (sinergia). Podem ser encontrados na literatura inúmeros casos de aplicação do enfoque de fusão de tecnologias (Kodama, 1992; Sorensen e Levold, 1992). No entanto, a fusão de tecnologias requer novas práticas gerenciais e comportamentais e habilidades intelectuais.

Para a implementação do enfoque de fusão de tecnologias três princípios essenciais devem ser seguidos pelas organizações: sensibilidade às necessidades e anseios do mercado, capacidade de internalização dos conhecimentos e P&D em parceria.

Sensibilidade às Necessidades do Mercado

Ser sensível às necessidades dos clientes representa uma nova interpretação do papel do mercado como o principal fator de definição das atividades de P&D e para o desenvolvimento de novos produtos, com variedade e customização suficientes para que a maioria das pessoas possa obter exatamente o que se deseja.

Sensibilidade às necessidades do mercado demanda novas formas de se identificar os desejos dos consumidores ou de oportunidades de negócios. Trata-se de traduzir os desejos e anseios, explícitos ou implícitos, dos clientes em um conjunto muito bem definido de produtos. É um processo que envolve duas etapas: a primeira, converte os dados de mercado em especificações de produtos; a segunda, decompõe os produtos conceituais em um conjunto de projetos de desenvolvimento.

Capacidade de Internalização de Conhecimentos

O ambiente deve promover o envolvimento de todos os empregados e em todos os níveis na busca e disseminação da informação tecnológica onde quer que ela esteja. Para isso é necessário um eficiente sistema de comunicação e uma moderna estrutura organizacional de modo a facilitar o fluxo de informações.

As diretrizes de P&D são inócuas sem o conhecimento completo de todas as alternativas técnicas envolvidas. A amplitude das alternativas técnicas abrange, entre outros, um sistema de monitoração das inovações tecnológicas externas à organização e externas ao setor industrial ao qual a organização está inserida.

As indústrias necessitam coletar informações de todo espectro de competidores sejam eles visíveis ou invisíveis (Kodama, 1992). Nos competidores visíveis estão incluídos os concorrentes conhecidos do mesmo setor industrial, os que utilizam tecnologia similar ou têm sistemas de produção similares. Nos competidores invisíveis estão os potenciais concorrentes desconhecidos e não familiares por estarem em setores industriais diferentes.

Manter sob observação o freqüente e diversificado crescimento das tecnologias demanda sofisticada forma de aquisição de conhecimento que inclui capacitação formal e informal. A capacitação formal envolve a implantação de uma rede de escritórios espalhados pelo mundo para monitorar aplicações de patentes, analisar publicações tecno-científicas e descobrir empresas e

empreendedores inovadores. A capacitação informal baseia-se no entendimento por todos os empregados - executivos, pesquisadores, operários - da responsabilidade pela disseminação da informação e pela promoção da inovação tecnológica.

Internalizando os novos conhecimentos associados à demanda de mercado, a organização seguirá um caminho progressivo na diferenciação, evoluindo para estados de maior complexidade.

Pesquisa e Desenvolvimento em Parceria

O processo de internalização de conhecimentos ou de competências favorece o domínio crescente de tecnologias externas à empresa. No entanto, para melhorar a eficácia e eficiência do processo de capacitação, as empresas devem promover projetos cooperativos da pesquisa e desenvolvimento.

Conhecendo-se as necessidades do mercado e conhecendo-se a disponibilidade de tecnologia, a escolha de parceiros e projetos ocorre naturalmente.

Para que as parcerias sejam qualificadas como adequadas à fusão de tecnologias, elas devem ser substanciais e recíprocas. Para uma parceria tecnológica ser substancial necessita de:

- Um comitê conjunto de P&D que coordene os projetos desde seu início (exploratório) até o estágio final de desenvolvimento do produto, e
- Garantias de que os altos dirigentes das empresas envolvidas encamparão a idéia e darão continuidade do projeto de inovação até o seu estágio final.

A parceria recíproca constitui a essência da fusão de tecnologias e parte do princípio de que todos os parceiros são iguais e assumem a responsabilidade pela sua especialidade, bem como compartilham de todos os benefícios. Em outras palavras, responsabilidade, respeito, confiança e benefícios mútuos são exercidos em sua plenitude.

Sistemas de Engenharia e Fusão de Tecnologias

Sistema Aberto

O modelo descreve as organizações como um sistema que recebe, transforma e produz energia (inclusive matéria e informação), com parte do fluxo de saída retornando para o sistema (retroalimentação).

As manufaturas são sistemas abertos, porque a entrada de energia sob diversas formas e sua transformação em produto proporcionam um fluxo de retroalimentação que consiste em um intenso intercâmbio de informações entre a organização e seu meio ambiente (Bresciani, 1993; Katz e Kahn, 1987).

Como sistemas abertos, as organizações sobrevivem somente quando forem capazes de manter entropia negativa, isto é, importação de energia sob todas as formas, em quantidades maiores do que as que devolvem ao ambiente sob a forma de produto.

Os sistemas ou subsistemas voltados para inovação consomem energia sob a forma de conhecimento e proporcionam novas tecnologias que chegam ao mercado na forma de novos produtos e serviços. O fluxo de retroalimentação proporciona mais ou menos energia conforme a sensibilidade da organização em atender as necessidades dos consumidores.

Auto-Organização

O fenômeno de auto-organização é um processo que pode ocorrer em um sistema aberto (organizado) e sua presença se verifica pelo aumento da complexidade, variedade, informação e ordem e pela redução da redundância, incerteza, ambigüidade e entropia desse sistema. A forma mais comum de um sistema auto-organizado é aquela onde a organização segue um caminho progressivo na diferenciação, evoluindo naturalmente de estados de menor para maior complexidade com a conseqüente diminuição da entropia (Bresciani, 1993; Katz e Kahn, 1987).

A adoção da fusão de tecnologias e a conseqüente capacidade de operacionalizar recursos variáveis e virtuais (conhecimento) ao invés de recursos físicos (capital) para atender a demanda de mercado em tempo adequado e, ainda, a capacidade de integração efetiva entre empresas, fornecedores, parceiros e clientes proporcionam as principais condições favoráveis para que ocorra o fenômeno de auto-organização.

A manufatura, que busca, através da fusão de tecnologias, vantagens competitivas em um mercado dinâmico e instável, deve proporcionar o balanceamento energético (fluxo de conhecimento) adequado de maneira a compensar o aumento de entropia causado pelos processos internos de organização (por exemplo, projetos de inovação envolvendo especialistas de diferentes disciplinas e parcerias tecnológicas). A colocação de novos produtos que atendem às necessidades do consumidor é a energia que realimenta o processo e dá motivação ao grupo.

As organizações devem criar as condições ambientais para que o fenômeno de auto-organização ocorra. A implantação de rede de comunicações não basta para interfacear processos, banco de dados e pessoal. É necessário também uma reorganização das atividades e disposição para o trabalho em equipe, ou em rede de equipes, para que a informação flua rapidamente e a empresa possa ser ágil. O trabalho em rede de equipes constitui o núcleo do processo de desenvolvimento integrado de produtos.

Adaptabilidade dos Sistemas de Engenharia

As ferramentas mais comuns utilizadas pelos sistemas de engenharia são: CAD ("Computer Aided Design"), CAE ("Computer Aided Engineering"), CAM ("Computer Aided Manufactoring"), CAPP ("Computer Aided Process Planning"), CASE ("Computer Aided Software Engineering"), CAT ("Computer Aided Inspection and Testing"), GT ("Group Technology") e outras.

A eficácia da utilização dessas ferramentas e da capacidade de adaptação dos sistemas de engenharia está na facilidade de integração dos recursos computacionais e no compartilhamento (e transparência) da base de conhecimentos, bem como na disponibilidade de um sistema de auxílio à tomada de decisão e de controle de versões.

Adaptabilidade ou capacidade de adaptação dos sistemas de engenharia, segundo Agostinho (1993), pode ser entendida como a capacidade de implementar novos produtos seqüencialmente. Ela mede o estado de organização desses sistemas, quando acionada para introduzir novos produtos em regime de alta diversificação, necessário às novas regras de mercado. Esse conceito pode ser formalizado pela equação abaixo:

$$A_{i,i+1} = \frac{T_i}{T_{i+1}}$$

onde: $A_{i,\,i+1}$ representa o índice de adaptabilidade do sistema de engenharia para produzir o produto $i+1$ após ter produzido o produto i; T_{i+1} representam, respectivamente, os tempos para produzir os produtos i e $i+1$, ambos seguindo atividades comuns do ciclo de desenvolvimento, envolvendo as atividades de marketing, engenharia e produção, ou seja, T é o tempo ou a capacidade de implementar novos produtos.

A adaptabilidade será neutra para $A_{i,\,i+1} = 1$, com $T_i = T_{i+1}$, progressiva quando $A_{i,\,i+1} > 1$, com $T_i > T_i + 1$, e regressiva quando $A_{i,\,i+1} < 1$, com $T_i < T_{i+1}$. À organização cabe proporcionar meios para que ocorra a adaptabilidade progressiva para, assim, alcançar a desejada redução do ciclo de desenvolvimento de produtos (Agostinho, 1993).

É na capacidade de adaptação dos sistemas de engenharia que residem as facilidades de implementação da fusão de tecnologias e, conseqüentemente, do desenvolvimento integrado de produtos e da engenharia simultânea como resposta à complexidade crescente e à redução do ciclo de vida dos produtos. A mecatrônica é um caso típico.

Desenvolvimento Integrado de Produtos

Produtos são objetos tangíveis, coisas que podem ser vistas, tocadas e usadas. O processo de desenvolvimento de novos produtos depende do fluxo de informaçoes da mesma maneira que o produto depende do fluxo de materiais para sua fabricação.

A empresa pioneira no lançamento de um produto inovador tem melhores condições de estabelecer preços que permitam um retorno adequado sobre os custos de desenvolvimento, bem como assegurar uma fatia melhor do mercado.

O fluxo de informações para o desenvolvimento integrado de produtos provém das áreas de marketing, engenharia e processo. A empresa deve promover transformações organizacionais e culturais de modo que os obstáculos normalmente existentes entre marketing, engenharia e processo sejam superados. Deve-se proporcionar um ambiente que permita, simultaneamente, a contribuição e interação entre os profissionais dessas áreas no desenvolvimento conjunto de novos produtos. A Engenharia simultânea (ES) é a técnica eficaz que permite o desenvolvimento integrado de produtos.

A implantação da ES no ambiente de desenvolvimento de produto da empresa envolve a criação de times multidisciplinares, a implementação de mecanismos que assegurem a qualidade durante o desenvolvimento, o melhoramento contínuo, o aumento da sensibilidade aos anseios dos clientes e a implementação de mecanismos que agilizem o fluxo, vertical e horizontal, de informações, possibilitem a tomada de decisões de forma negociada e cooperativa, e motivem os profissionais abrirem mão de prerrogativas inerentes ao cargo que ocupam em prol ao objetivo comum.

O time de desenvolvimento atuando conforme os princípios de ES atuará como um sistema auto-organizado, recebendo influências externas - no caso dos clientes e fornecedores - e evoluindo para uma complexa e efetiva integração humana produzindo as inovações tecnológicas esperadas. A interação entre os membros do grupo tende a aumentar a entropia, porém a união é mantida se os objetivos visando atender as necessidades do mercado são mantidos e constantemente relembrados.

Os produtos refletem o estágio da organização e o processo de desenvolvimento que os criou. A plena aceitação do produto pelo mercado consumidor demonstrará o sucesso da aplicação da ES pela empresa e a integração, consistência e evolução profissional da equipe de desenvolvimento.

Conclusões

A estratégia da fusão de tecnologias amplia a visão de mercado permite um fluxo intenso e estimulante de informações para dentro da empresa. No entanto, exige uma postura avançada de organização que dê margem ao surgimento do processo de auto-organização. A empresa deve ser ágil o suficiente para fazer os ajustes necessários entre as exigências dos clientes e seus objetivos institucionais. As oportunidades de negócio incluem parcerias tecnológicas que, conseqüentemente, dão maior alcance à capacitação multitecnológica.

Se a estratégia de fusão de tecnologias direciona as atividades de pesquisa e desenvolvimento a médio e longo prazos, a opção pela engenharia simultânea permite a organização ser eficiente e eficaz no desenvolvimento e fabricação de novos produtos em prazos curtos.

Assim, as decisões por fusão de tecnologias, adaptabilidade dos sistemas de engenharia, flexibilidade dos sistemas de manufatura e desenvolvimento integrado de produtos (engenharia simultânea) são solidárias e complementares no processo inovação tecnológica.

Referências

Agostinho, O. L., 1993, "Adaptability of Engineering and Marketing Structures: a New Approach to Attend the Consumer Market Needs in CIM Environment", Proceedings of the 2nd International Conference Computer Integrated Manufacturing, vol. 1, p. 62, Singapore.

Bresciani Filho, E., 1993, "Inovaçao Tecnológica Através da Pesquisa como Processo de Auto-Organização em Empresa Industrial", Seminário de Auto-Organização e Informação, Centro de Lógica e Epistemologia e História da Ciência, UNICAMP.

Drucker, P. F., 1992, "The New Society of Organization", Harvard Business Review, vol. 70 (5), p. 95.

Katz, D. K. and Kahn, R. I., 1987, "Psicologia Social das Organizações", Atlas, São Paulo.

In this sense, even the inquiry of function costs, foreseen in the Value Analysis methodology as an "assessment step" (Csillag, 1985), seems to be more adequate for the judgement of already existing technical systems design, than for the conception phase. It should also be useful in the detection of weak spots and/or improvement of products which have already been developed.

Thus, during this phase of product design, the comparative assessment of conception variants is expected to be more significant as an aid for the decision-making of adequate conception solutions. More often than not, despite the unfavourable assessment results, some conception variants can still be utilized, and the definitive decision can only be taken after a greater concretization of the solution and as the idea takes shape - something that should occur in the following phases of the embodiment design and detailed design.

Therefore, to "assess" a solution alternative, at this point of product conception, means to analyze this solution in light of objectively defined criteria - bearing in mind that this could result in a merely provisional classification.

In case there is more than one alternative, each one of them must be submitted to the same criteria, so that a hierarchical order of importance ranked among the several solutions can be defined. After the ranking, it is possible to make a choice among them, that is, it is possible to identify the most favourable conception, according to the designer's view and design objectives.

An additional aspect is noteworthy: product design professionals know that a choice must be made as objectively as possible. However, very often the final decision falls upon an alternative which is not in the top of the ranking. Unweighted criteria - such as "solution originality", "beauty", decision-maker's "feeling" - sometimes overlap with purely technical criteria, and are those criteria adopted as elements of the final judgement for determining an alternative purported as the most adequate.

In spite of this, the technical evaluation of choices among conception alternatives is conducted considering the overall solution syntheses obtained for the product under study. Therefore, this work is carried out based on the set of conception alternatives which have been developed so far, and establishes a comparison between the available conception alternatives.

The specific bibliography includes several methods for the evaluation of solution alternatives (Seel, 1992; Blanchard and Fabrycky, 1990; Pahl and Beitz, 1988; Back, 1983, to name a few), which offer different approaches to analyze objectively product conception alternatives.

As far as the designer's point of view is concerned, it might be interesting to choose an evaluation method that is mainly based on the Requirements List (VDI 2225, 1984; Beitz, 1972). It is a simple method that can be quickly applied; it weighs the degree to which each conception variant meets the needs of design requirements classified in the early stage of the study as "desirable". It goes without saying that all requirements classified as "compulsory" have been met by the conception alternative being analyzed (otherwise, this conception would be incomplete and, therefore, it would have been ruled out as unacceptable in one of the previous evaluation stages).

The classification method mentioned above assigns different values to each of these desirable requirements. For example, grade 3 can be assigned to the desirable requirement of minor importance that is fulfilled; grade 6 to the desired requirement of medium importance, and grade 10 to the desirable requirement of great importance; grade zero will be assigned to a desired requirement that is not fulfilled by the conception variant. In recording the desirable requirements that are individually fulfilled by the solution alternatives, it is possible to calculate an average grade for each of the existing conception alternatives. This average grade will be useful to compare solution alternatives, and it will establish a hierarchy among the compared conceptions.

In this way, the relative importance of solution alternatives will be established in function of the average value that is calculated, which represents how each alternative meets the "desired" design requirements.

Another evaluation model - more complex and more complete - which also uses the Requirements List initially established to create value assignment criteria of concept solutions, was suggested by Beitz (1972, 1973) and referred to in other publications (Pahl and Beitz, 1988; Back, 1983).

In this model, the designer, aided by the Requirements List originally created, must establish his own conception assessment criteria, trying to spot important qualities of the product to be evaluated

and, after doing so, set objectives to verify the fulfillment of these qualities and then create the evaluation criteria.

Special care must be taken to make sure that the individual objectives on which the assessment criteria will be based are as independent as possible from the one another (Beitz, 1973). This aspect was also stressed by Sell (1992), and is meant to avoid a possible contradiction. If this contradiction occurs, the measures adopted to increase the utility value according to a criterion of some variant (or the extent to which an objective is fulfilled) might provoke the decrease of the utility values of other objectives. Therefore, care must be taken so that the fulfilment of an objective will bring, by itself, a contribution to the general utility of the conception variant, regardless of conflicts with the fulfillment of other objectives.

In the event that the starting point for the search of conceptions has been the Requirements List created with the "house of quality" (Hauser and Clausing, 1988), these assessment criteria can be adapted directly from the design requirements developed by the utilization of that technique. The criteria obtained through the "house of quality" would probably encompass a larger portion of the company's, consumer's and design's interests. Nevertheless, in order to get to the criteria of the "house of quality", the company needs a proper managerial and operational infrastructure to collect and to interpret the necessary data, infrastructure not commonly found in most companies nowadays (Campos, 1992).

Back to the systematic procedure for the assessment of conception variants discussed by Beitz (1972, 1973), in order to create its own criteria and to make the evaluation of conception variants, the designer must pay special attention to the following working steps:

1) Identification of evaluation criteria;
2) Weighing of evaluation items;
3) Weighing of evaluation sub-items;
4) Definition of evaluation parameters;
5) Setting of parameter values;
6) Calculation of overall value for each conception variant, and
7) Ranking of conception variants.

The first step ("identification of evaluation criteria") consists of establishing a set of objectives from which the evaluation criteria may be derived.

Taking the Requirements List into account, the factors that will be useful for evaluating conceptions are listed. For example, should there be an "assembly" requirement, factors such as "small utilization of movable parts", "low suceptibility to vibration", "small number of components", "low complexity of components", etc., can be established. Thus, the item "assembly" will have some sub-items (Fig. 1).

Item/Sub-item
1. Assembly:
1.1 - small utilization of movable parts;
1.2 - low suceptibility to vibration;
1.3 - small number of components;
1.4 - low complexity of components.

Fig. 1 Example of item and sub-items identified as conception evaluation criteria.

Two levels were adopted here (item and sub-item) in order to create the evaluation criteria. With them, the obtained results are already considered sufficient for the purpose of this paper. There is no other restraint to establish more levels, except for some additional efforts to be made on the evaluation procedure: in the same way that it was developed for two levels, the procedure can be extended to others, so as to meet the needs of jobs that require it.

The selection of evaluation items and sub-items from the design Requirements List is justified by the fact that it is in this list - and nowhere else - that are found all the requirements that

must be fulfilled by the product under study. This list is, then, the starting point from which evaluation criteria are built in order to assess the conception variants that have already been obtained.

Therefore, with the Requirements Lists, the designer writes down as many items and respective sub-items he considers important in order to compare his conceptions.

In the second step ("weighing of evaluation items"), weighting factors of each one of the previously listed items are judged, establishing their differences in function of their importance to the product and to the design. According to traditional theory, judgement factors are chosen based on a scale with grades ranging from 0 to 100 (which indicate nill or maximum importance, respectively). In addition, the sum of the factors assigned to the criteria must be equal to 100. Evidently, in case there is a single criterion item, it will be assigned maximum importance, with a weighting factor 100.

Likewise, in step three sub-items related to each listed item will be weighed according to a 0 - 100 value range.

For each evaluation criterion, it is useful to have a parameter with which to compare with the conception. Thus, step four ("definition of evaluation parameters"), tries to spot the parameter that is more suitable for this comparison. It must be quantifiable or, if this is not possible, it must be expressed by statements constructed as concretely as possible. During this step parameter magnitude must also be evaluated, considering that this "magnitude" represents the value (quantitative) regarded as ideal for the criterion that is being applied; later, conceptions will be graded in function of their "distance" from this "ideal" quantitative value, the highest grades are assigned to those conceptions that are closer to the "magnitude" value.

For example, in Fig. 2 one of the evaluation criteria is "low fuel consumption"; in this case, the parameter will be "fuel consumption", and the unit of measure, "g/kWh" - that is, fuel mass relative to the energy that this mass generates. The magnitude regarded as ideal, in this case, was 240 g/kWh, and will serve as a comparison standard to assess all conception alternatives that have been created. Another example, also from Fig. 2, has the evaluation criterion "lightweight construction"; the parameter is "mass per unit power", with a unit of measure "kg/kW". Its magnitude was set in 1.7 kg/kW, establishing a comparison standard for the conception alternatives that were analyzed thereafter. On the other hand, if the evaluation criterion is not quantifiable, such as "simple production", the comparison parameter could be "component simplicity", without a unit of measure for this factor. The magnitude of this parameter will be "great simplicity", meaning that the greater the conception simplicity, the higher the grade that it will be assigned to this item during the evaluation process. Another example of evaluation criterion can be "long service life", the parameter of which will be "service life", and can be measured in kilometres covered during this service life. The ideal standard, in this example, is expressed in a magnitude equivalent to 180,000 km.

Beitz (1973) warns that magnitudes of objects adopted as a basis for evaluation must be mentioned only when it is possible to assign quantitative numeric values to the respective criteria with sufficient accuracy. Or else, it is more convenient to make verbal statements of assessment (ex.: high, medium, low), with a degree of accuracy that can be clearly recognized. According to the author, it is dangerous to assign numeric values that are likely to be incorrect, because it might convey an information reliability which, in fact, does not exist.

In the example of Fig. 2 "Nr." means the order in which appear the evaluation criteria to be applied to the conceptions; the "criteria" themselves are the sub-items identified in the previous step; "weight wi" is the weighting assigned to this sub-item i, calculated as a product of the weighting assigned to the item by the weighting of each one of its sub-items: "parameters" are the reference values which the designer will use to assess the conception, and are measured in their respective "unit"; "variant Sj" represents each of the conception variants available for analysis, with gradings based on a scale of values ranging from zero, assigned to the lowest end ("absolutely useless solution") to ten ("ideal solution"), in the upper end; and "weighted value" will be the result of product (Vij.wi), the addition of which will represent the value of each conception alternative that is being evaluated.

Evaluation Criterion			Parameter			Variant S_j	
Nr.	Criterion	Weight (w_i)	Parameter	Unit	Magnitude	Value (V_{ij})	Weighted Value ($V_{ij} \cdot w_i$)
1	low fuel	0.3	fuel consumption	g/kWh	240		
2	lightweight product	0.15	mass per power	Kg/kW	1.7		
3	simple product	0.1	component simplicity	--	great		
4	long service life	0.2	life service	Km	180,000		
...	...	...					
i	...	...					
...	...	...					
n	...	...					
Addition (w_i) = 1							Addition ($V_{ij} \cdot w_i$)

Fig. 2 Typical criteria for selection of an automobile internal combustion engine (source: Pahl and Beitz, 1988 - adaptation)

In step five ("setting of parameter values"), the designer must assign values to each one of the evaluation criteria which have been previously determined, considering one criterion at a time. These values are shown in grades, according to a previously defined scale. An example of such scale can be seen in Fig. 3: points are placed between the ends zero (indicating that that particular evaluation item is not fulfilled by the solution variant in question) and 10 (showing that the solution variant fulfills that evaluation item in the best possible way). Intermediate situations between these two ends will be represented by internal points of the referred interval.

The designer must grade the evaluation items of each one of the conception variants. All available conception variants must be analyzed for each criterion.

Value scale for the grading of criteria	
Meaning	Pts.
Absolutely useless solution	0
Very inadequate solution	1
Weak solution	2
Tolerable solution	3
Adequate solution	4
Satisfactory solution	5
Good solution with few drawbacks	6
Good solution	7
Very good solution	8
Solurion exceeding the requirements	9
Ideal solution	10

Fig. 3 Example of value scale for the grading of criteria.

Step six ("calculation of overall value for each conception variant") occurs after the assignment of the last value to the last conception variant, referring to the last evaluation criterion: the sum of grades obtained by each conception is then calculated. This sum of grades can either be calculated through the addition of values assigned to the parameters (addition of the Vij, varying i),

without weighting the criteria; or through the weighted addition of the values assigned to the parameters (addition of Vij.wi, varying i). These sums indicate that the highest value of addition of Vij (obtained with the variation of i) is the best solution; or, in the other case, the highest value of the addition of Vij.wi (obtained with the variation of i) is the best solution.

In step seven ("ranking of conception variants"), solution variants are ranked according to a sequence based on the addition of the (Vij), or through the addition of the (Vij.wi). The comparison, according to either addition (with or without weighing the criteria) can lead to different results for rankings of conception variants.

Given possibility of mistakes and uncertainties due to evaluation errors, its is likely that the conception variant with the highest total of weighted value is really not the best solution among all the possibilities. In addition, when the weighted values are to close, there might be uncertainty as too the correct ranking - since it is always possible to expect inaccuracies to occur during the evaluation. In face of these problems, a Solution Profile (Pahl and Beitz, 1988; Back, 1983; Beitz, 1973) can be built to aid in the comparison of solution alternatives.

Conclusion

Although the evaluation models that have been analyzed in this paper can be utilized satisfactorily, this field probably still needs improvement with regards to conception evaluation. It is possible to verify that the model described by Beitz is not sufficiently generic; the "house of quality" model is demanding in terms of company organization; the Value Analysis model is more suitable for redesign, and so forth: there is no model objectively developed to evaluate products during the conception phase. Moreover, none is specifically designed for use with CAD systems.

This seems to be a promising field for research, especifically if the current trend of attempting to find conception with the aid of computers is taken into account (Fiod, 1993). This trend aims at the integration of this product idealization phase to CAD systems that are available in the market today.

With assessment mechanisms integrated to a computerized system for product conception research, we can hope that automation of all design process is very close to becoming a reality.

References

Back, N., 1983, *Metodologia de Projeto de Produtos Industriais (Industrial Products Design Methodology)*. Rio de Janeiro, RJ, Brazil: Guanabara Dois.

Beitz, W., 1972, "Bewertungsmethoden als Entscheidugshilfe zur Auswahl von Lösungsvarianten". Konstruktion 24, pp. 493-498.

Beitz, W., 1973, "Bewertungsmethoden als Entscheidugshilfe zur Auswahl von Lösungsvarianten (Fortsetzung)". Konstruktion 25, pp. 29-32.

Blanchard, B.S. nad Fabrycky, W.J., 1990, *Systems Engineering and Analysis*. New Jersey: Prentice Hall, 2nd. ed.

Campos, V. Falconi, 1992, TQC - *Controle da qualidade total (no estilo japonês) (TQC: Total Quality Control - Japanese Style)*. Belo Horizonte, MG, Brazil: Fundação Christiano Ottoni, Escola de Engenharia, Universidade Federal de Minas Gerais.

Csillag, J.M., 1985, *Análise de Valor. Metodologia do Valor (Value Analysis. Value Methodology)*. São Paulo, SP, Brazil: Atlas.

Fiod Neto, M., 1993, "Desenvolvimento de Sistema Computacional para auxiliar a concepção de produtos industriais". ("Development of a Computer-aided design system for the conception of industrial products"). Florianopólis, SC Brazil: PhD Thesis, Federal University of Santa Catarina.

Fiod Neto, M. and Back, N.,1991, "O processo do projeto de produtos industriais" ("The process of industrial products design"). Annals of the North-Northeast Congress of Mechanical Engineering (CEM-NNE/91. Natal, RN, Brazil.

Fiod Neto, M. and Back, N.,1992, "A sistematizacão da concepção do produto". ("The systematization of product conception"). Annals of the II North-Northeast Congress of Mechanical Engineering (CEM-NNE/92). João Pessoa, PB, Brazil.

Hauser, J.R. and Clausing, D., 1988, "The house of quality". Harvard Business Review, May-June, pp. 63-73.

Pahl, G. and Beitz, W., 1988, *Engineering design: a systematic approach*. Berlin: Springer-Verlag, 2nd. ed.

Sell, Ingeborg, 1992, "Avaliação de alternativas de produtos: metodologia". ("Evaluation of product alternatives: a methodology"). Paper presented during the selection examination for professor promotion: Federal University of Santa Catarina, Florianópolis, SC, Brazil.

VDI 2225 (Richtlinie), 1984, "Konstruktionsmethodik. Technischwirtschaftliches Konstruieren Vereinfachte Kostenermittlung, Blatt 1 - Entwurf". Berlin: VDI-Richtlinien.

RBCM - J. of the Braz. Soc. Mechanical Sciences
Vol. XVII - nº1 - 1995 - pp. 116-118

ISSN 0100-7386
Printed in Brazil

Abstracts

Tomasini, E. P., 1995, "Advances and Applications of Laser Velocimetry", RBCM - J. of the Braz. Soc. Mechanical Sciences, Vol. 17, no. 1, pp. 1-13.

This paper is a critical review of the most recent advances in laser measurement techniques and their different applications. It is worth underling that these techniques are used both for measuring fluids motion characteristics and conditions, and for measuring motion, vibrations in particular, in solids.

Those applications which, until today, had been carried out in laboratories, are now being extended to the industrial field, especially in the control of processes and products. It is therefore desirable that associations, meetings and conferences will contribute to a more extensive use and knowledge of these techniques.

Keywords: Laser Doppler, Dual Focus, PIV, Doppler Global Velocimetry, Scalar Quantities, Laser Vibrometry, Vibrations, Flames.

Moura, L. F. M., Rego, A. J. C. and Avancini, J. R., 1995, "Numerical Simulation of the Two-Phase Flow Redistribution Between Two Passes of a Heat Exchanger", RBCM - J. of the Braz. Soc. Mechanical Sciences, Vol. 17, no. 1, pp. 14-25. (in Portuguese)

This work deals with the numerical simulation of the two-phase flow distribution inside a common header placed between two passes of a shell-and-tube heat exchanger. The Numerical results have been obtained from a computer code based on the two-dimensional two-fluid model. The interfacial momentum transfer was modeled as a function of the flow patterns observed in the heat exchanger common header. The influence of the total mass flow rate and the mixture quality (the inlet flow conditions) on the phase distributions at the common header outlet were investigated. The numerical simulations of the two-phase flow distribution inside the common header were compared qualitatively with other numerical and experimental results, showing the capability of the proposed model.

Keywords: Two-Phase Flow, Numerical Simulation, Two-Fluid Model, Heat Exchanger.

Siemek, J., Stopa, J. and Rybicki, C., 1995, "Peculiarities of Two-Phase Flow in Coalbeds", RBCM - J. of the Braz. Soc. Mechanical Sciences, Vol. 17, no. 1, pp. 26-34.

The theorical aspects of the two-phase gas-water flow, with sorption, in the coalbed treated as the double porosity system is presented and the equivalence of such model with the three phase flow model in classical porous medium is proved. Then, the results of computer simulation are presented and discussed to show the peculiarities of the flow in coalbeds.

Keywords: Degasification, Coalbeds, Porous Medium, Two-Phase Flow.

Hernández-Vaquero, R. M. S., 1995, "Information Integration in Computer Integrated Manufacturing (CIM)", RBCM - J. of the Braz. Soc. Mechanical Sciences, Vol 17, no. 2, pp. 35-48.

One of the main problems when implementing the CIM concept concerns information integration. In order to support information integration an information system provided with suitable data models is required. In this paper, an information system is presented, which fulfils the requirements for an appropriate information management in CIM.

In order to make the information system transportable and worlwide accepted, it has been built on the basis of an international standard ISO 10303 (STEP). In this paper, an overview of STEP will be given as well as two of the most interesting aspects of STEP: the EXPRESS language and the neutral exchange file.

The EXPRESS language is used in the information system as data model. The users of the information system (CIM tool user) must establish their data models in EXPRESS and the information system will store them in the database. This makes the information system flexible because the implemented interface is independent of the database schema. Some access functions are provided by the information system for the storage and retrieval of instances of the model when the designer is working with the CIM tool. The data exchange format is the one used in STEP.

The information system was developed in the frame of the ESPRIT 2202 CIM-PLATO project of the European Community.

Keywords: CIM, Information Integration, STEP, EXPRESS.

Scotti, Américo, 1995, "The Welding Arc Pressure", RBCM - J. of the Braz. Soc. Mechanical Sciences, Vol 17, no. 2, pp. 49-55.

The aim o the present article is to contribute for a best understanding of the phenomena which occur in an arc column during welding. The origin o pressure on the weld pool is described and discussed. Consensus and disagreement on the matter amongst author are also stated. Practical importance of the subject is conclusively pointed out.

Keywords: Welding, Physics of Arcs Plasma Jet, Arc Pressure.

Torii, Kahoru and Nishino, Koichi, 1995, "Thermal Contact Resistance of Wavy Surfaces", RBCM - J. of the Braz. Soc. Mechanical Sciences, Vol 17, no. 2, pp. 56-76.

Experimental and analytical studies were made on the thermal contact resistance (TCR) of wavy surfaces. An emphasis was placed on the influence of the surface waviness on the overall TCR in a high vacuum. A nearly spherical waviness with a large radius of curvature was prepared on a metal surface made of copper, aluminum alloy or stainless steel. Heat transfer experiments performed at a high vacuum indicated a power law behavior of the TCR against the nominal contact pressure. The value of the exponent was, however, dependent on the material and the magnitude of surface roughness, and it was substantially smaller than those of the previous correlations. A technique for predicting TCR was developed by using a pressure-measuring film which was capable of visualizing a distribution of contact pressure. Predicted values of the overall TCR agreed reasonably well with the experimental values. It was shown that the macroscopic constriction resistance was predominant for the present wavy surfaces. Effects of the interstitial gas were also examined by varying the ambient air pressure from vacuum to atmospheric. As expected, the overall TCR decreased as the air pressure increased. Such behavior was analyzed by using a simple two-stage heat conduction model which took into account gas conductions through the waviness gap and the roughness gap. The model was shown to be adequate to explain quantitatively the effect of the interstitial gas on the overall TCR for wavy surfaces.

Keywords: Thermal Contact Resistance, Wavy Surface, Prediction Technique, Interstitial Gas.

Palma, Ernani S., 1995, "Modelling the Flow Stress in Metals as a Function of the Temperature and Strain-Rate", RBCM - J. of the Braz. Soc. Mechanical Sciences, Vol 17, no. 2, pp. 77-88.

This work presents a mathematical model which describes the plastic deformation of metals. A constitutive equation, based on microstructural aspects of metal is derived. This equation establishes the dependence of the flow stress on the temperature and strain rate. The mathematical model results are then compared with experimental data produced by the authors, indicating the feasibility of the method.

Keywords: Modelling, Plastic strain, Sintered Materials, Steel.

Springer, H. and Ecker, H., 1995, "Modelling, Simulation and Optimization of a Printer Sled Driving System", RBCM - J. of the Braz. Soc. Mechanical Sciences, Vol. 17, no. 1, pp. 89-101.

An electromechanical system is considered that is composed of a sled, which is guided by two parallel guide rods and carrying a printer head elastically attached to the sled. The sled is driven by a two-phase step motor through an elastic belt and pulley system. The step motor torque characteristics are generated by frequency and amplitude modulated currents in the two phases controlled by a microprocessor. Nonlinear equations of motion for the system are established and numerically integrated by the simulation code ACSL. A new optimization routine GOMA is applied to the simulation model in order to optimize the current modulation parameters so that the dynamical position error of the printer head approaches a minimum.

Keywords: Printed Sled Driving System, Control of a Mechanical System.

Cardoso Jr., J. L., Agostinho, L. O. and Breciani Filho, E., 1995, "Technology Fusion System and New Product Development", RBCM - J. of the Braz. Soc. Mechanical Sciences, Vol. 17, no. 1, pp. 102-108. (in Portuguese)

This article the generation process of knowledge by tecnology fusion system as a self-organizing process and new product development catalyst. As a result of technology fusion the concept of adaptability of engineering system within an integrated product development enviroment is considered.

Keywords: Adaptability of Engineering Systems, Technology Fusion, Technology Innovation, Concurrent Engineering.

Fiodi Neto, M. and Back, N., 1995, "Assessment of Product Conception: A Critical Review", RBCM - J. of the Braz. Soc. Mechanical Sciences, Vol. 17, no.1, pp.109-115

During the product-conception phase assessment criteria are used to select promising alternatives among the optimal solutions encountered by the designer. A correct evaluation of the obtained results is necessary during the conception phase, so that further efforts for product realization are not wasted on ideas which are identified as no promising at an early stage.

Keywords: Conception Evaluation, Conception of Product, Methodology of Project.

"Srs. Autores, os artigos poderão ser entregues em meio magnético, editados por qualquer processador de texto do ambiente Windows".

Revista Brasileira de Ciências Mecânicas Revisores - 1994

Journal of the Brazilian Society of Mechanical Sciences Referees - 1994

Álvaro Toubes Prata	*UFSC*
Angela Ourivio Nieckele	*PUCRJ*
Anselmo Eduardo Diniz	*UNICAMP*
Antonio Batocchio	*UNICAMP*
Antonio Carlos Bannwart	*UNICAMP*
Arno Blass	*UFSC*
Arthur José Vieira Porto	*EESC*
Aureo Campos Ferreira	*UFSC*
Claudionor Cruz	*UFU*
Clovis Raimundo Maliska	*UFSC*
Clovis Sperb de Barcellos	*UFSC*
Edson Gomes	*EPUSP*
Eduardo Vila Gonçalves Filho	*EESC*
Euclides de Mesquita Neto	*UNICAMP*
Eugenio Spano Rosa	*UNICAMP*
Fernando Iguti	*UNICAMP*
Francisco José Simões	*UFPB*
Henrique Rosenfeld	*EESC*
Hernani Brinatti	*EPUSP*
João Batista Aparecido	*UNESP Illha Solteira*
João Carlos Meneses	*ITA*
João Fernandes Gomes de Oliveira	*EESC*
João Manuel Domingos de Almeida Rollo	*EESC*
José João de Espindola	*UFSC*
Kamal Abdel Radi Ismail	*UNICAMP*
Ney Augusto Dumont	*PUCRJ*
Nivaldo Lemos Coppini	*UNICAMP*
Olivio Novaski	*UNICAMP*
Paulo Roberto Sousa Mendes	*PUCRJ*
Renato Pavanello	*UNICAMP*
Ricardo Luiz Utsch de Freitas Pinto	*UFMG*
Walter Lindolfo Weingaertner	*UFSC*
Webe João Mansur	*COPPE/UFRJ*
Wilson Sérgio Venturini	*EESC*

ISSN 0100 - 7386

REVISTA BRASILEIRA DE CIÊNCIAS MECÂNICAS
JOURNAL OF THE BRAZILIAN SOCIETY OF MECHANICAL SCIENCES

VOL. XVII - Nº 1 - 1995